Max-Planck-Institut
für Meteorologie

MAX-PLANCK-GESELLSCHAFT

International Max Planck Research School
on Earth System Modelling

Causes for regional changes in heavy precipitation over Europe

Christine Radermacher

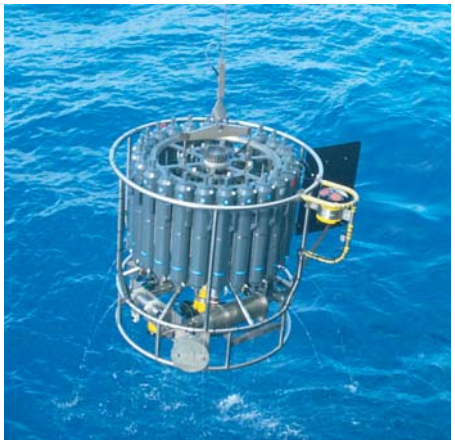

Berichte zur Erdsystemforschung 133/2013

Reports on Earth System Science

Hinweis

Die Berichte zur Erdsystemforschung werden vom Max-Planck-Institut für Meteorologie in Hamburg in unregelmäßiger Abfolge herausgegeben.

Sie enthalten wissenschaftliche und technische Beiträge, inklusive Dissertationen.

Die Beiträge geben nicht notwendigerweise die Auffassung des Instituts wieder.

Die "Berichte zur Erdsystemforschung" führen die vorherigen Reihen "Reports" und "Examensarbeiten" weiter.

Notice

The Reports on Earth System Science are published by the Max Planck Institute for Meteorology in Hamburg. They appear in irregular intervals.

They contain scientific and technical contributions, including Ph. D. theses.

The Reports do not necessarily reflect the opinion of the Institute.

The "Reports on Earth System Science" continue the former "Reports" and "Examensarbeiten" of the Max Planck Institute.

Anschrift / Address

Max-Planck-Institut für Meteorologie
Bundesstrasse 53
20146 Hamburg
Deutschland

Tel.: +49-(0)40-4 11 73-0
Fax: +49-(0)40-4 11 73-298
Web: www.mpimet.mpg.de

Layout:

Bettina Diallo, PR & Grafik

Titelfotos:
vorne:
Christian Klepp - Jochem Marotzke - Christian Klepp
hinten:
Clotilde Dubois - Christian Klepp - Katsumasa Tanaka

Berichte zur Erdsystemforschung 133/2013

Causes for regional changes in heavy precipitation over Europe

Christine Radermacher

aus Aachen

Hamburg 2013

Reports on Earth System Science 133/2013

ISSN 1614-1199

Christine Radermacher
Max-Planck-Institut für Meteorologie
Bundesstrasse 53
20146 Hamburg

Als Dissertation angenommen
vom Department Geowissenschaften der Universität Hamburg

auf Grund der Gutachten von
Prof. Dr. Daniela Jacob
und
Dr. Lorenzo Tomassini

Hamburg, den 3. April 2013
Prof. Dr. Jürgen Oßenbrügge
Leiter des Departments für Geowissenschaften

ISSN 1614-1199

Causes for regional changes in heavy precipitation over Europe

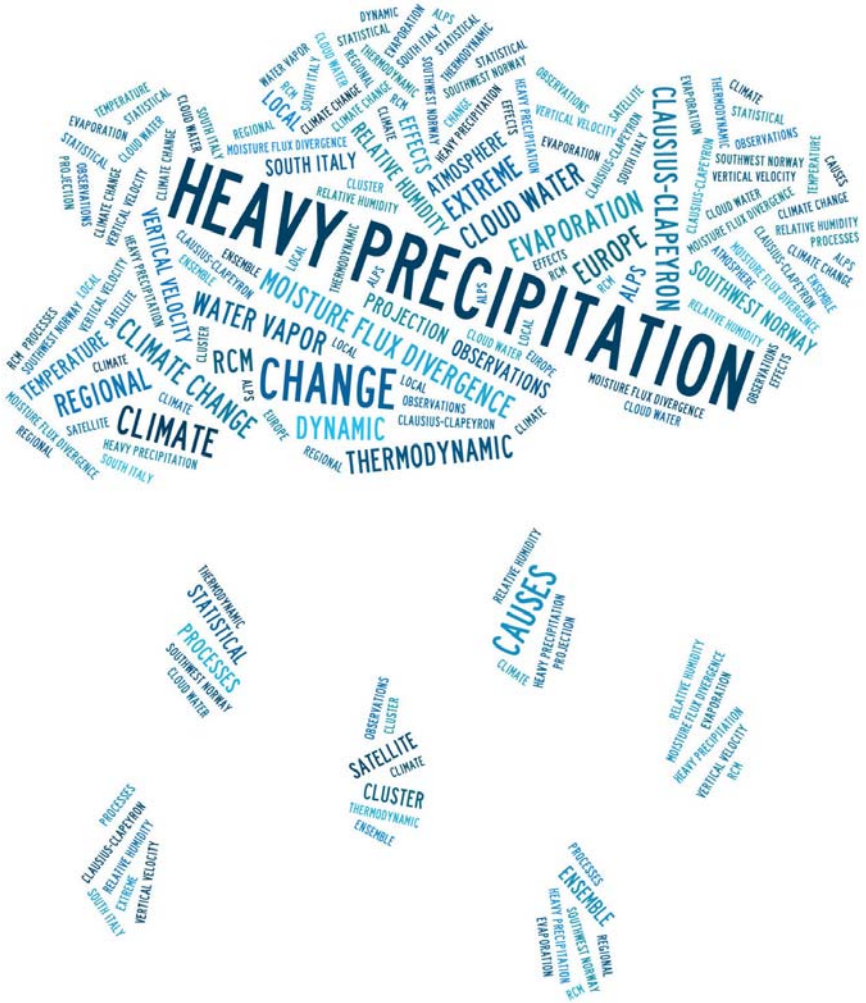

Christine Radermacher

Hamburg 2013

Abstract

In a warming future climate, heavy precipitation events are expected to change in frequency and intensity due to alterations of dynamic and thermodynamic processes. In particular the amount of atmospheric moisture is expected to increase when the temperatures are rising, which invigorates the moisture flux convergence and could lead to enhanced precipitation intensities. Also, heavy precipitation characteristics may change due to shifts in the large-scale circulation of the atmosphere as well as changes in the boundary layer stability. Particularly complex are causes for changes on regional scales, which are still not fully understood and have so far mainly been investigated with global climate models. Regional climate models may instead be more appropriate since meso-scale storms, convection, and other regional scale features are often associated with the strongest precipitation events and cannot be resolved by global models. This study presents a detailed investigation of causes for changes in heavy precipitation on regional scales. Quantities, which mainly govern the formation of heavy precipitation events over Europe and alter their characteristics are identified in a regional modeling framework and by application of extreme value statistics. The role of dynamic versus thermodynamic aspects is assessed. The results indicate limitations to the scaling of heavy precipitation changes with atmospheric moisture and stress the role of cloud liquid water and relative humidity on regional scales. Furthermore, changes in the atmospheric dynamics are found to play a decisive role overall.

Contents

List of Figures

List of Tables

1 Introduction

In the scientific community there is general consensus that the characteristics of precipitation as one of the most important variables in our Earth's climate system will change as the climate changes due to increased greenhouse gas emissions (Semenov and Bengtsson 2002; Trenberth et al. 2003; Frei et al. 2006; Hegerl et al. 2007). Changes may involve the mean, the frequencies, or the intensities of precipitation events. The understanding of the processes involved in their formation is essential to understand their changes and to improve climate model projections to the future. These processes may range from the large-scale dynamics down to local cloud and precipitation microphysics.

Of particular relevance are changes of heavy and extreme precipitation events, i.e. events in the uppermost quantile range of the probability distribution. Often, natural hazards are associated with these events (Van Aalst 2006), with destroying impacts on infrastructure, property, or human lives. Heavy rainfall may result in floods in riverine or severe landslides in mountainous regions. Heavy snowfall events can cause avalanches, severe damages through snow debris, or traffic breakdowns.

Changes in the global average precipitation are controlled by the hydrological cycle which is constrained by the global energy budget (Boer 1993), in particular by the balance of the radiative effects and an upward latent heat flux through evaporative cooling at the surface and latent heat release to the troposphere by precipitation. For an ensemble of global climate model simulations under CO_2 doubling, Allen and Ingram (2002) found the increase of global average precipitation to be about 3.4 % per kelvin.

Future changes in heavy precipitation events are not bounded by the energy budget but are suggested to be constrained by the Clausius-Clapeyron relation (Allen and Ingram 2002). This relation describes the exponential increase of the saturation vapor pressure with temperature. The hypothesis of a scaling of heavy precipitation changes with the Clausius-Clapeyron relation is based on several assumptions (Trenberth et al. 2003). First, heavy precipitation is assumed to be determined by the amount of moisture which is already in the atmosphere at the start of a storm and can be fed to a precipitation event by the large-scale circulation and low-level moisture convergence. Only a small amount of moisture is provided by local evaporation (Trenberth 1998). If second, the relative humidity of the atmosphere remains constant as the climate changes, the atmospheric moisture, also known as precipitable water, increases with temperature at the same rate as the saturation specific humidity, i.e. following the

Clausius-Clapeyron relation. For the global mean temperature of about 281 K at the 850 hPa pressure level, this scaling is about 7 $\%/K$, which can be considered as a good approximation overall (Trenberth et al. 2003). Under the third assumption that the atmospheric circulation does not change considerably in a warming climate, the intensity of precipitation is expected to increase at a similar rate. Heavy precipitation is suggested to be favored thereby in a warming climate (Trenberth et al. 2003).

The argument of constant relative humidity with climate change is supported on the global scale by studies with general circulation models (GCMs) (Pall et al. 2007; Allen and Ingram 2002; Hegerl et al. 2007). Yet, regionally, the assumption may not be fulfilled everywhere, which causes deviations from the Clausius-Clapeyron scaling of atmospheric moisture (Held and Soden 2006; Lorenz and DeWeaver 2006). Also, the non-changing nature of the atmospheric circulation is not generally supported by climate models. Changes in the dynamics, such as shifts in the storm tracks due to changes in the meridional gradient of the sea surface temperature (SST), have been found in several GCM studies (Bengtsson et al. 2006; Ulbrich et al. 2008). Such changes could modify the pattern of the moisture flux convergence and might lead to shifts of heavy precipitation to different locations or changes in the frequency and intensity of such events (Emori and Brown 2005a; Meehl et al. 2005). In a global model study, Pall et al. (2007) test the Clausius-Clapeyron constraint on different spatial and temporal scales and suggest that with regard to regional changes one has to consider both dynamic and thermodynamic aspects.

Also, the immediate scaling of heavy precipitation changes with the vertically integrated water vapor has been questioned. O'Gorman and Schneider (2009a) assess a scaling which is based on the condensation rate. They find that heavy precipitation changes scale more closely with the moist-adiabatic derivative of saturation water vapor than with the vertically integrated amount. This is due a weakening of the moist-adiabatic temperature lapse rate caused by increased latent heat release, which causes a damping of the increase in the condensation rate. Berg et al. (2009) find changes of heavy summer precipitation to be limited by the moisture availability rather than the by the atmospheric saturation water vapor on regional scales over Europe.

In general, the causes for heavy precipitation formation differ regionally and the same may be true regarding the causes for their changes. Changes in the static stability, local evaporation, or convective processes may be important aspects. On regional scales, dynamic and thermodynamic causes for future changes in heavy precipitation have not been investigated in detail so far, in particular not with regional climate models (RCMs).

High-resolution RCMs represent appropriate tools to investigate atmospheric processes on limited area domains in a physically consistent and three-dimensional framework. For the simulation of heavy precipitation events regional modeling is important in particular as meso-scale storms and convection are often features of the strongest

rain events and cannot be resolved by global models. Furthermore, increased model resolution improves the simulation of heavy events over complex orography (e.g. Kunz and Kottmeier 2006; Zängl 2007). Figure 1 displays the topography of the European continent in the RCM REMO at a spatial resolution of about 25 km.

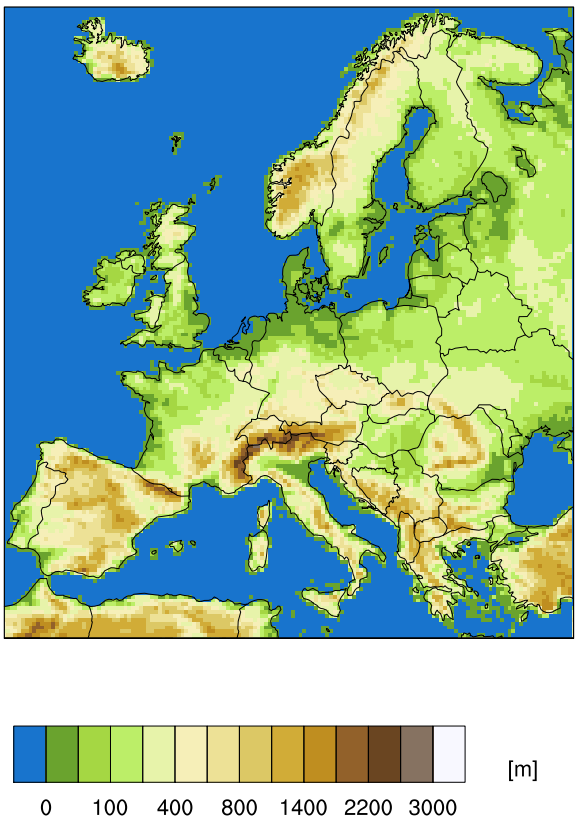

Figure 1.1: Topography of Europe in meters above sea level as used in the regional climate model REMO at 25 km spatial resolution.

The climate on the European continent exhibits a variety of regional differences, from subtropical climate in the south to arctic climate in the very north, with coastal and continental areas, the Alps as weather barrier between northern and southern regions, and the Mediterranean Sea as large water reservoir. Europe therefore incorporates various mechanisms forming heavy precipitation events and is a suitable region to study their changes.

Since extreme events are by definition rare in occurrence, the investigation of their statistics exhibits some obstacles. It is for example often desired to estimate the probability distribution of events that exceed the range of the observations. Standard prob-

ability density estimation techniques are appropriate for the part of the distribution with the highest frequency of observations, but can be biased towards the largest or smallest events, described by the tails of the distribution (Coles 2001; Embrechts et al. 1997). Extreme value theory (EVT) tackles the problem of estimating the probability density within the tails. Besides investigating the stationary, non-varying distribution of extremes, EVT can also be applied to investigate temporal trends by introducing the time as explanatory variable. Also, physical reasons for extreme events can be explored by extending a statistical model by covariates, i.e. by variables that may possibly control the extreme variable. Since heavy precipitation events occur rarely, a robust assessment of their causes with sensitivity studies is not possible. The EVT provides an appropriate framework for this.

In this study, projected changes in heavy daily precipitation are analyzed in regional climate models and their causes are investigated using extreme value statistics. The key aim is to assess which dynamic and thermodynamic aspects control changes in heavy precipitation on regional scales. Particular attention is turned on the Clausius-Clapeyron scaling and regional deviations from it.

1.1 The research questions

The study aims to answer the following research questions:

1. How is heavy precipitation projected to change regionally over Europe for a future climate change scenario? Are the changes robust across an ensemble of regional climate model simulations?
2. Is there an immediate scaling of changes in heavy precipitation and precipitable water, predicted by the Clausius-Clapeyron relation?
3. Which dynamic and thermodynamic quantities mainly govern the formation of heavy precipitation events? How do they interact and cause changes of heavy precipitation in different regions of Europe?

1.2 Outline of the study

The research questions are investigated in three main chapters which are written in the style of journal publications. Therefore, each of the Chapters 2, 3, and 4 contains its own introduction and conclusions. Chapter 2 has been published in the Journal of Climate (Radermacher and Tomassini 2012). Chapter 3 is going to be submitted to

the Geophysical Research Letters. Submission to a scientific journal is also planned for Chapter 4. For editorial consistency, the abstract of the publication underlying Chapter 2 has been omitted. Also, some editorial changes and minor modifications have been made to the text to make it consistent with other parts of the thesis, e.g. to avoid repetition. Finally, in Chapter 5, the work is wrapped up and conclusively discussed. A short outlook to possible continuations of the study is given.

The main contents of the three chapters are as follows:

- Chapter 2: In this chapter, the first and the second research question are tackled with the following analyses:
  - Extreme value analysis of future changes in heavy precipitation projected by an ensemble of RCM simulations over the European domain and assessment of the robustness of the results across the ensemble.
  - Analysis of the regional scaling of heavy precipitation with total column water vapor and column cloud liquid water, with focus on the expectations from the Clausius-Clapeyron relation.
- Chapter 3: After having analyzed the regional connections of future changes in heavy precipitation with precipitable water and cloud liquid water in Chapter 2, the aim of this chapter is to investigate whether these connections are found in an RCM simulation for present-day climate and agree with observations. This chapter therefore contributes to the second research question. The following analyses are carried out:
  - Comparison of heavy precipitation in a present-day high-resolution RCM simulation and meteorological observations.
  - Analysis of the relationship between moisture variables and temperature in model and observations.
  - Investigation of total column water vapor and cloud water as covariates for heavy precipitation using an extreme value model for present-day climate.
- Chapter 4: Whereas the focus of Chapter 2 and 3 is mainly on the thermodynamic aspects of heavy precipitation, the dynamic causes and their interplay with the thermodynamics are investigated more detailed in Chapter 4. The aim of this part is to answer the third research question by carrying out the following investigations:
  - Cluster analysis of characteristic patterns of the moisture flux divergence favorable for heavy precipitation formation in present and future.
  - Identification of suitable sets of dynamic and thermodynamic covariates for heavy precipitation in different European regions using an extreme value statistical model.

2 Future changes in heavy precipitation and thermodynamic causes

In this chapter, an extreme-value analysis of projected changes in heavy precipitation is carried out for an ensemble of eight regional climate model simulations over the European domain. The consideration of several regional models that are forced by different global models allows for an assessment of the robustness of the trends in terms of inter-simulation agreement. This leads to answering the first research question of the study, posed in Chapter 1.1. In the second part of the chapter, thermodynamic aspects for changes in heavy precipitation are discussed. Changes of variables that are related to the process of precipitation formation, such as vertically integrated water vapor and cloud liquid water, are examined. The scaling of changes in heavy precipitation and thermodynamic quantities with temperature is explored. In this context, the validity of the Clausius-Clapeyron scaling for heavy precipitation is assessed on regional scales, which is aimed at answering the second research question (Chapter 1.1).

2.1 Introduction

Among the consequences that may result from warmer climatic conditions, changes in extreme events can locally have the most devastating effects. Heavy precipitation events are critical in particular as they can cause floods in riverine areas and land slides in mountainous regions. Such hazards can result in enormous losses of infrastructure, ecosystems, or human lives. A detailed exploration of the causes for heavy precipitation and possible changes in heavy precipitation characteristics is therefore important.

Causes for changes in heavy precipitation can broadly be classified as being of dynamic or thermodynamic nature (Emori and Brown 2005b; Muller et al. 2010). Dynamic causes refer to changes in the atmospheric circulation while thermodynamic causes encompass changes in temperature and atmospheric moisture content. Yet, the separation is not clear-cut and overlapping is possible. Changes in atmospheric stability and convective activity, for instance, are related to thermodynamic characteristics of the boundary layer and induce alterations in the dynamics of the atmosphere.

As explained in Chapter 1, a starting point for the discussion of thermodynamic aspects of changes in heavy precipitation is the Clausius-Clapeyron equation (Allen and Ingram 2002; Pall et al. 2007; Allan and Soden 2008; Trenberth 2011). On its basis it

is suggested that heavy precipitation and atmospheric moisture scale with temperature in a similar way, i.e. at a rate of about $7\%/K$. However, several issues remain. For instance, there is a widespread decrease in surface relative humidity over land in global warming simulations (O'Gorman and Muller 2010; Sherwood et al. 2010). Moreover, warming and moistening does not take place uniformly over the troposphere (Soden et al. 2005) under changing greenhouse gas concentrations. This can have an effect on the static stability of the atmosphere and subsequently on the frequency and intensity of convective activity (Genio et al. 2007; Frierson 2008; O'Gorman and Schneider 2009b). Furthermore, the temperature increase over land significantly outpaces changes over the ocean in global warming simulations, especially in northern hemisphere summer. This may lead to a drying of arid land areas (Mariotti et al. 2008). In the absence of strong dynamic forcing and moisture advection, the availability of moisture can be limited over land, which has an impact on precipitation formation, although the link between soil moisture and precipitation is not straightforward (Hohenegger et al. 2009). In Europe, the increased amount of convective precipitation that falls over wet compared to dry soils is not necessarily steered directly by the local amount of evaporation. Instead, convective precipitation over land might be driven by the build up of a shallow boundary layer in which heat and moisture are accumulated and provide a source of convective instability through a high concentration of low-level moist entropy (Schär et al. 1999).

Dynamic causes for heavy precipitation are often intertwined with thermodynamic effects. For instance, strong convective activity can occur in warm cores of baroclinic eddies (Korty and Schneider 2007). Changes in atmospheric circulations also imply changes in horizontal temperature gradients and moisture convergence (Held and Soden 2006). Weakening of convective activity can have both local causes as well as causes related to changes in water vapor mass flux and wind stress due to alterations in the large-scale flow. For example, a poleward expansion of the Hadley cell implies a strengthening of subsidence and associated drying in certain subtropical regions like the Mediterranean (Lu et al. 2007; Frierson et al. 2007; Lionello et al. 2008). Related may be also a shift in mid latitude storm tracks (Ulbrich et al. 2008; Bengtsson et al. 2009) and changes in modes of variability like the North Atlantic Oscillation (Gerber and Vallis 2009). Moreover, changes in the meridional temperature gradient due to polar amplification can affect the moisture dynamics of the atmosphere (Boutle et al. 2010). In Europe, for the formation of precipitation the influence of local evaporation versus moisture advection into a region is more dominant in summer when convective effects are more pronounced in relation to large-scale transports (Frei et al. 1998).

So far it is suggested from the discussion of RCM simulation results that causes for changes in heavy precipitation can be quite different regionally and seasonally (Lenderink and van Meijgaard 2008; Berg et al. 2009). In the present study an ensemble of high-resolution RCM simulations is used to estimate changes of heavy precipitation in a warming climate and to investigate causes for these changes. Limited area mod-

els have been shown to well reproduce the statistics of heavy precipitation on a daily timescale (Frei et al. 2003; Semmler and Jacob 2004; Frei et al. 2006; Hohenegger et al. 2008; Hanel and Buishand 2010).

Extreme value statistics represent an appropriate tool to analyze the occurrence rate of extreme weather events (Coles 2001; Embrechts et al. 1997) and have been applied in hydrology, meteorology, and climatology for many years (e.g. Buishand 1989; Katz 1999; Katz et al. 2002; Naveau et al. 2005; Friederichs et al. 2009; Friederichs 2010). Based on an extreme value analysis including time-dependent parameters seasonal characteristics of trends in heavy precipitation events over Europe are examined under climate change conditions. Also a discussion of changes in variables that govern precipitation formation is provided. The focus of this part of the study is the understanding of the interplay between trends in heavy precipitation and changes in thermodynamic aspects as simulated by high-resolution climate models.

The structure is as follows. Section 2 gives an overview over the climate model simulations that are analyzed. A description of the extreme value statistical techniques that are applied is provided in section 3. In section 4 the results of the statistical analysis of trends in heavy precipitation events over Europe are presented. Additionally, the trends in heavy precipitation are set in relation to changes in other variables that govern precipitation formation, with focus on the Clausius-Clapeyron relation. Finally, in section 5, a discussion of the results is given and conclusions summarize the findings.

2.2 Climate model simulations

The regional climate model simulations analyzed in this study were performed in the ENSEMBLES project, which was part of the Sixth Framework Programme (FP6) by the European Union. The domain covers the whole European area with a spatial resolution of about 25 km. The period 1961 to 2099 was simulated with anthropogenic forcing due to the emission of greenhouse gases and sulphate aerosols as defined by the Special Report on Emissions Scenarios SRES A1B emission scenario (Nakicenovic and Swart 2001).

The RCMs considered for the present work are RACMO (Lenderink et al. 2003) run by the Royal Netherlands Meteorological Institute (KNMI), RCA (Kjellström et al. 2005) run by the Swedish Meteorological and Hydrological Institute (SMHI) and the Community Climate Consortium for Ireland (C4I), HadRM3 (Collins et al. 2006) run by the Hadley Centre, CLM (Böhm et al. 2006) run by the Swiss Federal Institute of Technology Zurich (ETHZ), and REMO (Jacob 2001) run by the Max Planck Institute for Meteorology (MPI-M).

The RCMs are driven by data from different GCMs at their lateral boundaries. The RCM-GCM combinations are displayed in Table 2.1. In the case of the driving global model HadCM3, two versions are used: HadCM3Q0 is the standard model version

and HadCM3Q16 is a version with higher sensitivity to climatic variability which was obtained by changing some of the model parameters. A detailed description of the modifications can be found in Collins et al. (2006). Also shown in Table 2.1 are the convection parameterizations of the regional climate models. For reasons of clarity only a subset of simulations from the ENSEMBLES project is considered in the present work. The simulations are selected because they cover simulations from the same RCMs driven by different GCMs as well as simulations with the same GCMs driving different RCMs. Also, all well-established convection parameterization schemes are covered. Yet, this selection is not exhaustive and the results will to some extent depend on the chosen models, their parameterization schemes, and the dynamics of the driving global models. Nevertheless, the range of the chosen combinations is expected to show which climatic trends in heavy precipitation over Europe are robust with respect to the selection of the RCM and the driving GCM. In this context robustness is defined as the agreement of the majority of simulations on the sign of the trend in a specific region.

In the present work no validation of the regional climate models is performed since this is not the aim of this study. In the framework of the ENSEMBLES project, the regional climate model simulations analyzed in this study have been validated against observations with respect to temperature, precipitation, geopotential height and cloud fraction (Kjellström et al. 2010; Lenderink 2010; Lorenz and Jacob 2010; Sanchez-Gomez et al. 2009; Christensen et al. 2010). For an attempt to validate the regional climate model REMO over Germany with regard to trends in heavy precipitation events the reader is referred to Tomassini and Jacob (2009).

2.3 Extreme value analysis

The focus of this chapter is on trends in heavy daily precipitation totals. Naturally, the probability density of precipitation events decreases towards the upper tail of the distribution. Extreme value theory tackles the problem to estimate the distribution of rare events. In the present work the Poisson point process approach is used. The occurrence of exceedances over a high threshold u (i.e. heavy precipitation events in the context of the present paper) is modeled by a Poisson process. The parameters of the Poisson point process likelihood correspond to the parameters of the GEV distribution for block maxima. Thereby, the Poisson point process approach is connected to the traditional extreme value theory. This connection is described in more detail in Tomassini and Jacob (2009) (see also Embrechts et al. 1997; Coles 2001). One advantage of the Poisson point process is the independence of the scale parameter σ on the choice of the threshold u. Also covariates can be introduced immediately. As the aim is to analyze the climatic trends of heavy precipitation, time is introduced as covariate here; the statistical model is then a non-homogeneous Poisson point process.

Let X_i be a series of independent and identically distributed random variables. If

Table 2.1: Climate model simulations considered in the present work. Regional climate models: Regional Model (REMO), Climate version of Lokal-Modell (CLM), Hadley Centre Regional Model version 3 (HadRM3), Regional Atmospheric Climate Model (RACMO), and Rossby Centre Regional Atmospheric Climate Model (RCA). Driving global climate models: ECHAM5/Max Planck Institute Ocean Model (ECHAM5/MPI-OM), third climate configuration of the Met Office Unified Model (HadCM3), Institute Pierre Simon Laplace Climate Model (IPSL), and Bergen Climate Model (BCM).

RCM	Institution	convection scheme	# vertical levels	driving GCM
REMO	MPI-M	Tiedke-Nordeng	27	ECHAM5/MPI-OM
CLM	ETHZ	Tiedke	32	HadCM3Q0
HadRM3	Hadley Centre	Gregory-Rowntree	19	HadCM3Q0
RACMO2	KNMI	Jakob-Siebesma	40	ECHAM5/MPI-OM
RCA	SMHI	Kain-Fritsch	24	ECHAM5/MPI-OM
RCA	C4I	Kain-Fritsch	31	HadCM3Q16
REMO	MPI-M	Tiedke-Nordeng	27	IPSL
RCA	SMHI	Kain-Fritsch	24	BCM

the threshold u is sufficiently large, a sequence of point processes N_n with $N_n = \left\{(\frac{i}{n+1}, X_i) : i = 1, \ldots, n\right\}$ converges on regions $(0,1)\times[u,\infty)$ for any $z > u$ to a Poisson point process with intensity Λ on $A = [t_1, t_2] \times (z, \infty)$, where

$$\Lambda(A) = (t_2 - t_1)\left(1 + \xi\left(\frac{z-\mu}{\sigma}\right)\right)^{\frac{-1}{\xi}}. \tag{2.1}$$

Let T_j be the time of the j-th exceedance and $\tilde{X}_j > u$ the value of the jth exceedance of the threshold u, $j = 1, \ldots, n_u$ with n_u being the number of exceedances. Denote the whole time period by the interval $[0, T]$. It can be shown that the likelihood function of the Poisson process (for each grid box separately) is given by

$$L = \exp\left\{-\int_0^T \left[1 + \xi\left(\frac{u-\mu_t}{\sigma_t}\right)\right]_+^{\frac{-1}{\xi}} dt\right\} \prod_{j=1}^{n_u} \frac{1}{\sigma_{Tj}} \left[1 + \xi\left(\frac{\tilde{X}_j - \mu_{T_j}}{\sigma_{T_j}}\right)\right]_+^{\frac{-1}{\xi}-1} \tag{2.2}$$

where $a_+ = a$ if $a > 0$ and zero otherwise. Similarly to Smith (2003), the temporal dependence of the location parameter μ_t and the scale parameter σ_t is chosen as

$$\mu_t = \mu_0 + \beta_1 \cdot t, \qquad \sigma_t = \sigma_0 e^{\beta_2 \cdot t}, \tag{2.3}$$

where μ_0, σ_0, β_1, and β_2 are constants. The shape parameter ξ is assumed to be constant in time. It characterizes the tail of the heavy precipitation distribution. Positive values

of ξ imply a heavy tail which is associated with the Fréchet family. In contrast, negative values of ξ imply a bounded tail associated with the Weibull family and values very close to zero indicate an exponential tail behavior.

For the present work the threshold u is defined to be the 95% quantile of the time series of daily precipitation totals for each grid point and for each simulation of the ensemble separately. Considering the findings by Smith (1999) the choice of this threshold is reasonable since this analysis focuses on the investigation of climatic trends of heavy 24-hour precipitation events and not on return periods of very extreme events at the far end of the distribution tails. A validation of this threshold choice applying W statistics has been carried out by Tomassini and Jacob (2009). The 95% quantile is constant in time and is estimated empirically for the whole time period from 1961 to 2099, including days without precipitation. All grid boxes for which the 95% quantile is smaller than 0.5 mm of precipitation are excluded from the analysis.

The Poisson point process model assumes the threshold exceedances to be independent. Therefore declustering is applied to the data in advance. In this analysis heavy precipitation events are assumed to be dependent (belonging to the same precipitation front) when they are separated by at most one day. This is reasonable for precipitation because strong events occur mostly in highly dynamic meteorological situations, passing a location quickly, or as convective events, which are rather short-lived with timescales of no more than a day. Accordingly, declustering is applied as follows. Two threshold exceedances are considered to belong to the same cluster if no more than one day lies in between them, except if at this day in between no precipitation has occurred. Each one of these clusters is then treated as one heavy precipitation event and the maximum of the exceedances within each cluster is considered as the corresponding precipitation amount (Davison and Smith 1990). Inspection of the data has shown that the declustered time series do not feature temporal autocorrelation any longer, which justifies this method.

Maximum likelihood parameter estimation is carried out for μ_0, σ_0, β_1, β_2 and ξ by minimizing the negative log-likelihood. The integral in (2.2) is approximated numerically. For more details the reader is referred to Tomassini and Jacob (2009).

From the estimated parameters of the inhomogeneous Poisson point process, high quantiles of the distribution of the data can be calculated in the following way:

$$q_t = u + \frac{\tilde{\sigma}_t}{\xi}((\zeta_u m)^{\xi} - 1), \tag{2.4}$$

with $\tilde{\sigma_t} = \sigma_t + \xi(u - \mu_t)$, m pointing to the m-observational return value (equivalent to the $(100 - m^{-1})$% quantile), and ζ_u being the probability that the threshold is exceeded.

For this analysis, the statistical computing language *R* (R Development Core Team 2010) is used, with the packages *POT* (Ribatet 2011) and *ismev* (Coles and Stephenson 2011) in particular.

2.4 Results

2.4.1 Trends in heavy precipitation over Europe

The statistical analysis is carried out separately for the summer (JJA) and winter (DJF) season. In the following the focus will be mainly on trends in the 99.9% quantile of total daily precipitation for winter and summer over the time period 1961 to 2099. The 99.9% quantile corresponds to a value of $m = 1000$, i.e., an event which occurs once in 1000 observations, including days without precipitation. In the present study this is once in about 11 seasons.

Winter

Figure 2.1 shows the relative linear trend of the 99.9% quantile of daily winter precipitation for the eight-member ensemble of RCM simulations. With high consistency the RCMs project a generally positive trend (indicated by green and blue color scaling) in northern Europe which is strongest over northern Scandinavia. Nevertheless, along the Atlantic coast of Norway, where the average precipitation is known to be high, heavy precipitation is projected to decrease or remain constant, depending on the driving GCM. In southern Europe, particularly on the Iberian Peninsula and around the Mediterranean Sea, the RCMs suggest no change in heavy precipitation or even a decrease. In general, the increase of heavy precipitation is found to be stronger over the continents than over the oceans, consistent with the pattern of temperature changes.

Figure 2.2 shows the number of models which agree on an increase in the 99.9% quantile of daily winter precipitation. The large-scale pattern of heavy precipitation changes is found to be broadly consistent across the models. Inconsistencies occur mainly over the Alpine ridge, the Pyrenees, and along the western coast of Norway. Furthermore, the simulations do not match well with regard to the sign of the change in a rather narrow transition zone between small positive and small negative trends, located over the Mediterranean region.

Figure 2.1 indicates that the regional climate models are strongly determined by the large-scale forcing provided by the driving global climate models. In comparison to the HadCM3 forced RCMs, the three ECHAM5/MPI-OM driven RCMs all similarly show a less strong increase in heavy precipitation over northern Scandinavia and more pronounced decreasing trends along the western coast of Norway and in the Mediterranean region. In the simulation of the Community Climate Consortium for Ireland (C4I), the regional climate model RCA is driven by a high-sensitivity version of HadCM3 (HadCM3Q16). The zonal band of large positive trends indicated by blue colors over the central continent becomes more pronounced and covers parts of the Atlantic as well. It also shows quite a pronounced decrease of heavy precipitation over the Alpine ridge and the Pyrenees, and an increase south of the Alps. The ECHAM5/MPI-OM driven

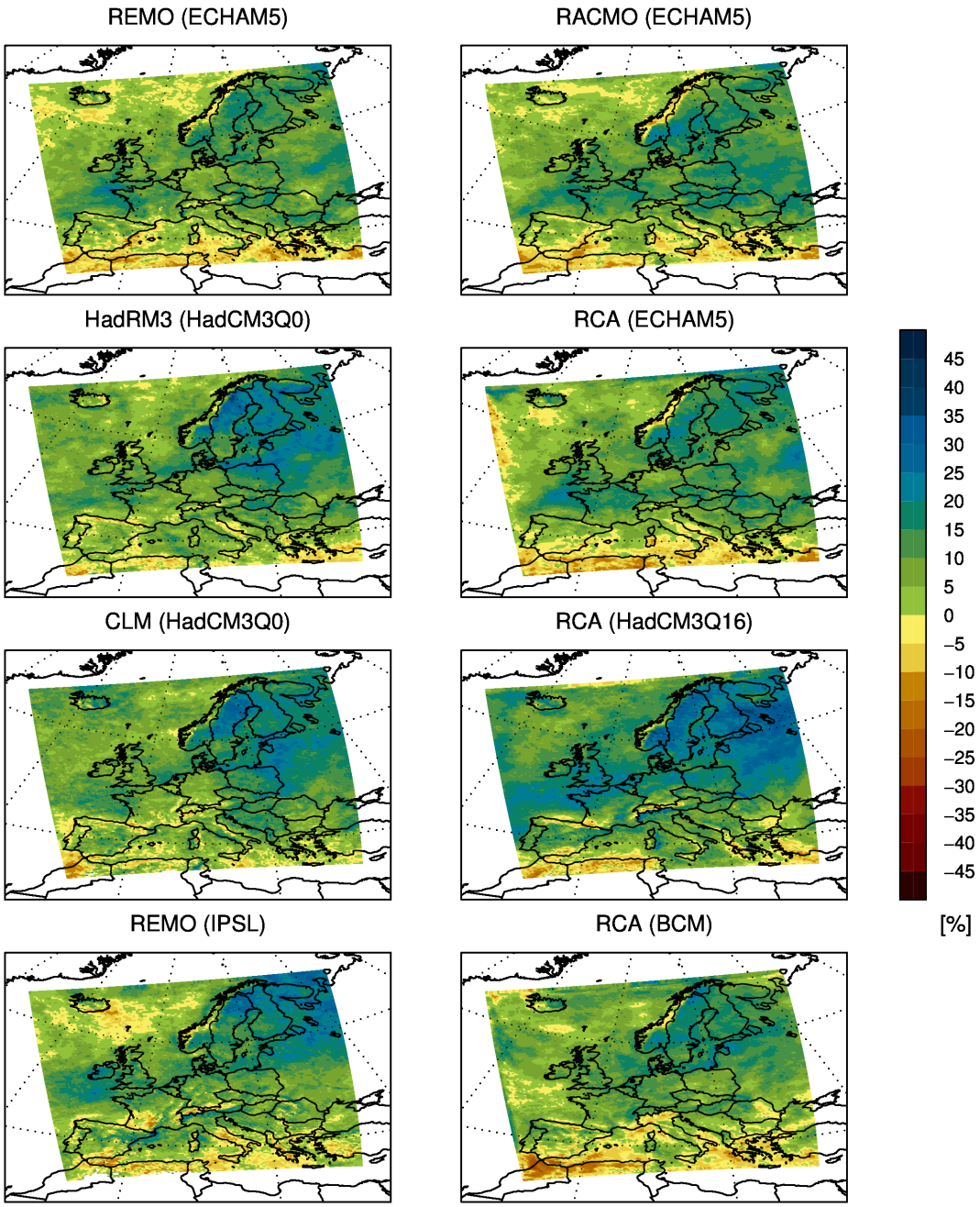

Figure 2.1: Relative trends of the 99.9% quantile of daily winter precipitation.

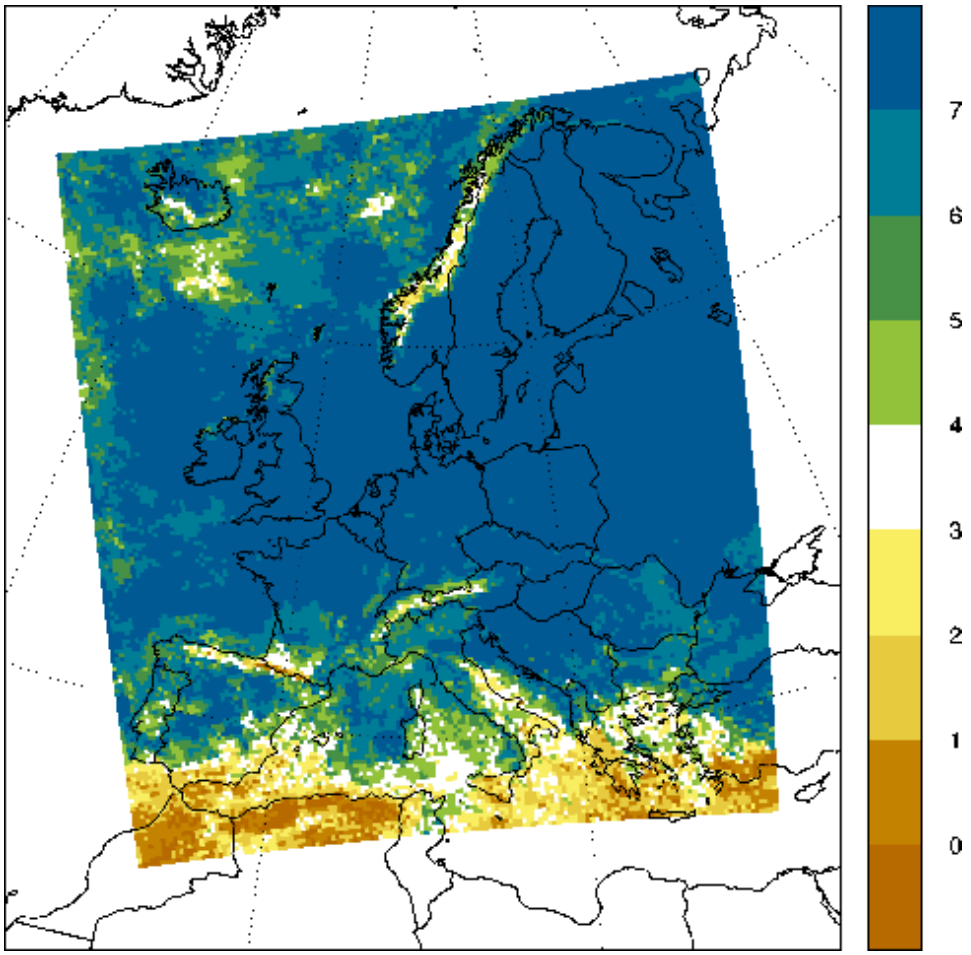

Figure 2.2: Number of models that agree on a positive relative trend of the 99.9% quantile of daily winter precipitation. A number of 8 indicates that all simulations agree on a positive trend, a number of 0 indicates that all simulations agree on a negative trend.

simulations do not show clear trends in Central Europe including the mountainous areas.

The pattern of change in the 99.9% quantile corresponds to the trend pattern in the location parameter μ (Figure 2.3), which is essentially commensurate to the mean of the heavy precipitation distribution. The trend of μ gives indications about a shift in the distribution of precipitation events. Strong increases stretch from northwest to northeast of the continent, while in the southern Mediterranean pronounced decreases can be observed. Generally, the areas where the location parameters show negative trends exhibit a somewhat larger extent than for the 99.9% quantiles. This indicates that in southern regions an increase in variance plays a decisive role for the sign of trends in the quantiles. The behavior of the scale parameter σ tends to confirm this interpretation (Figure 2.4).

The scale parameter σ is essentially analogous to the variance of the heavy precipitation distribution and indicates changes in the day to day variability of the intensity of precipitation events. Trends in σ are not very distinct in any of the climate model simulations. The strong north to south gradient in trends as prevalent for the location parameter μ and for the quantiles is not present for σ. Also in the very southern part of Europe, where μ is projected to decrease markedly, the scale parameter remains essentially constant. The regional climate model simulation that is driven by the high-sensitivity version of HadCM3 shows a clearer positive trend in σ in most areas including the Mediterranean. When seen as part of the changes in the 99.9% quantile, the trends in σ seem to damp the strong trends in μ partly, especially where the changes in μ are negative. Small changes in σ can obviously play a large role for changes of the 99.9% quantile.

Figure 2.5 shows the values of the shape parameter ξ to be mostly close to zero, which indicates an exponential tail behavior. The largest positive values occur over the Mediterranean coast lines, largest negative values over Scandinavia, except over the Atlantic coast of Norway. The different simulations are surprisingly consistent in this respect. Over the Alps, however, the estimates show some ambiguity among the various models. The values of ξ in climate model simulations are to some extent dependent on the resolution. Increased resolution tends to lead to higher values in ξ (Tomassini and Jacob 2009).

Summer

Figure 2.6 shows the relative trend of the 99.9% quantile of daily summer precipitation for all the regional climate model simulations. As mentioned in Section 2.3, grid boxes for which the 95% quantile of daily precipitation is smaller than 0.5 mm are excluded from the analysis. They appear as white areas in the figures.

The simulations show a slight positive trend in heavy precipitation over northern

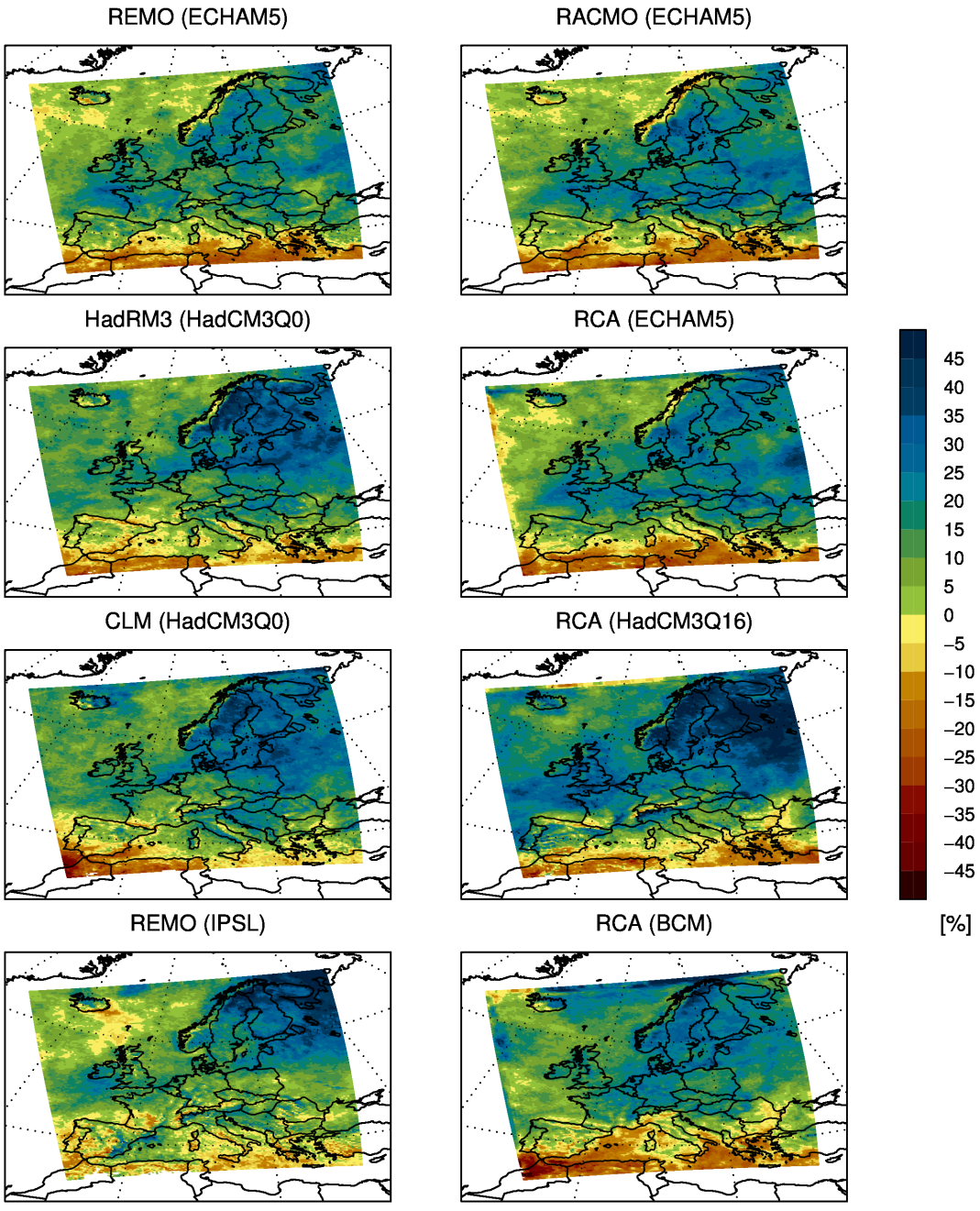

Figure 2.3: Relative trends of the location parameter μ for winter.

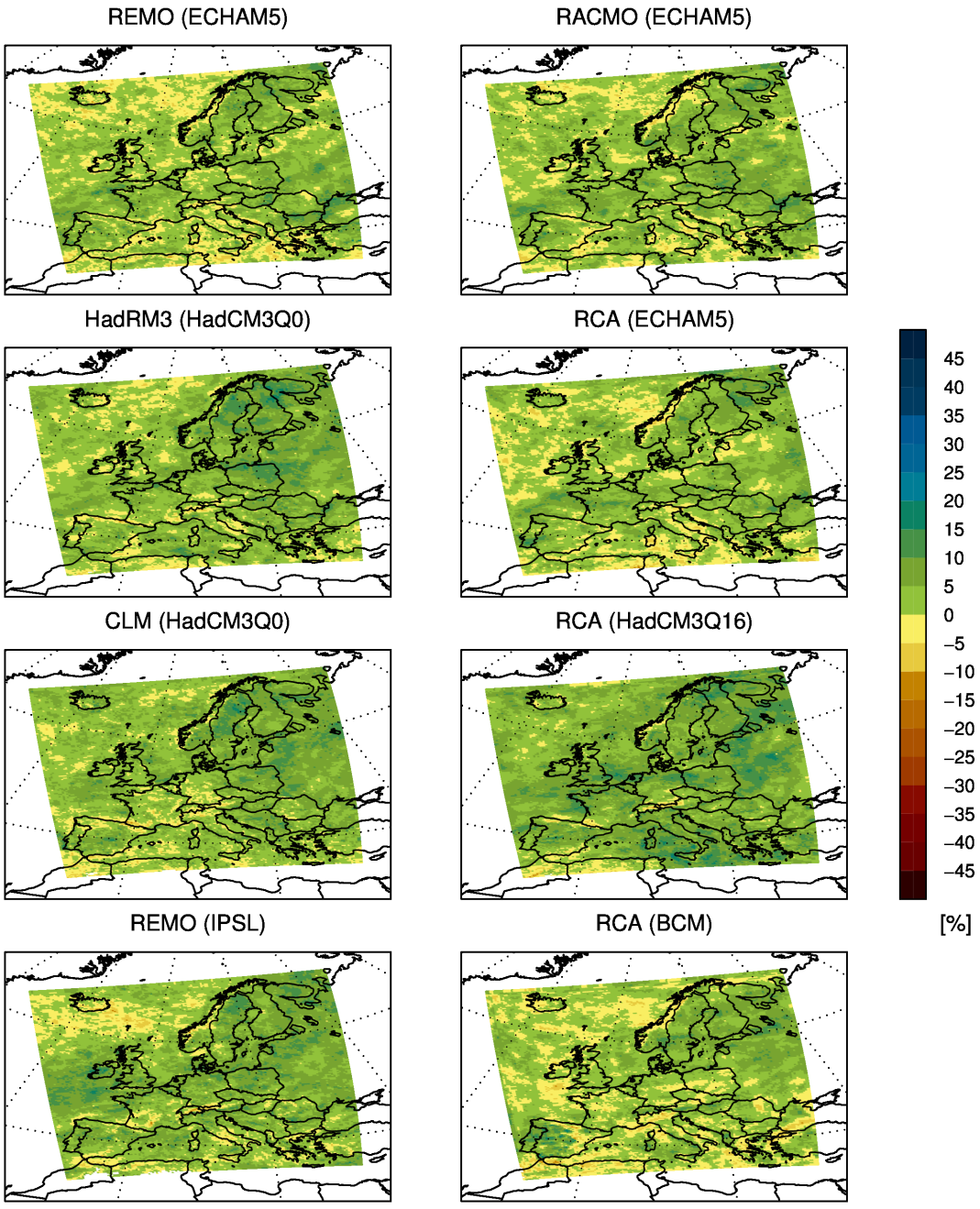

Figure 2.4: Relative trends of the scale parameter σ for winter.

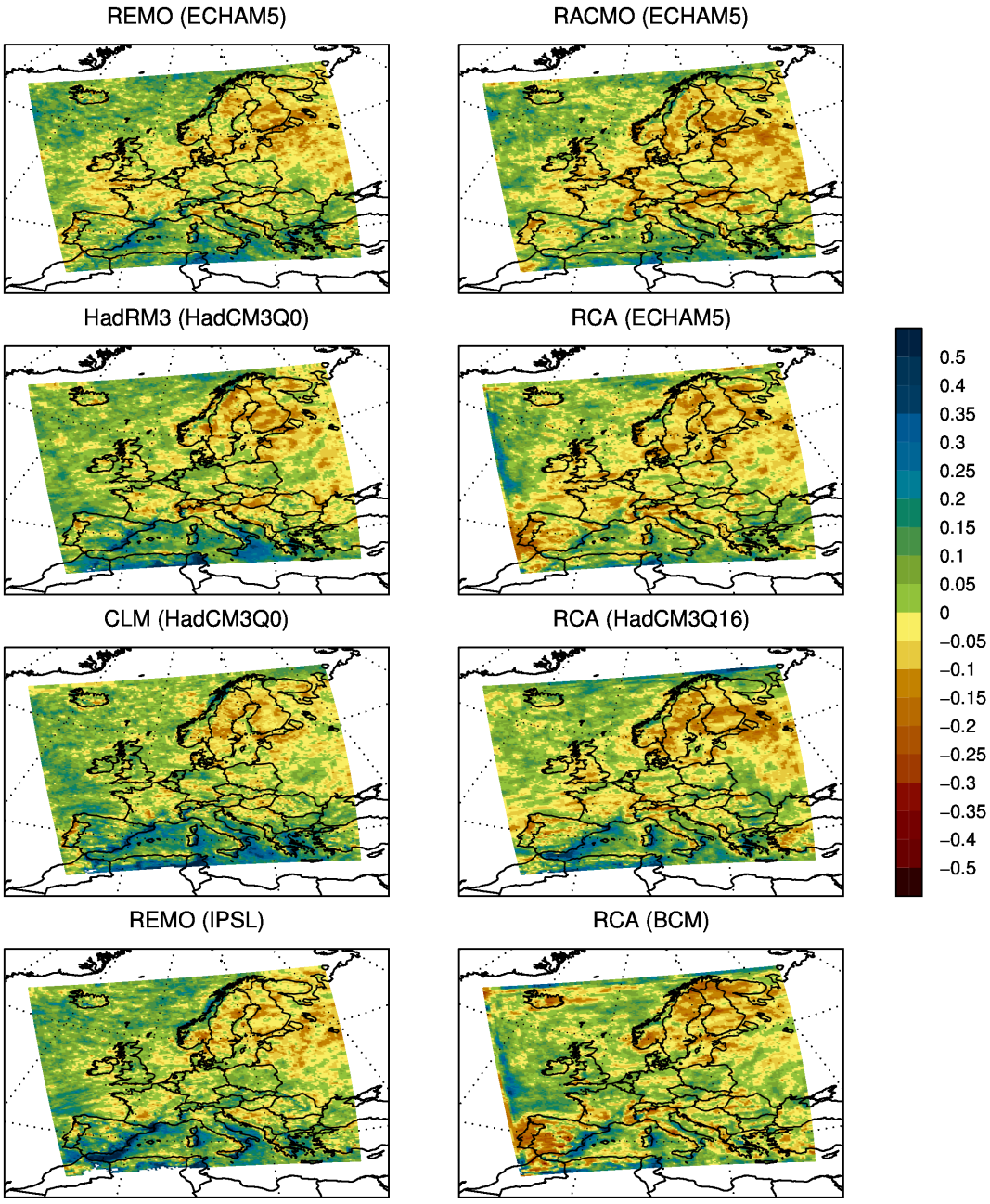

Figure 2.5: Estimated shape parameter ξ for winter.

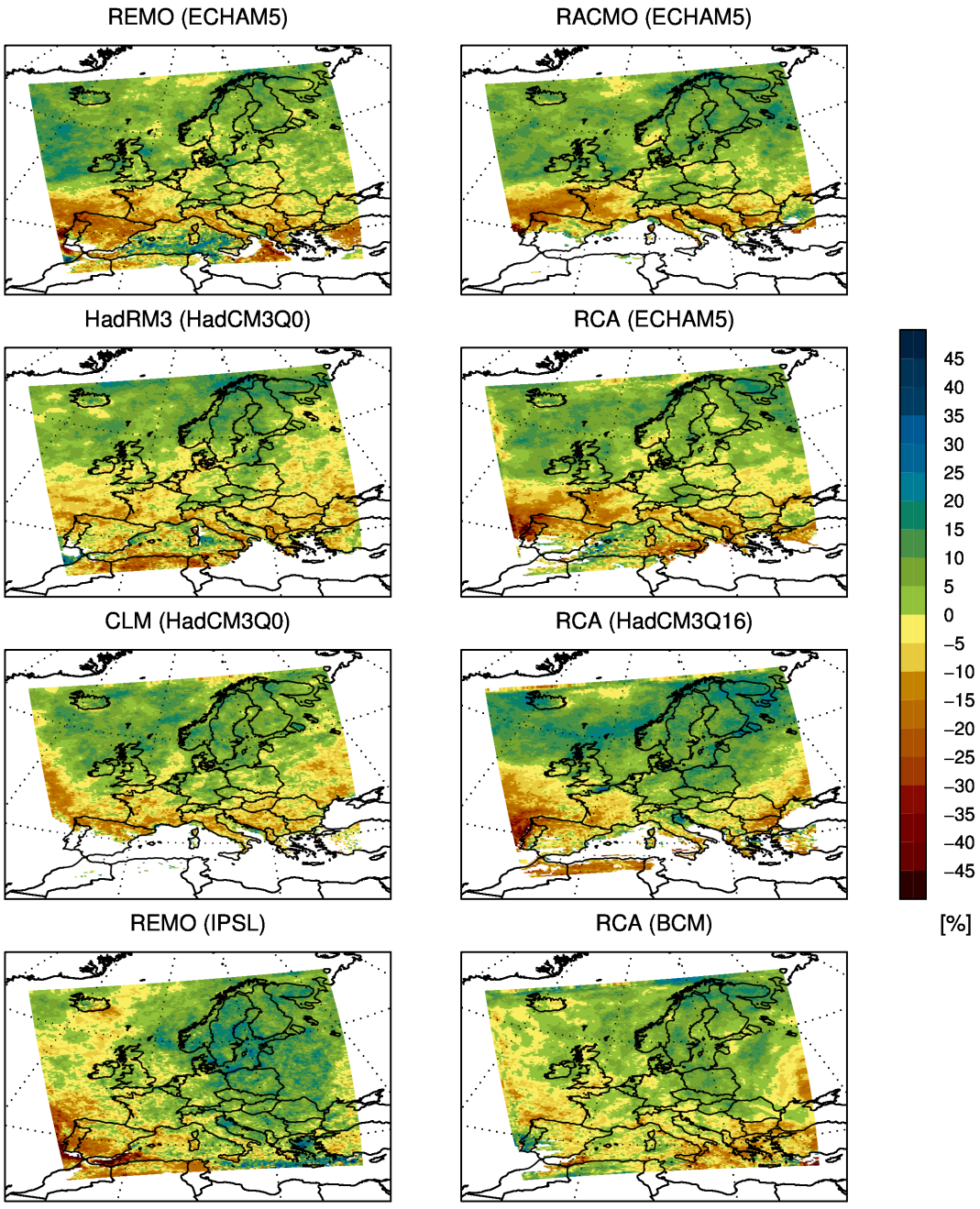

Figure 2.6: Relative trends of the 99.9% quantile of daily summer precipitation.

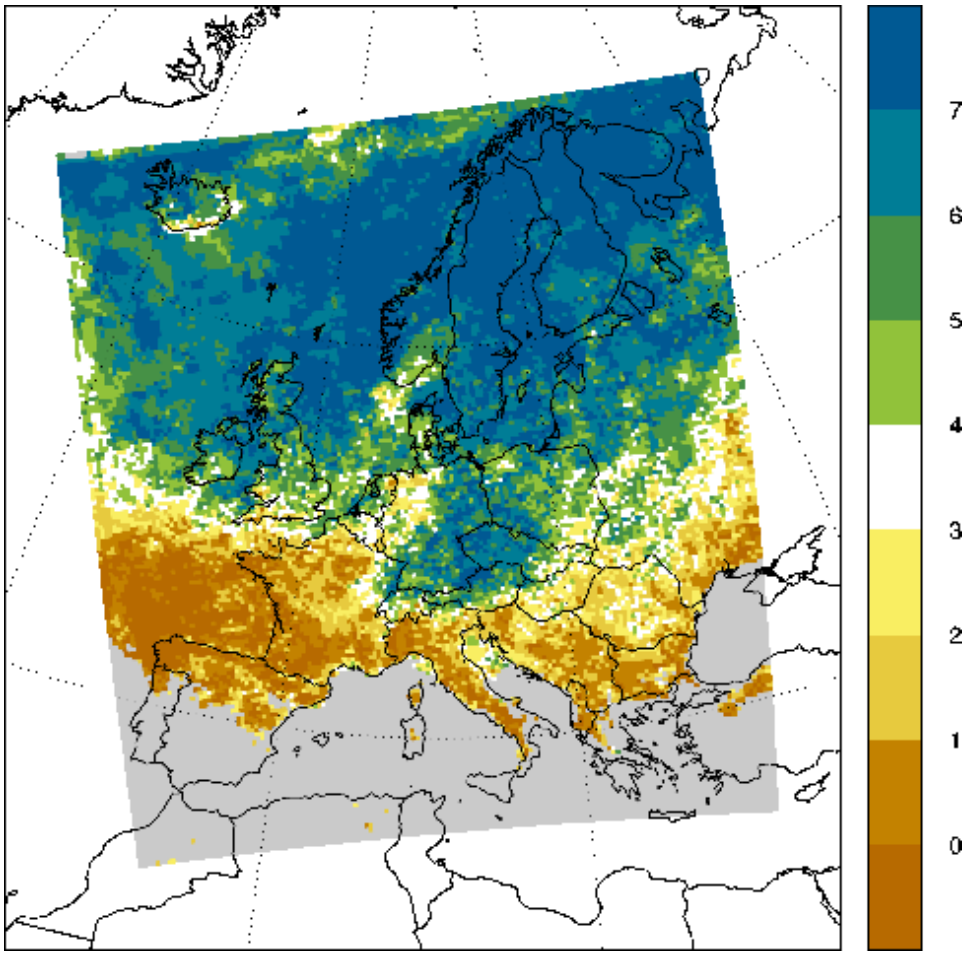

Figure 2.7: Number of models that agree on a positive relative trend of the 99.9% quantile of daily summer precipitation. A number of 8 indicates that all simulations agree on a positive trend, a number of 0 indicates that all simulations agree on a negative trend. Gray areas denote grid boxes for which the 95% quantile of daily precipitation is smaller than 0.5 *mm* in at least one simulation. These grid boxes are excluded from the analysis.

Europe whereas negative values occur in the south. In the transition zone between positive and negative trends and over the Mediterranean Sea, the agreement between the simulations is low (Figure 2.7). In the regions with stronger positive and negative changes the simulations show high consistency. The magnitude of the changes differs especially for the decrease in heavy precipitation over southern Europe (Figure 2.6). Whereas in the ECHAM5/MPI-OM driven simulations and in the RCA simulation driven by HadCM3Q16 a relatively clear border is prevalent between negative and positive trends at the latitude of the British Channel in the west and at the latitude of the Alps further east, the pattern is less distinct in the other simulations. All models project positive trends in some regions in the Mediterranean and Alpine area, but they are not consistent in location.

Similar to the situation in winter, the trends in the location parameter μ show patterns which resemble the trends in the 99.9% quantiles (Figure 2.8), but substantially amplified in relative terms. In Scandinavia a strong increase is projected, while in the Mediterranean region, France, and eastern Europe the location parameter shifts to smaller values. The RCM simulations are consistent with respect to the geographical pattern. Trends in the scale parameter σ exhibit a somewhat clearer north to south gradient than in winter, with negative sign in many regions in the south. Yet, the changes are not large in relative terms (Figure 2.9). In comparison to winter, the trends in the scale parameter σ in summer show a pattern which is more similar to the pattern of changes in the 99.9% quantiles. This indicates that changes in the variability of heavy precipitation events play a larger role in summer.

The values of the shape parameter ξ (not shown) are essentially positive in summer and larger than in winter. Positive values of ξ imply heavy tails, which means that even the far tail of the distribution holds some mass. Higher values of ξ thus indicate an increasing impact of changes in σ on changes in the 99.9% quantiles. The highest values of around 0.5 are obtained over the Mediterranean Sea. Over continental Europe the values of ξ range in general between 0 and 0.35. In the northern parts of the domain, including Scandinavia, ξ takes values close to zero, and no systematic differences can be found between land and sea areas.

2.4.2 Heavy precipitation and the Clausius-Clapeyron relation

The Clausius-Clapeyron scaling of precipitable water is examined by dividing its relative linear trend by the linear trend of $2m$-temperature at each model grid point. Cloud liquid water and heavy precipitation trends are treated likewise. This gives a first idea on how closely the processes of cloud and precipitation formation follow the Clausius-Clapeyron scaling on regional scales. For this section, four simulations of the ensemble are selected for reasons of brevity. Nevertheless, the chosen simulations represent a large range within the ensemble, since different RCMs, different driving GCMs, and different

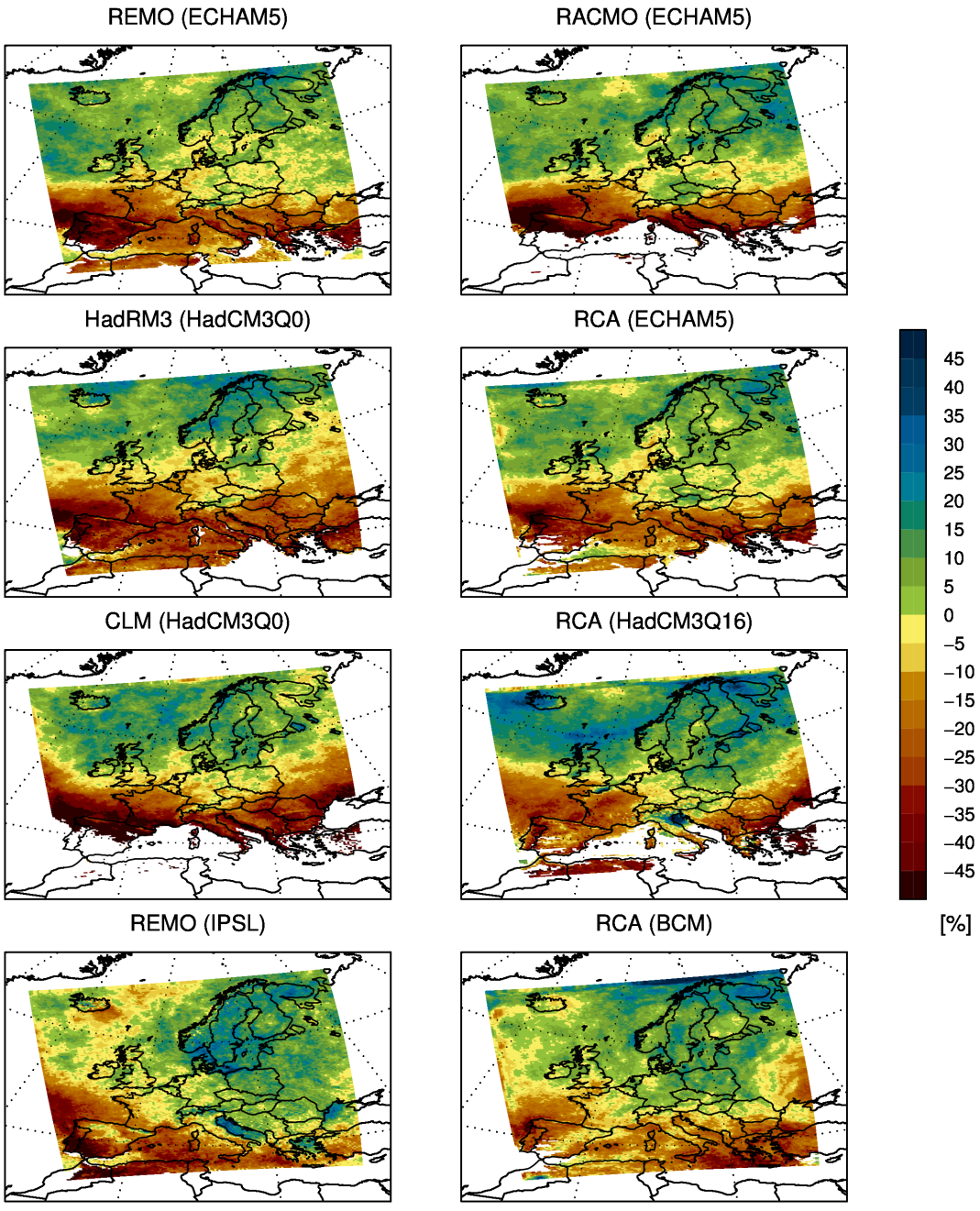

Figure 2.8: Relative trends of the location parameter μ for summer.

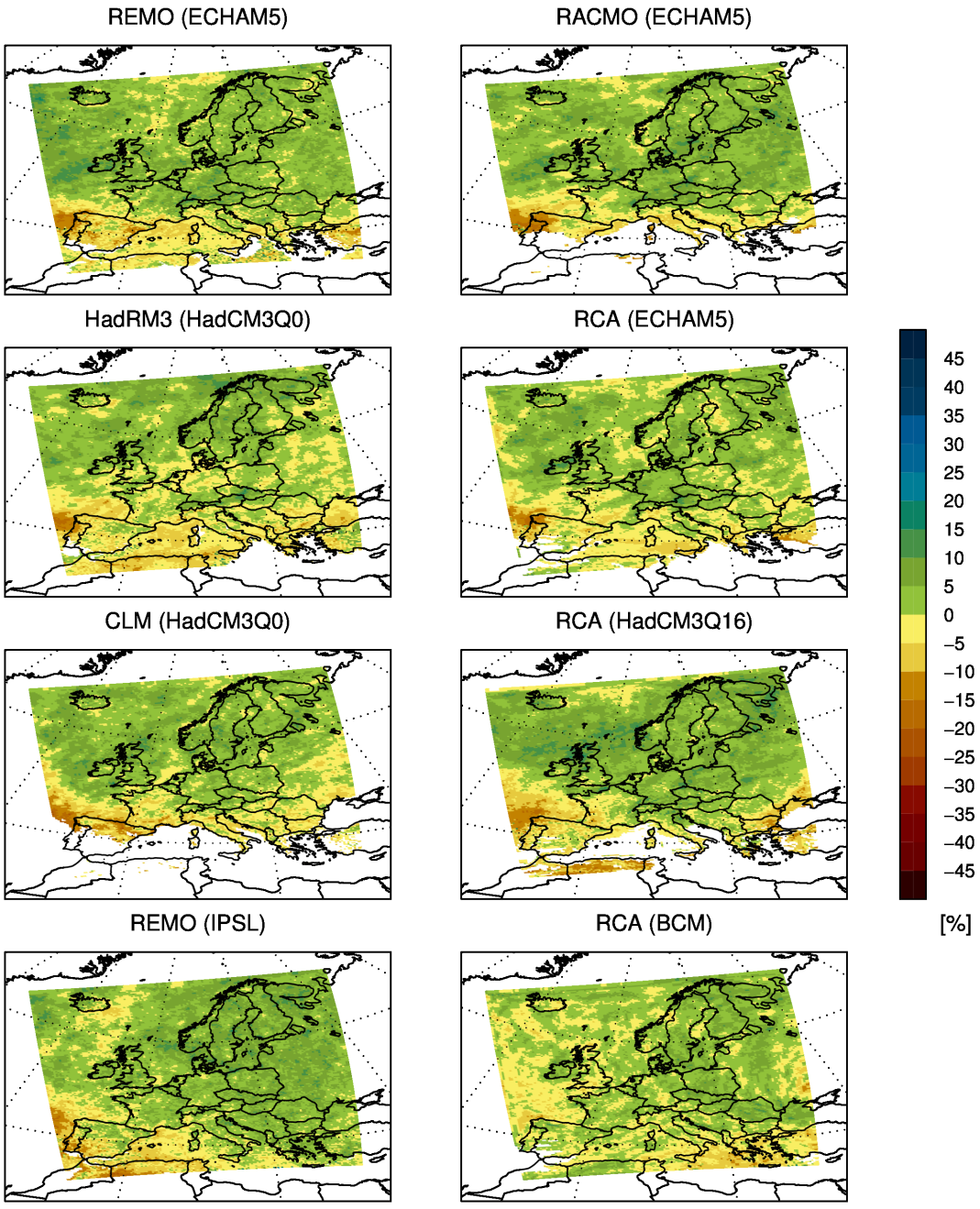

Figure 2.9: Relative trends of the scale parameter σ for summer.

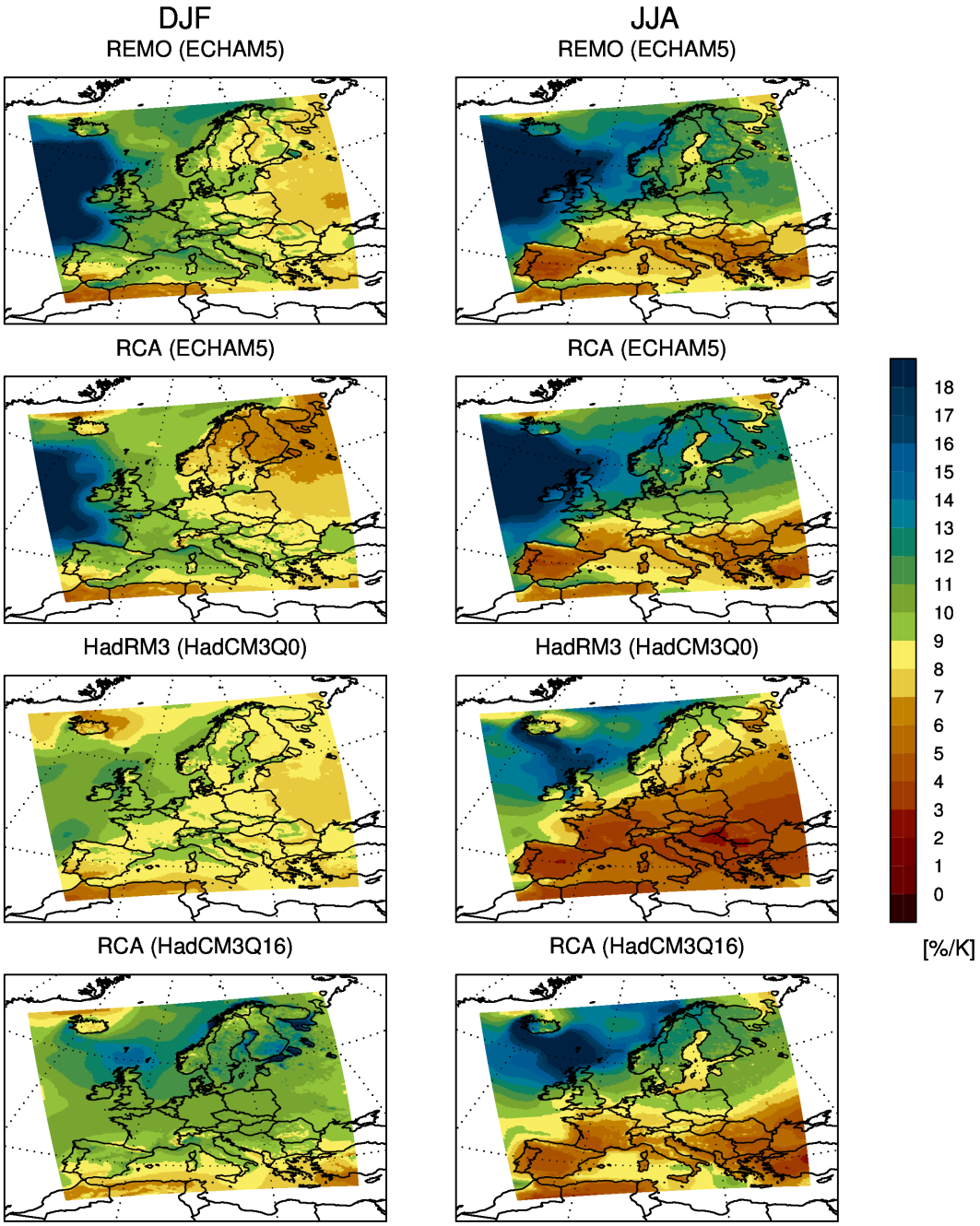

Figure 2.10: Relative trends of the precipitable water in % per K temperature change for winter (left) and summer (right).

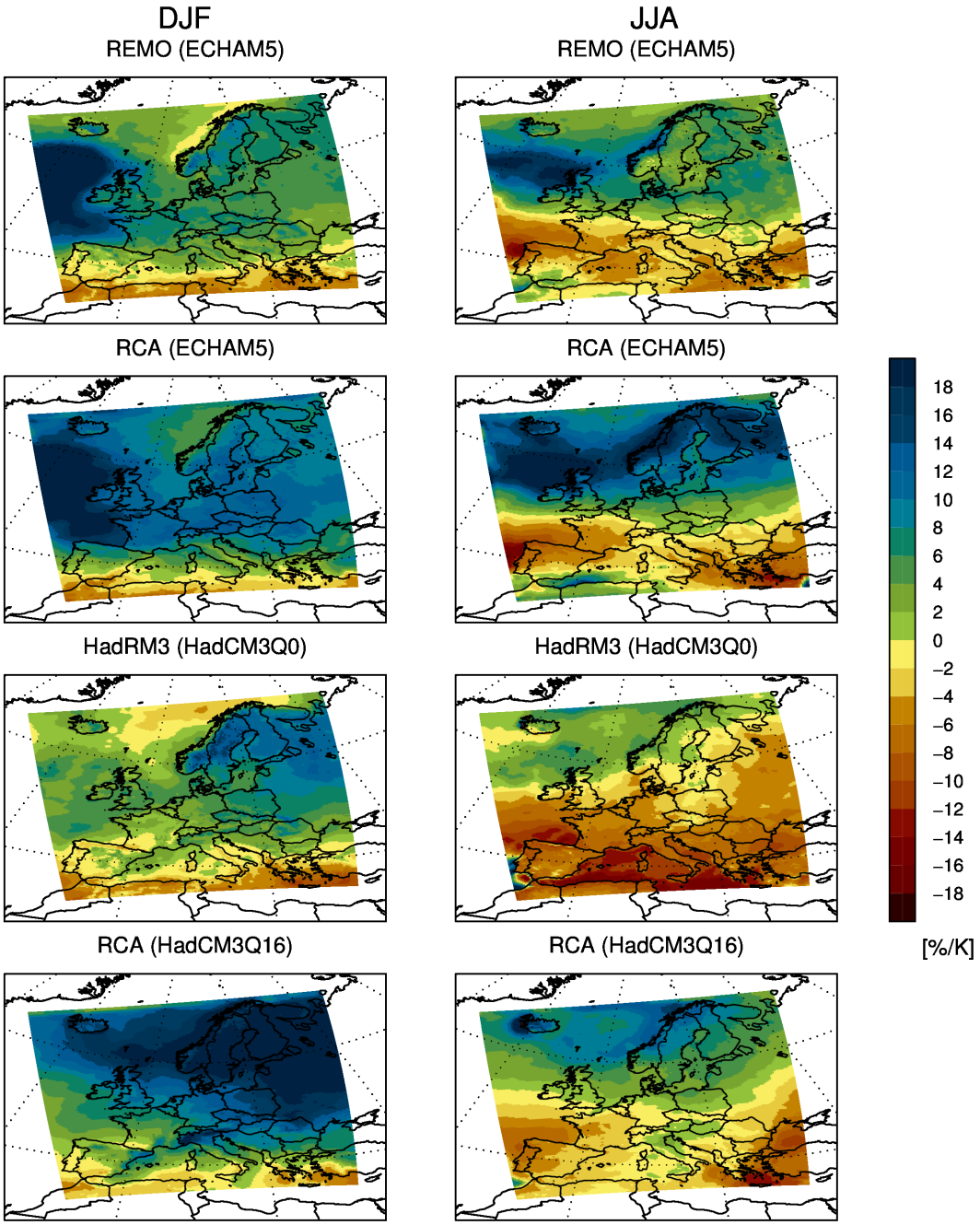

Figure 2.11: Relative trends of the cloud liquid water in % per K temperature change for winter (left) and summer (right).

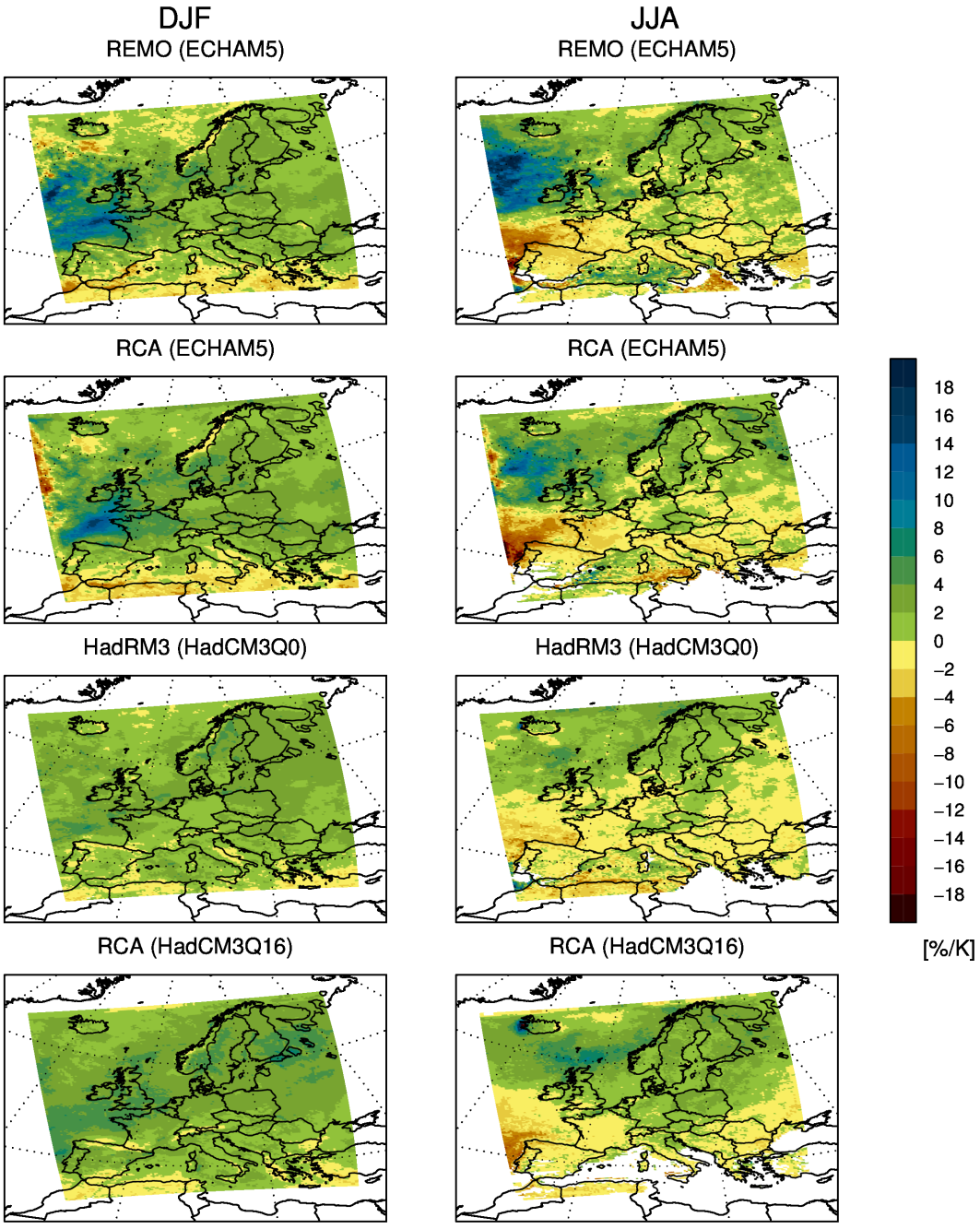

Figure 2.12: Relative trends of the 99.9% quantile of daily precipitation in % per K temperature change for winter (left) and summer (right).

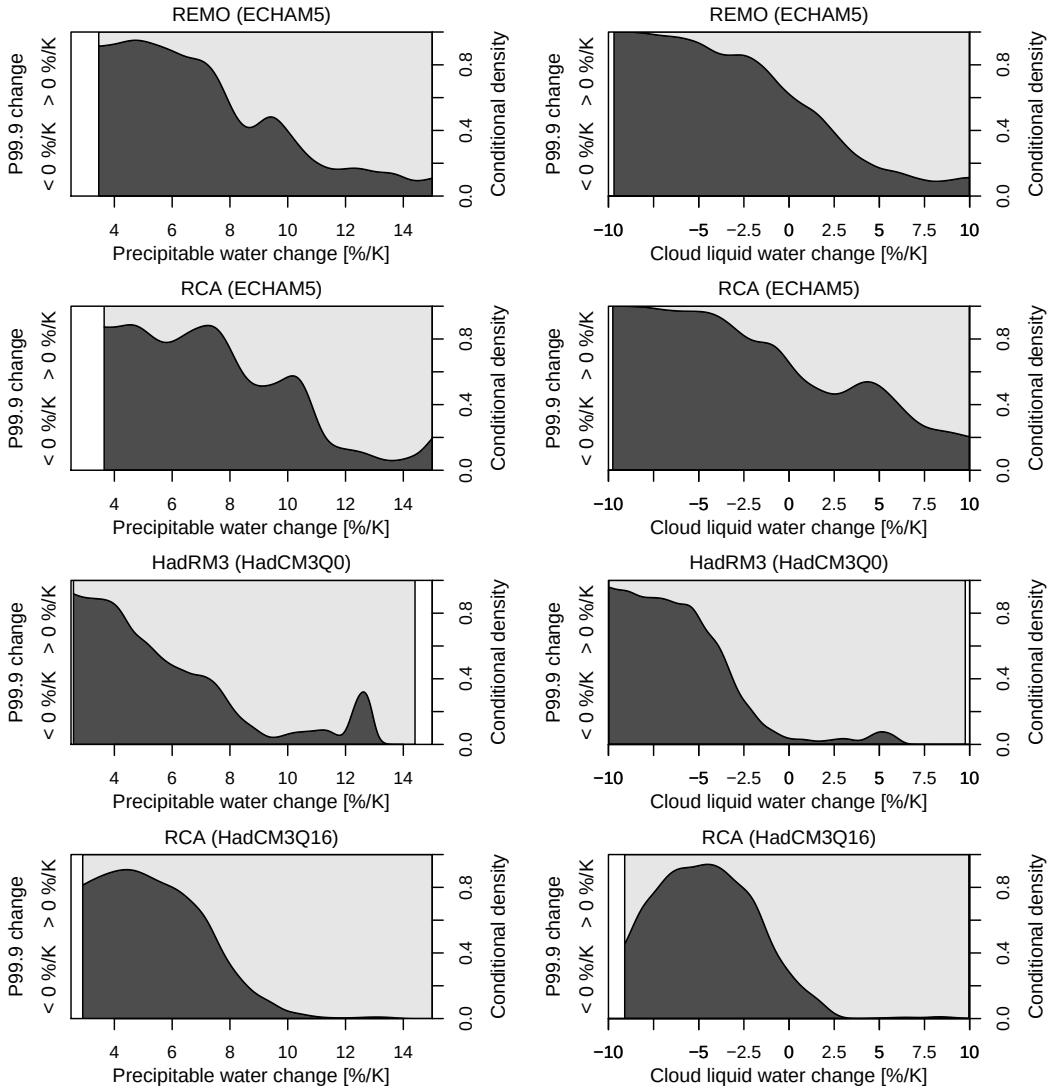

Figure 2.13: Conditional density of precipitable water (left) and cloud liquid water (right) on positive values (gray) and negative values (black) of changes in the 99.9% quantile of precipitation (P99.9) per K warming for summer. Only land points are considered.

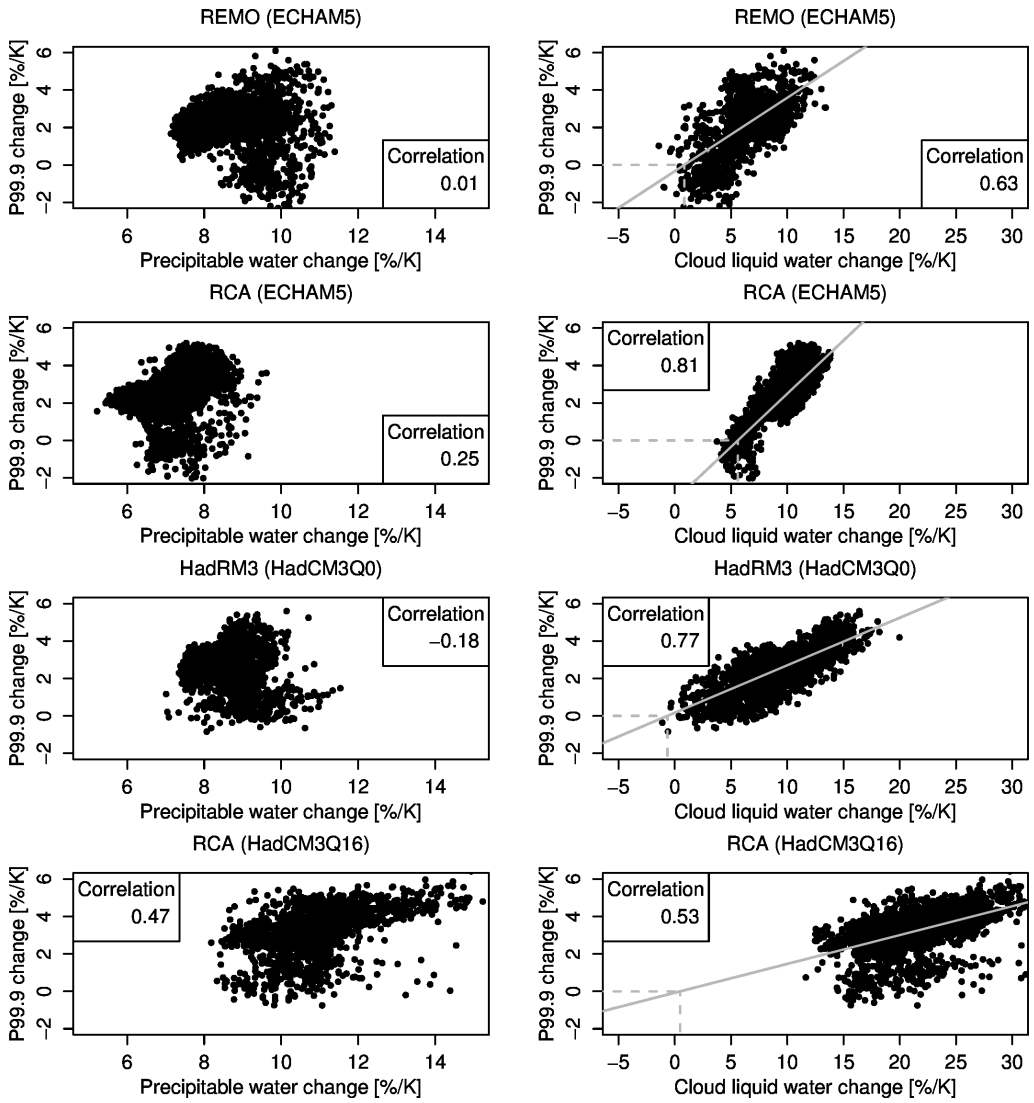

Figure 2.14: Scatter plots of the pointwise changes of heavy precipitation versus precipitable water (left) and cloud liquid water (right) over Scandinavia in winter. The regression is shown as solid gray line, the dashed lines show the intercept of the regression line with the x-axis at the point of zero changes in heavy precipitation.

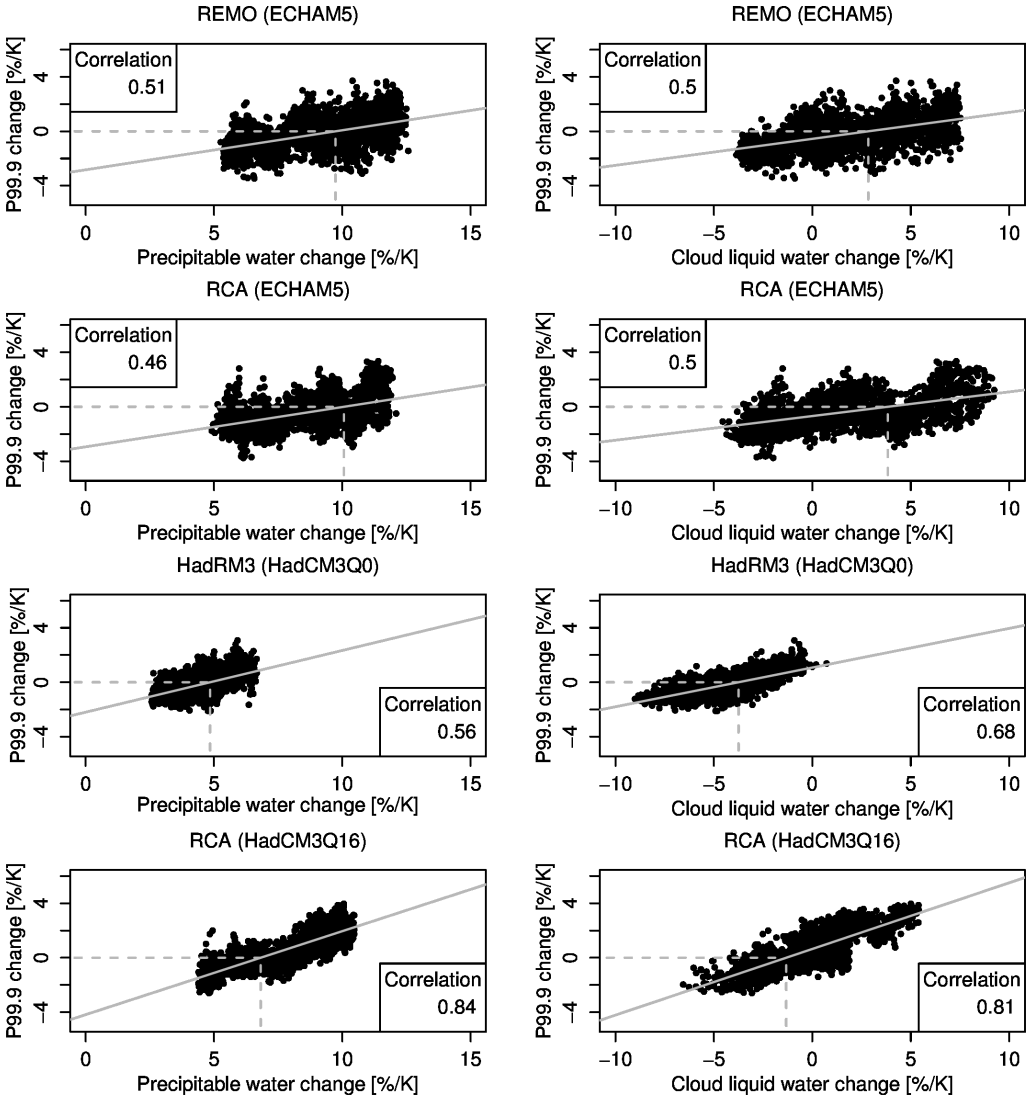

Figure 2.15: As Figure 2.14, but for East Europe in summer.

convective parameterization schemes are covered (see Table 2.1). The results show that the driving global climate models play an important role for heavy precipitation trends in the RCM simulations. In order to analyze the influence of the large-scale forcing for the Clausius-Clapeyron scaling, two RCM simulations driven by ECHAM5/MPI-OM and two driven by HadCM3 are selected. Linear trends of all variables are estimated for the time period 1961 to 2099.

On a regional scale the analyzed RCM simulations suggest some variation in the trends of precipitable water per kelvin temperature increase over Europe (Figure 2.10, note that all colors in this figure denote positive values). In all simulations, the changes are positive over the entire domain and strongest over the Atlantic Ocean, where they take values up to 18 $\%/K$. Over land in winter, the changes range from 8 to 12 $\%/K$ in the west and from 6 to 8 $\%/K$ in the east. However, the spatial variability is to a large extent due to regional differences in the amplitude of the temperature increase. In absolute terms, the trend in precipitable water in winter is showing a rather uniform increase over the whole domain in all simulations. In summer, the increase in precipitable water per kelvin is distinctly smaller in southern Europe, with values between 0 and 6 $\%/K$, compared to northern parts of the continent. This is reflected by the relative humidity markedly decreasing by up to -4 $\%/K$ in these regions (see Figure A.1 in Appendix A). The strong contrast between land and ocean in the precipitable water trends in summer over southern Europe indicates that atmospheric water vapor is limited by the local availability of water.

The relation between the trends of cloud liquid water and temperature depends to a considerable extent on the driving GCM (Figure 2.11). In winter, the ECHAM5/MPI-OM driven RCMs show weak positive (green to blue color scaling) and negative (yellow to red color scaling) changes around the Mediterranean, and give values from 4 to 10 $\%/K$ over the land masses further north. Over the Atlantic Ocean, an increase of up to 18 $\%/K$ is suggested. This is again related to the small absolute temperature increase of only about 1 K in this area over the whole time period. The RCA simulation driven by the high-sensitivity global model HadCM3Q16 shows values of more than 18 $\%/K$ over a large band ranging from Iceland southeastwards over northern and central Europe to the Black Sea. The trends in cloud liquid water in winter correspond closely to the changes in heavy precipitation (Figure 2.12), although there is an offset between the two variables. While heavy precipitation changes by around 5 $\%/K$ over land, the trends in cloud liquid water are considerably stronger.

In summer cloud liquid water increases with temperature in northern Europe and decreases in southern Europe, again in qualitative agreement with the changes in heavy precipitation (Figure 2.12). This feature is robust across all four simulations. Nevertheless, the magnitude of the trends differ between the RCMs. The HadRM3 simulation exhibits negative trends over the complete European land mass except Scandinavia whereas the other simulations show a relatively clear line between positive trends in

the north and negative trends in the south. Areas of positive and negative trends match well for cloud liquid water and heavy precipitation, only the amplitude of the pattern is more pronounced in the case of cloud liquid water.

To better quantify the relationships between the trends in precipitable water, cloud liquid water, and heavy precipitation with temperature, we investigate whether a threshold exists for precipitable water and cloud liquid water changes below which heavy precipitation decreases in the regional climate model simulations. Figure 2.13 shows conditional density diagrams for the summer season. Only land points are considered. The graphics show the probabilities of heavy precipitation trends to be positive or negative, given a certain value of precipitable water or cloud liquid water. The black areas denote the conditional densities for negative trends, the gray areas for positive trends.

For changes in precipitable water a threshold below which at least 80 % of the changes in heavy precipitation are negative is found to be 5–7 $\%/K$, depending on the simulation. All four simulations show a gradual decrease for the probability of negative heavy precipitation trends to occur with increasing magnitudes of changes in precipitable water per kelvin temperature increase.

Negative changes in heavy precipitation are found to concur with negative changes in cloud liquid water. One can find a value of -5 to -2.5 $\%/K$ for cloud liquid water change as threshold below which 80 % of the changes in heavy precipitation are negative. As for precipitable water changes, the driving global model has some influence on the shape of the conditional distribution. In the HadCM3 driven simulations the density decreases more rapidly towards zero, whereas it changes more gradually for the ECHAM5/MPI-OM driven simulations.

We exemplify the scaling behavior of trends in heavy precipitation with changes in precipitable water and cloud liquid water in more detail for two selected regions: Scandinavia (5–30°E, 55–70°N), possessing a rather wet and oceanic climate, and East Europe (16–30°E, 44–55°N), being characterized by dryer continental conditions. The regions are selected based on the definitions by Christensen and Christensen (2007) and again only land points are taken into account. Scatter plots of the changes of the 99.9% quantiles versus changes in precipitable water and cloud liquid water are shown in Figure 2.14 for Scandinavia in winter, and in Figure 2.15 for East Europe in summer. All trends are scaled by the respective change in near-surface temperature.

For the winter months in Scandinavia (left column of Figure 2.14), the changes in heavy precipitation show hardly any dependence on the changes in precipitable water, except for the RCA simulation driven by the high-sensitivity global model HadCM3Q16. In the other simulations the change of precipitable water is rather uniform with a mean value of 7–8.8 $\%/K$. Distinctly stronger correlations from 0.53 to 0.81 are found between the changes in heavy precipitation and cloud liquid water (right column of Figure 2.14). The dashed lines point to the offsets between the changes of cloud liquid

water and heavy precipitation. They essentially scatter around zero, indicating that in winter the qualitative behavior of trends in heavy precipitation is closely connected to changes in cloud liquid water.

In the summer months in East Europe (Figure 2.15), correlations of changes in heavy precipitation with changes in precipitable water and cloud liquid water are similar and range between 0.46 in the RCA simulation driven by ECHAM5 and 0.84 in the RCA simulation driven by HadCM3Q16. This suggests that the regional water budget governs both precipitable water and cloud liquid water. An increase of about 7 $\%/K$ in precipitable water is needed to maintain the level of heavy precipitation (dashed lines in the left column). The decrease in relative humidity caused by moisture availability limitations affects all variables. Cloud liquid water scales quite closely with heavy precipitation, although the slope of the regression line in the right column of Figure 2.15 proves to be clearly smaller than 1: changes of 5 $\%/K$ in cloud liquid water correspond to trends of 1–2 $\%/K$ in heavy precipitation. A qualitatively similar behavior can be observed in other regions in southern Europe as well.

2.5 Discussion and Conclusions

An extreme value analysis of projected changes in heavy precipitation in an ensemble of eight high-resolution regional climate model simulations over the European domain is presented. In general, the different models agree well on the qualitative nature of the trends. The results show robust trends for heavy precipitation over many parts of Europe in a warming climate. In winter the changes are positive over most of the European continent, with changes of up to 30 % in high quantiles over northern Europe. A north-south gradient in the trends can be observed, and in the most southern parts of Europe they are close to zero or even negative. In summer, despite strong increases in near-surface temperatures, negative trends in heavy precipitation occur over a large area which extends from central to southern Europe. These negative trends can reach up to -30 % in regions like Spain, southern France, southern Italy, or Greece. In northern Europe, changes in heavy precipitation are positive also in summer.

The changes in the extreme value distributions mainly originate from shifts in the location parameter. For some parts of southern Europe in summer, negative trends in the location parameter contrast with positive changes in the scale parameter, suggesting a general decrease in heavy precipitation in conjunction with increased variability. However, these areas are not widespread, and negative trends in the location parameter generally are accompanied by negative trends in the scale parameter.

In other studies for Europe similar results for changes in heavy precipitation were found with different RCM-GCM combinations (e.g. Durman et al. 2001; Frei et al. 2006). Due to the parameterization of processes at scales below the resolution of the RCMs, such as convection, radiation, land surface processes, and cloud microphysics,

RCMs have limitations, which can lead to model uncertainties. The convective parameterization scheme can particularly be an issue for summer precipitation and on sub-daily timescales (Lenderink and van Meijgaard 2008). Also, in summer the simulation of soil moisture can highly affect changes in temperature and precipitation via the alteration of changes in evapotranspiration (Seneviratne et al. 2010). In this chapter the RCM results for heavy precipitation changes are found to be to some extent influenced by the large-scale patterns of their driving GCMs. Despite the limitations, the robustness of the results found in this analysis from an ensemble of various RCMs with different driving GCMs and different parameterization schemes gives confidence in the pattern of heavy precipitation changes.

The relative changes in the 99.9% quantile of daily precipitation totals, precipitable water, and cloud liquid water are divided by the temperature changes to test the Clausius-Clapeyron scaling (see 2.1) for these variables.

In winter the change in precipitable water is rather uniform in absolute terms. The scaled pattern reflects mostly the differences in temperature trends over the domain. Over the European continent changes are close to the Clausius-Clapeyron relation, i.e. 7 $\%/K$. Although qualitatively the situation is not very different for cloud liquid water, the spatial pattern of changes of cloud liquid water better correlates with changes in heavy precipitation per kelvin temperature increase. The scaling factor is about 2 to 4, i.e. a change of 1 $\%/K$ in heavy precipitation corresponds to a change of 2–4 $\%/K$ in cloud liquid water.

This suggests that overall in winter the large-scale dynamics plays a decisive role. Patterns of trends in moisture related variables reflect changes in storm track densities and storm intensities (Bengtsson et al. 2006). Thereby changes in precipitable water do not relate to changes in cloud condensate and precipitation in an immediate and straightforward way. Alterations in dynamical processes which lead to the formation of clouds and rainfall are not governed by the amount of precipitable water alone. Other aspects like changes in meridional temperature gradients or static stability contribute to the mechanism.

The most robust sub-Clausius-Clapeyron behavior in precipitable water is found over the southern European land masses in summer. This is associated with decreases in relative humidity of about -4 $\%/K$ in these regions. The distinct differences between changes over land and ocean indicate that here moisture is limited by the local availability of water which can evaporate from the soil or vegetation (Seneviratne et al. 2010). Humidity changes in the atmospheric boundary layer can affect cloud and precipitation formation (Hohenegger et al. 2009). Accordingly, cloud liquid water decreases over southern Europe in summer. Both cloud liquid water and precipitable water show a qualitatively similar scaling behavior with regard to heavy precipitation. Ultimately, the changes in the local hydrological cycle and the moist static stability in the region are also an expression of alterations in the large-scale circulation and indicate a pole-

ward extension of the Hadley cell associated with a poleward shift of the subtropical dry zones, for example to the Mediterranean area (Lu et al. 2007; Frierson et al. 2007; Mariotti et al. 2008).

In many regions of Europe the results of this chapter question the dominant role of precipitable water as a governing factor for changes in heavy precipitation. It is shown that the trends in heavy precipitation are smaller than predicted by the Clausius-Clapeyron relation. Moreover, in the mid-latitudes, processes of cloud and precipitation formation also depend on dynamic aspects such as moisture convergence and baroclinic storm activity. Also, changes in moist static stability may play a role. A more complete picture of the physical mechanisms determining changes in heavy precipitation over Europe can only be gained by also considering these dynamic aspects.

Summary of Chapter 3

In this chapter, projected future changes of heavy daily precipitation totals are examined in detail for the European domain through application of a non-stationary extreme value analysis. The link of changes in heavy precipitation with precipitable water and cloud liquid water is assessed and the connections with changing temperatures are examined with respect to the Clausius-Clapeyron relation on regional scales. The results highlight the importance of changes in cloud liquid water and relative humidity for changes in heavy precipitation and reveal only a limited scaling with changes in precipitable water. In southern Europe in summer, the assumption of constant relative humidity with increasing temperatures is not fulfilled and a limited local availability of water may cause deviations from the Clausius-Clapeyron scaling of changes in precipitable water and thus cloud liquid water and heavy precipitation. In the higher latitudes, limitations may be caused by changes in the dynamics, which alter the moisture flux divergence.

3 Modeled and observed heavy summer precipitation and thermodynamic relations

Chapter 2 has indicated that in particular in summer and in the warm southern regions of Europe, the changes in precipitable water per unit temperature increase might be less than predicted by the Clausius-Clapeyron relation, probably due to a limited local availability of water vapor, associated with decreasing trends in relative humidity. Also, for parts of Europe, heavy precipitation changes show a better scaling with cloud liquid water than with precipitable water, indicating that condensation and cloud formation play an essential role for changes in heavy precipitation. In Chapter 2 these relationships have been found for an ensemble of regional climate change projections. For a better understanding of the processes in the models, the dependencies of thermodynamic quantities on temperature in the summer season are examined in Chapter 3 in present day regional climate model simulations driven by reanalysis data for different European sub-regions. Furthermore, the relationships between heavy precipitation and vertically integrated water vapor and cloud water are investigated. To assess whether the modeled connections agree with reality, the results are compared to observational data from satellites and meteorological stations. In addition, the representation of heavy precipitation events in the regional climate model is validated against the observations for different regions in Europe. In conjunction with Chapter 2, Chapter 3 contributes to answering the second research question posed in Chapter 1.1.

3.1 Introduction

Heavy precipitation events are expected to change their frequency and intensity in a warmer climate due to alterations in dynamic and thermodynamic processes. Because of the often regional to local scale nature of heavy precipitation events, RCMs are adequate to investigate their climatology and future changes. To understand projected future changes in heavy precipitation it is however indispensable to understand the physical processes behind.

As explained in Chapter 2.1, the thermodynamic process is expected to intensify in a warmer climate (Allen and Ingram 2002) due to an increase in the atmospheric water

holding capacity following the Clausius-Clapeyron relation. The hypothesis that heavy precipitation intensity would consequently increase at the same rate as predicted by the Clausius-Clapeyron equation has been examined in Chapter 2. On regional scales large deviations from this simple scaling were found. Besides, related studies have shown recently that the rate of heavy precipitation increase per degree of warming is lower in climate model simulations (O'Gorman and Schneider 2009a,b; Trenberth 2011).

In agreement with Berg et al. (2009), it has been shown in Chapter 2 that projected heavy precipitation trends over Europe scale better with trends in cloud water than with trends in the total column water vapor, in particular in summer. The dependency of heavy daily precipitation on daily mean temperatures in RCM simulations over Europe has been evaluated by Berg et al. (2009), who found generally good agreement between observations and models.

This study aims to investigate heavy precipitation statistics and their connection with total column water vapor and cloud water for the summer season (June – August, JJA) in high-resolution RCM simulations and observational data sets. A non-homogeneous extreme value analysis is used to analyze heavy daily summer precipitation from the RCM REMO and meteorological station data. In a second part the relationships of total column water vapor and cloud water with temperature are investigated in the model and in satellite observations. A similar analysis is carried out for the convectively available potential energy (CAPE). Deviances in the behavior of total column water vapor from the Clausius-Clapeyron relation are discussed. In the last part the extreme value model is extended by total column water vapor and cloud water as covariates. The focus of this study is on four European sub-regions which are characterized by different climate characteristics.

3.2 Data and methodology

3.2.1 The REMO simulation setup

The regional climate model REMO is a three-dimensional atmospheric circulation model, which dynamically simulates the physically relevant processes (Jacob and Podzun 1997; Jacob 2001; Jacob et al. 2001, 2007). In this study REMO is used at a horizontal resolution of $0.088\,^\circ \times 0.088\,^\circ$, which is approximately $10\,km \times 10\,km$. The model is hydrostatic and has a vertical resolution of 27 levels. REMO as a Limited Area Model needs lateral boundary forcing data like temperature, wind, surface pressure and moisture and as surface boundary conditions sea surface temperature and sea ice extent. The boundary data are provided by the ERA-Interim reanalyses, which have a spatial resolution of $0.75\,^\circ \times 0.75\,^\circ$. In a single nesting approach REMO is directly driven by the ERA-Interim data. The simulations are carried out for the time period 1989 to 2008 with model domains covering three different European sub-regions: Northern Europe,

Eastern Europe, and Italy/the Alps (Figure 3.1a)). For the analyses, the REMO output data is cut to the same time periods which are covered by the respective observational data sets.

Due to different geographic features, solar irradiation, and atmospheric dynamics, the analyzed relationships of heavy precipitation and related variables may vary substantially across different parts of Europe. Smaller sub-regions with different climatic characteristics are selected from the RCM simulation domains. The investigated areas are Southwest Norway, the Alps, South Italy, and East Romania/Moldova. The sub-regions are chosen such that they are expected to exhibit nearly homogeneous distributions of daily precipitation totals and similar daily mean temperatures within the region. The sub-domains are shown as hatched areas in Figure 3.1a.

3.2.2 Observational datasets and methods

The observational precipitation data is composed of meteorological station measurements from different datasets. For the Norwegian domain it stems from the climate database of the Norwegian Meteorological Institute for Norway, publicly available on the eKlima webserver; for the other areas, station data is extracted from the National Climatic Data Center (NCDC) observational data base and from the European Climate Assessment (ECA) dataset (Klein Tank and Coauthors 2002). The data set consists of measurement data from automatic stations as well as from synoptic stations and simple rain gauges for the time period 1989–2008 or parts of it.

Daily statistics of the total column water vapor have been obtained from the combined SSM/I–MERIS L3 product which was developed in the framework of the ESA DUE GlobVapour project. It consists of retrievals from the SSM/I and MERIS instruments over ocean and land, respectively. In this study the data are used only over the land masses at a spatial resolution of $0.05^\circ \times 0.05^\circ$ for the time period 2003–2008. For further details and description of the MERIS instrument retrievals, the reader is referred to Lindstrot et al. (2012).

The observed cloud water path retrievals used in this study have been produced by The EUMETSAT Satellite Application Facility on Climate Monitoring (CM-SAF) (Schulz et al. 2009) from measurements of the polar-orbiting imagers NOAA and METOP-AVHRR. The data has a resolution of $15\,km \times 15\,km$ and covers the time period 2004–2008. Both the liquid and the ice phases are included in the retrievals. In the following, the cloud water path, consisting of both phases, is referred to as cloud water.

To analyze the connection of total column water vapor and cloud water to the temperature variability, the $2m$-temperatures at grid point basis are divided into bins of 2 kelvin within each region. Only time steps with at least one precipitation event in the region exceeding the 95% quantile are taken into account. For each temperature

bin, the conditional areal averages of daily mean column water vapor and cloud water are calculated from REMO and from the satellite data. For the analysis of the satellite data, the reference temperatures are obtained from the gridded E-OBS observational data set, which was developed based on station measurements in the framework of the EU FP6 project ENSEMBLES (Haylock et al. 2008; Klok and Klein Tank 2009).

Cumulus convection plays a major role for the formation of heavy summer precipitation. The convectively available potential energy (CAPE) is an indicator for the potential of cumulus convection. In this study, mixed-layer CAPE is calculated from the ERA-Interim reanalyses and REMO output. In the used pseudo-adiabatic formulation of CAPE the water vapor is assumed to be converted into droplets and falls out as rain. The ascent then follows a so called pseudo-adiabat. For an description of the calulation method used here, the reader is referred to Riemann-Campe et al. (2009). CAPE is analyzed in the way described above for column water vapor and cloud water.

3.2.3 Extreme value analysis of daily precipitation

The statistics of heavy daily precipitation totals from observed and modeled data are investigated using an extreme value model with and without included covariates. In the second case, total column water vapor and cloud water are introduced as explanatory variables to examine their relationship with heavy precipitation occurrence.

To make the gridded precipitation data from the RCM comparable with the precipitation observations, the output corresponding to one meteorological station is chosen to be the average of the four closest grid boxes around the station location. The investigated time period covers the years 1989–2008 or a fraction depending on the availability of the observational data. To enlarge the amount of data available the total 24h precipitation amounts from all stations within each region are pooled together. This method is justified by the similarity of the precipitation statistics within each region, which was a criterion for the definition of their spatial extent.

In the present study, exceedances of daily precipitation events over a large threshold are modeled by a non-homogeneous Poisson point process (PPP). The parameters of the PPP are the location parameter μ, the scale parameter σ, and the shape parameter ξ, equivalent to the parameters of the corresponding generalized extreme value distribution (GEV).

The covariate-dependency is introduced into the PPP model by including the regional averages of column-integrated water vapor and cloud water as large-scale explanatory variables for heavy precipitation. Additionally, the station height and corresponding height of the regional model orography are included in the statistical model to account for altitude differences which possibly have an impact on heavy precipitation statistics.

The dependency of the parameters μ and σ on the covariates h (station height) and

q (total column water vapor or cloud water) is described as follows:

$$\mu(q,h) = \mu_0 + \beta_1 \cdot q + \beta_2 \cdot h, \qquad \sigma(q,h) = \sigma_0 \cdot e^{\beta_3 \cdot q + \beta_4 \cdot h}, \tag{3.1}$$

where μ_0, σ_0, β_1, β_2, β_3, and β_4 are constants. The shape parameter ξ is kept invariant with respect to the covariates. The parameters of the PPP are estimated using the maximum likelihood approach with the likelihood function of the Poisson process. For details on the PPP the reader is referred to Coles (2001); Katz et al. (2002).

For the Poisson point process model, independence of the threshold exceedances is assumed. Yet, heavy precipitation events can naturally occur in clusters of several days if for example large synoptic systems or series of systems are passing. The clustering of exceedances in the datasets was checked, but found to be negligible with no significant influence on the estimated parameters. Therefore, no declustering was applied in advance.

After the estimation, the parameters can be re-parameterized into quantiles in the following way:

$$Q(q,h) = u + \frac{\tilde{\sigma}(q,h)}{\xi}((\zeta_u m)^{\xi} - 1), \tag{3.2}$$

with $\tilde{\sigma}(q,h) = \sigma(q,h) + \xi(u - \mu(q,h))$, m pointing to the $(100 - m^{-1})\%$ quantile, and ζ_u being the probability that the threshold is exceeded. The model is evaluated at different values for the covariates h and q (see Eq. 3.1). In the present study a constant value of 100 meters is inserted for the altitude variable h. In this way, only the effect of the total column water vapor and cloud water on large precipitation quantiles is investigated as desired.

3.3 Results

3.3.1 Heavy precipitation statistics

At first, the PPP model is fitted without the explanatory moisture variables to investigate the distribution of heavy daily precipitation totals from model output and observational data. Only the station altitude is included as covariate to account for orographically caused differences in rainfall. Figure 3.1 shows the estimated parameters μ, σ, and ξ as well as the 99% quantile in the summer months (JJA) for REMO against station measurements in each sub-region (Figure 3.1a). The error bars show the corresponding standard errors; different colors mark the different sub-regions.

The location parameter μ (Figure 3.1b), which can essentially be understood as the center of mass of the heavy precipitation distribution, ranges from 17 mm in the summer dry region South Italy over moderate values in Romania and Moldova up to 43 mm in Southwest Norway and in the Alps. In the Alps, however, the day-to-day variability

of extremes, indicated by the scale parameter σ (Figure 3.1c), is much larger than in Southwest Norway, which is a consequence of the local nature of strong precipitation events in mountainous regions. This is also reflected in the shape parameter ξ (Figure 3.1d), showing heavy tail behavior for the Alpine region, which means that there is mass on the tail of the distribution and a few events exist which are very large compared to the bulk of the distribution.

Model and observations are in good agreement concerning the location and the scale of the heavy precipitation distribution in all sub-domains, but the model overestimates the strength of the tail in South Italy and Romania/Moldova, which can be seen by the shape parameters deviating from the identity line in positive direction (Figure 3.1d). This means that in these convectively dominated regions the observations exhibit a broader range of moderate and heavy precipitation events, whereas the model simulates a few heavy precipitation events which are outstandingly heavy compared to the rest of the distribution. However, this does not imply that the model overestimates heavy precipitation events in general, since the 99% quantiles (Figure 3.1e) are rather slightly underestimated by the model in South Italy and Romania/Moldova. These findings indicate that the frequency of heavy precipitation events may be underestimated by the model, whereas the intensity of convective events, which are produced by the parameterization scheme, may be overestimated.

3.3.2 Thermodynamic relations

Figures 3.2–3.5 a–c show the dependencies of the total column water vapor, the cloud liquid water, and CAPE on the temperature range for three European sub-regions in summer. The analyses are conditioned on days where the 95% quantile of daily summer precipitation was exceeded at least at one grid point within the region. Results are drawn in blue for the model output and in red colors for the satellite observations. The shaded areas highlight one standard deviation and dashed lines indicate an increase of $7\%/K$ which would be the approximate increase of column water vapor predicted by the Clausius-Clapeyron equation.

In Southwest Norway (Figure 3.2a) a positive connection between total column water vapor and temperature at a rate closely following the Clausius-Clapeyron relation is found both for model and observations. For the cloud water (Figure 3.2b) both show a similar Clausius-Clapeyron like increase with temperature in the lower temperature range up to approximately $8\,°C$, but a negative relationship above.

Over the Alps, the change of total column water vapor (Figure 3.3a) with temperature has similar characteristics as for Southwest Norway up to an average regional temperature of $15\,°C$. At higher temperatures, however, the curves flatten and show a sub-Clausius-Clapeyron behavior. Similar as for Norway is also the temperature relation of cloud water (Figure 3.3b), which increases at lower and decreases at higher

temperatures.

For South Italy as well as East Romania and Moldova the relationships are shifted towards higher temperatures (Figure 3.4 and 3.5 a and b). Whereas in Eastern Europe, total column water vapor increases with temperature only sligtly below the Clausius-Clapeyron change, the water vapor in South Italy shows no clear dependency on the temperature above $18\,°C$, but levels out completely. The cloud water in this region decreases for temperatures of $17\,°C$ and above. In general, the amount of cloud water is lower for South Italy compared to the other sub-regions.

The convective instability, described by CAPE at the time of heavy precipitation occurrence, is generally low in Southwest Norway (Figure 3.2c) where the summer precipitation is of large-scale rather than convective nature. With increasing areal average temperatures, convection becomes more likely, indicated by increasing CAPE values. This positive relation of CAPE with near-surface temperature can be observed in all sub-regions. However, the increase of CAPE with temperature is not strongest in South Italy (Figure 3.4c) where the highest temperatures occur. At a temperature of $20\,°C$, the highest areal CAPE average of 500 Jkg^{-1} is found for the Alpine region (Figure 3.3c), followed by East Romania and Moldova (Figure 3.5c). Model and observations agree on the analyzed relationships between CAPE and temperature within the range of one standard deviation. Yet, the differences are largest in South Italy, where CAPE is underestimated by REMO. A reason might be that the parameterization of convection in the model has no memory, in contrast to reality, where CAPE can accumulate over some time when the energy of the ascending parcels is not large enough to overcome the stability of lower atmospheric boundary layer and reach the level of free convection (Parker 2002). This is an issue in particular in regions where it rains rarely in summer, like in South Italy.

The results so far suggest that some limitations to the Clausius-Clapeyron behavior of total column water vapor exist for high areal average temperatures. This feature can most clearly be observed for South Italy. If one assumes that air which is dynamically advected to a region has obtained moisture by synoptic-scale moisture convergence over the ocean, the amount of water vapor should always be sufficient to reach saturation. A less dynamic nature of the synoptic situation at higher temperatures results in moisture being provided by evaporation from local sources like the ground, vegetation, or even small lakes. If the available amount of water is not sufficient to maintain constant relative humidity, the total column water vapor will show a sub-Clausius-Clapeyron behavior. This is reflected in the relationship of the cloud water with temperature. For cloud water, however, the scale of resulting precipitation events plays a role in addition. As the analysis of CAPE indicates, convective instability and thereby convective precipitation events dominate at higher temperatures. In the regional model, convection is parameterized by the sub-grid scheme for cumulus clouds. Precipitation in the convective scheme is produced and falls out within one simulation time step. Only the water

detrained in the updrafts is passed on to the large-scale cloud scheme and contributes to the total cloud water. With the growing convective nature of precipitation at higher temperatures, the mean daily amount of large-scale cloud water therefore decreases. In the observations, the relationships are supposed to be similar since convective events usually take place at sub-daily timescales and are very efficient in removing cloud water from the atmosphere. At lower temperatures, precipitation of synoptic temporal and spatial scales is dominant. At such situations, the increased amount of cloud water due to more water vapor is not removed as effectively, which leads to a positive relationship of daily mean cloud water and temperature.

3.3.3 Effect of thermodynamic covariates on heavy precipitation

The extreme value model used in section 3.3.1 is extended by total column water vapor and cloud water as covariates to examine their effect on the occurrence of heavy summer precipitation in model and observations. Additionally, the station altitude is introduced as covariate to account for orographic effects on heavy precipitation. Figures 3.2–3.5 d and e show the estimated relations of the 99% quantile of daily precipitation with total column water vapor and cloud water for the four sub-regions. The results are colored in blue for the model output and in red for the observations. Shaded areas highlight the range of 1000 random samples from the multivariate joint normal distribution of the PPP parameters.

The regional average of total column water vapor has no clear effect on the 99% quantile of daily summer precipitation in any of the sub-regions (Figure 3.2–3.5d). The relations obtained from observational data imply even a negative sign, however with small absolute values.

In contrast to the total column water vapor, the cloud liquid water (Figure 3.2–3.5e) is positively correlated with the occurrence of heavy precipitation events. This behavior is found in all sub-regions qualitatively similar for model and observational data. In Romania/Moldova and in Southern Italy (Figures 3.4e and 3.5e), the extreme value model suggests the 99% quantile of heavy precipitation to increase on average by 15 mm per 0.1 kgm^{-2} cloud water change in the observational dataset. In South-west Norway and in the Alps (Figures 3.2e and 3.3e), the increase ranges between 6.5 and 8 $mm/0.1kgm^{-2}$. The relationships are weaker in the model, ranging from 2-5 $mm/0.1kgm^{-2}$.

The results indicate that heavy summer precipitation increases with the cloud water in a region, rather than depending on the mean amount of vertically integrated water vapor in the region. On the investigated scales an increased water holding capacity of the air does not necessarily lead to an increase in the number or intensity of heavy precipitation events. Instead the condensation process of water vapor determined by the structure of the boundary layer appears to play an essential role for the formation

of heavy summer precipitation.

3.4 Conclusions

In contrast to the simple picture that changes of heavy precipitation events scale with changes in the column water vapor contained in the air, the analyses of observational data and regional climate model simulations in this study have indicated that heavy precipitation does not feature a strong relationship with the areal average of total column water vapor in the considered European sub-regions during the summer season. Instead, cloud water appears to be a more suitable covariate on regional scales. This is consistent with the findings from Chapter 2 and in agreement with the results by Berg et al. (2009), who find a positive connection of observed and simulated cloud water and heavy rainfall in summer and only a limited Clausius-Clapeyron scaling.

From these results one can conclude that the regional amount of column-integrated water vapor, which is available at the time a heavy precipitation event builds, does not by itself lead to more or heavier precipitation events. Instead, the value of high precipitation quantiles appears to be thermodynamically determined by the process of cloud formation, which is dependent on the moist static stability and the vertical air motions in the boundary layer. This is consistent with the results from O'Gorman and Schneider (2009b), who argue that heavy precipitation changes scale with changes in the condensation rate, which is proportional to the vertical derivative of saturation specific humidity along a moist adiabat rather than the vertically integrated saturation specific humidity.

At lower temperatures the interpretation of the positive connection between heavy precipitation and regional column cloud water is straightforward: a higher amount of stratiform regional cloudiness and cloud water leads to a higher possibility for heavier rains. For higher temperatures, the increase of CAPE with temperature implies that the fraction of convective precipitation increases. The connection between heavy precipitation and cloud water is then two-sided: On the one hand, more convection leads to a more efficient removal of convective cloud water by sub-daily rainfall. On the other hand, more intense convection leads to more detrainment of cloud water to the surroundings, which is why heavy precipitation has a positive relationship with the cloud water in the region. Inspection of the convective versus large-scale fraction of heavy daily precipitation totals has shown that the former increases while the latter decreases with temperature in the warmer range. Since convective precipitation events usually have a duration of much less than a day, their increase is smaller than the decrease in the large-scale, which leads to an overall decrease of heavy daily precipitation totals with temperature.

Not only show the results deviances from the expected relationship between total column water vapor and heavy precipitation, but also limitations to the Clausius-

Clapeyron like scaling of total column water vapor with temperature at the highest temperature range. This is likely due to a limited availability of water vapor caused by reduced advection of moisture in less dynamic synoptic situations dominating at high temperatures. The cloud water increases with temperature at low temperatures, but decreases at higher temperatures, probably due to an increase in the amount of convectively formed clouds from which water is more effectively removed by precipitation on sub-daily timescales.

Since the same analyses have been carried out with model simulations as well as with different observational datasets, they can be regarded as a validation for the regional climate model REMO. Besides deviances in the shape parameter, the model reproduces the distribution of heavy precipitation sufficiently well. Also, model and observations show good agreement regarding the analyzed physical relationships, which gives confidence that REMO performs adequately in future projections of heavy precipitation.

Summary of Chapter 4

In this chapter, thermodynamic relations relevant for heavy precipitation formation are investigated for present day summer climate in an RCM simulation and in meteorological observations. In the previous chapter, the results have indicated limitations to the increase of vertically integrated water vapor with the saturation value for the warm regions of Europe in summer. At the same time, decreasing changes with temperature have been found for the cloud liquid water. The results from Chapter 3 confirm these findings for the temperature dependencies in present day climate in modeled and observational data. The presented extreme value analysis highlights the importance of the cloud liquid water as regional scale covariate for heavy summer precipitation in different European sub-regions.

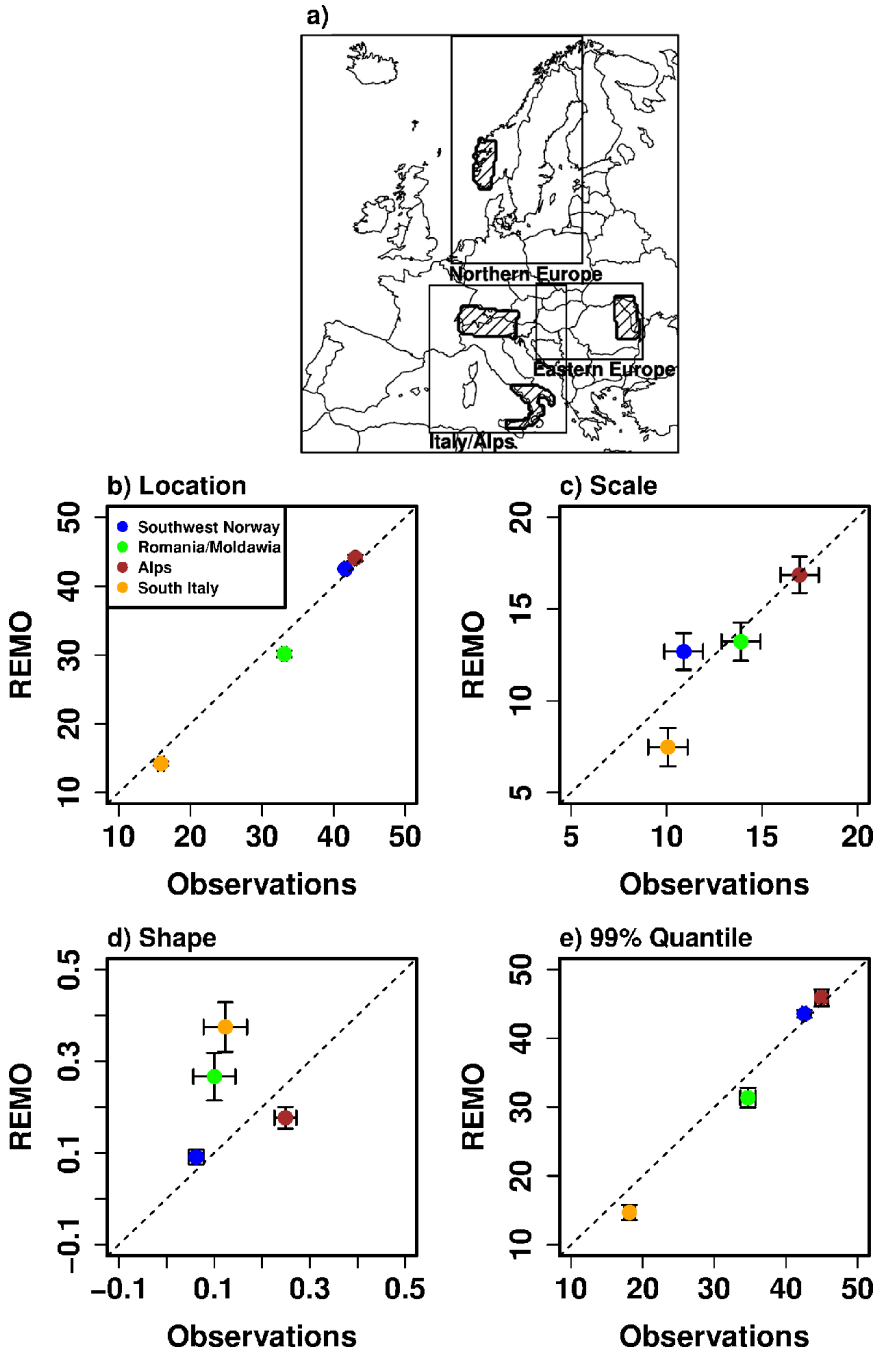

Figure 3.1: a) Map of Europe showing the sub-regions as hatches areas. b–d) Parameters of the Poisson point process for heavy daily summer precipitation in REMO vs. Observations. e) 99% quantile of the Poisson point process for heavy daily summer precipitation in REMO vs. Observations. The error bars in b)-d) show the corresponding standard errors. The error bars in e) denote the uncertainties of the quantiles obtained from the range of 1000 random samples from the multivariate joint normal distribution of the PPP parameters.

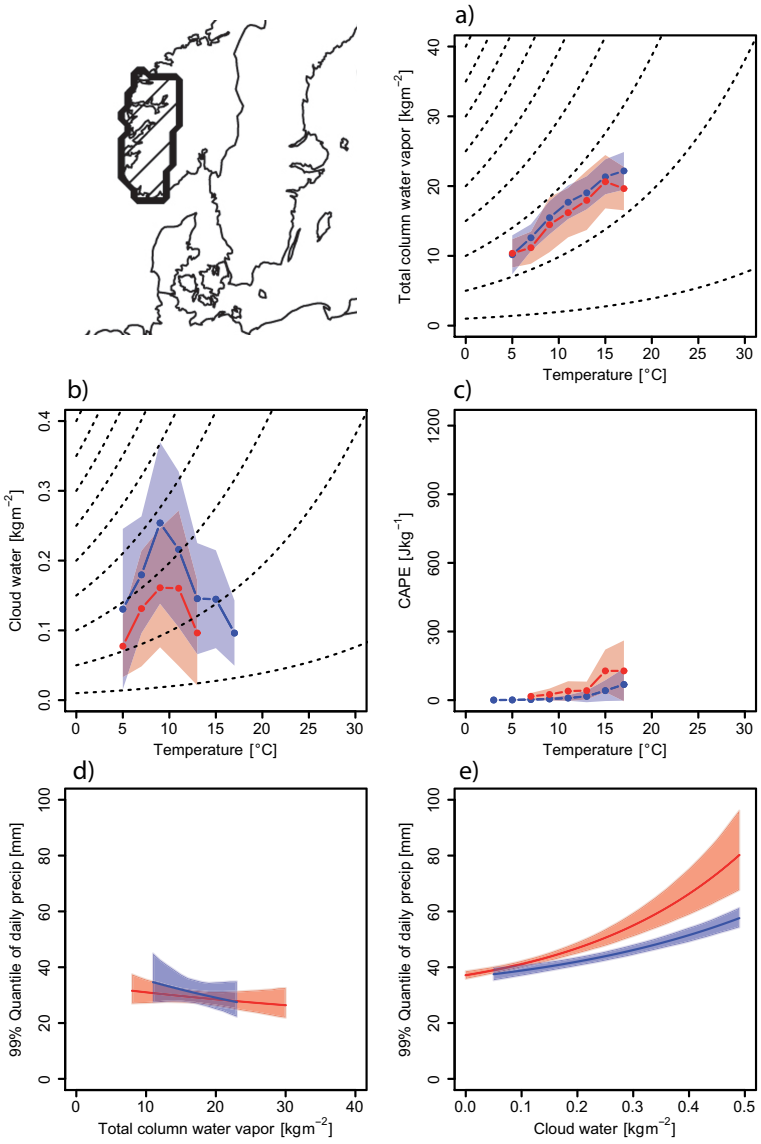

Figure 3.2: Southwest Norway: (a) Relationship of the daily mean total column water vapor and near-surface temperature in summer. Blue: REMO model output. Red: satellite observations. Shaded areas highlight one standard deviation and dashed lines indicate an increase of $7\%/K$ which would be predicted by the Clausius-Clapeyron equation. (b) Relationship of the daily mean cloud water and near-surface temperature in summer. (c) Relationship of daily mean mixed-layer CAPE and near-surface temperature, conditional on days with precipitation above the 95% quantile for summer. (d) Dependency of the 99% quantile of total daily summer precipitation in mm on the total column water vapor in kgm^{-2}. Shaded areas highlight the range of 1000 random samples from the multivariate joint normal distribution of the PPP parameters. (e) Dependency of the 99% quantile of total daily summer precipitation in mm on the column cloud water in kgm^{-2}.

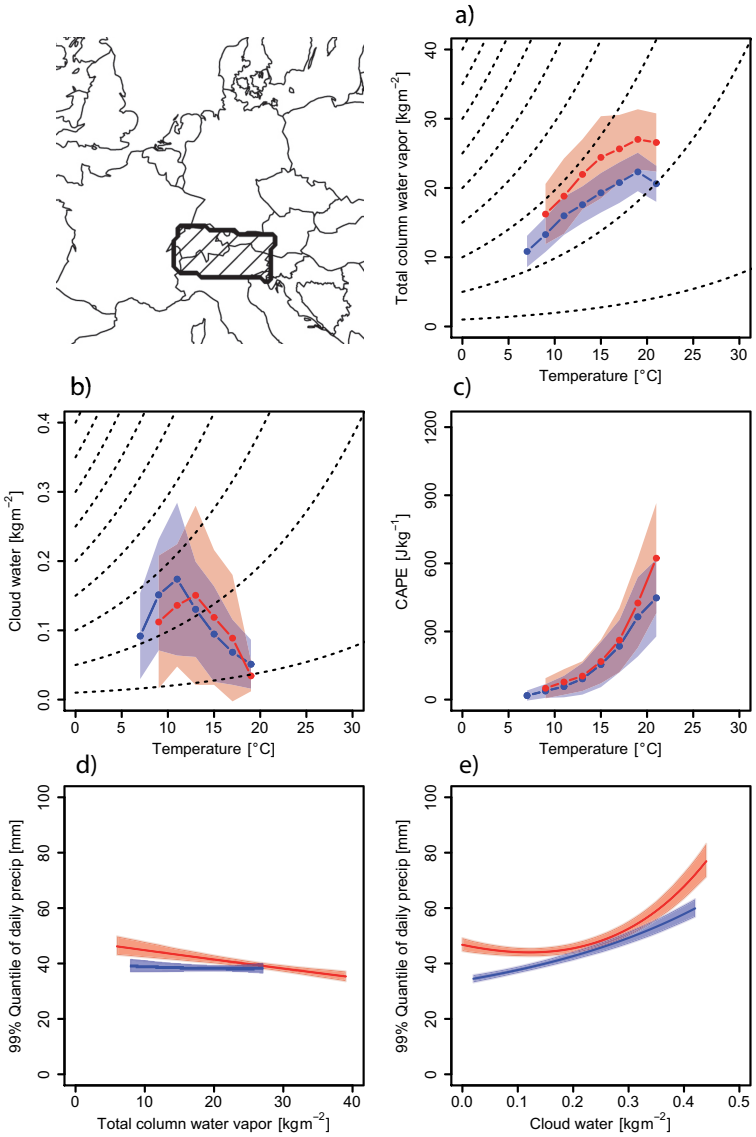

Figure 3.3: Same as Figure 3.2, but for the Alps.

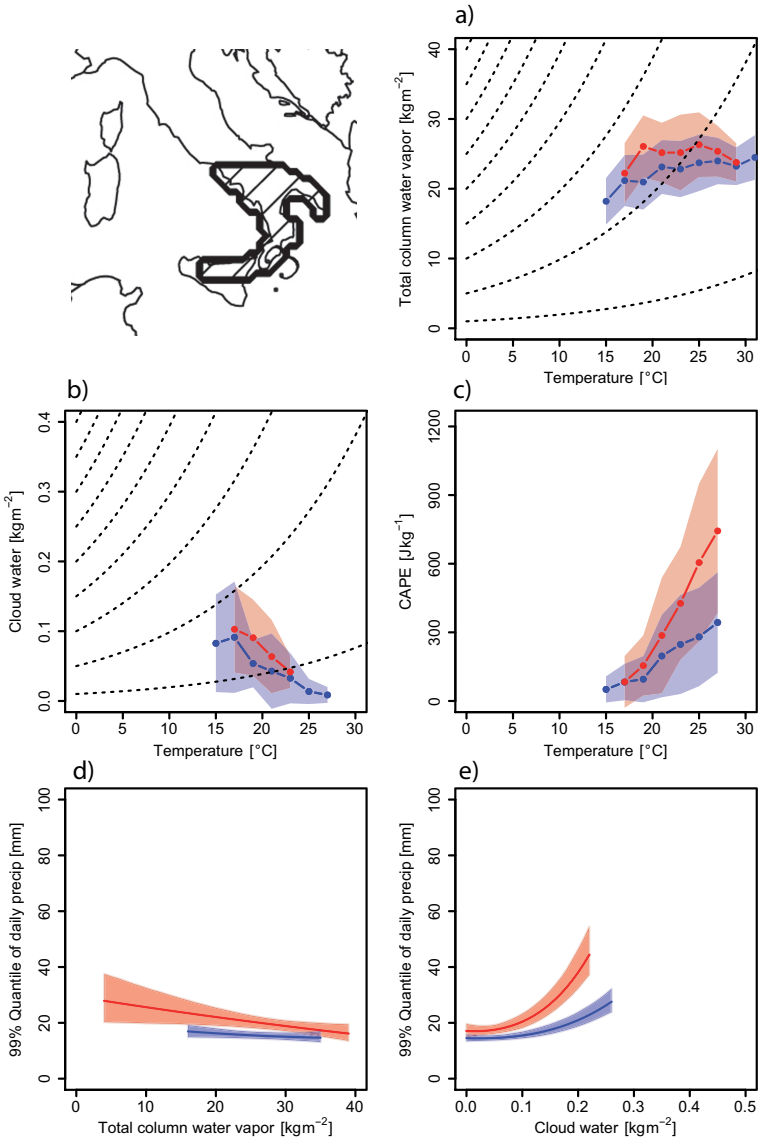

Figure 3.4: Same as Figure 3.2, but for Southern Italy.

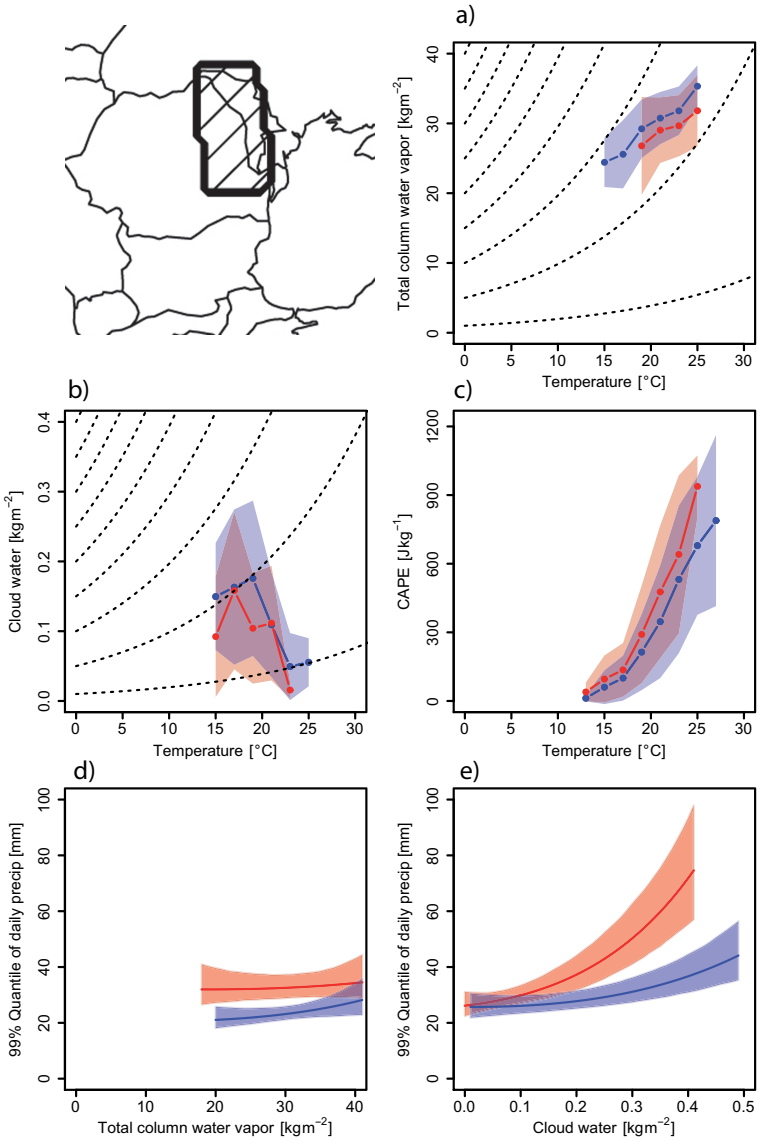

Figure 3.5: Same as Figure 3.2, but for East Romania and Moldova.

4 Dynamic and thermodynamic covariates for heavy precipitation changes

Whereas Chapter 2 and 3 are focused in particular on thermodynamic aspects of heavy precipitation formation and changes, the investigation of dynamic factors of influence is included in Chapter 4. In the first part of the chapter, synoptic scale patterns of moisture flux divergence are analyzed with a cluster analysis conditional on heavy precipitation occurrence in a regional climate model simulation for present and future. This allows to assess which dynamic situations favor heavy precipitation formation in different parts of Europe In the second part of this chapter, different combinations of dynamic and thermodynamic quantities as covariates for heavy precipitation are assessed with an extreme value analysis. Chapter 4 is aimed at answering the third research question posed in Chapter 1.1.

4.1 Introduction

The dynamic and thermodynamic processes forming precipitation are described by the water balance equation, which connects the dynamic transport of water with evaporation and precipitation as sources and sinks. In the mid-latitudes, the water often evaporates and converges at low tropospheric levels in remote regions, preferably over the oceans, and is advected by the flow through synoptic scale eddies to regions where it precipitates. Convergence and associated rising of the air then leads to adiabatic cooling and condensation resulting in the formation of clouds. The combination of advection and convergence of moisture is described by the moisture flux divergence (MFD) which balances the difference of evaporation and precipitation in the water budget. In a warming climate, the MFD can be modified either by changes in the flow field, or by changes in the amount of water in the lower atmosphere. The MFD thereby joins thermodynamic and dynamic aspects. The impact of its changes on precipitation has been discussed by Held and Soden (2006), who found that the MFD response to global warming is to a large extent determined by the Clausius-Clapeyron relation rather than by changes in the flow field. They argue that as a consequence, the poleward transport of moisture and the difference pattern of evaporation and precipitation change proportionally to the lower-tropospheric water vapor over oceans and other areas where relative humidity changes are assumed to be small.

The influence of dynamic and thermodynamic factors on future changes in mean and heavy precipitation in climate simulations has been discussed in several studies. Emori and Brown (2005b) decompose the changes in heavy precipitation into a dynamic and a thermodynamic part and show that in strong upward motion regimes, extreme precipitation increases mainly due to the thermodynamic component. Meehl et al. (2005) find mid latitude changes in the precipitation intensity to be controlled by both the increased water vapor and the atmospheric circulation. For the northern latitudes they suggest advective processes to have an enhancing effect on the increase of precipitation, in particular for the most intense events. O'Gorman and Schneider (2009b) propose a full scaling including the vertical velocity as dynamic component and the vertical derivative of the specific humidity as thermodynamic part. They find the best scaling for both components being considered, but the thermodynamics having the largest impact. Chou et al. (2012) derive a set of equations to directly estimate the contribution of dynamics and thermodynamics on precipitation frequency and intensity in the tropics. In a multi-model ensemble of global climate models they show a shift of the precipitation distribution towards more intense events to be mainly caused by the thermodynamic component. Yet, they find the dynamic component to be able to reduce precipitation frequency and intensity, and even enhance the heaviest events.

Most studies dealing with the impact of thermodynamic and dynamic components of the moisture balance are focused on global or tropical changes in heavy precipitation statistics simulated by GCMs. Detailed causes for extratropical changes on regional scales are not sufficiently investigated so far. Therefore, in this chapter, thermodynamic and dynamic contributions to heavy precipitation formation and changes in Europe are investigated with the regional climate model REMO.

In a first part, dynamic situations favorable for heavy precipitation formation are identified using a cluster analysis of the moisture flux divergence conditional on heavy precipitation occurrence in present and future. Changes in the anomalies of precipitation-related variables are examined for the dynamic patterns. In the second part extreme value statistics are used to asses which covariates are suitable to explain heavy precipitation occurrence and may govern causes for future changes. The analysis is focused on the four European sub-regions, which have been studied also in Chapter 3.

The chapter is structured as follows: A description of the analyzed RCM simulation and the applied methods is given in section 4.2. The results are presented in section 4.3 for the cluster analysis and in section 4.4 for the extreme value analysis of causes for heavy precipitation changes. Finally, the results are discussed and summarized in section 4.5.

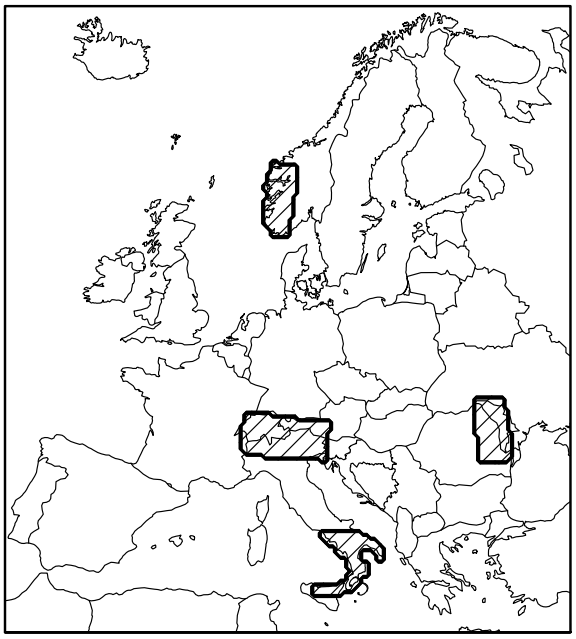

Figure 4.1: Map of Europe showing the selected sub-regions Southwest Norway, the Alps, East Romania and Moldova, and South Italy as hatched areas.

4.2 Data and methods

4.2.1 Regional climate model data

In this chapter a set of dynamic and thermodynamic variables and processes that govern the formation of heavy precipitation is analyzed in present and future climate. For this purpose, a model study is carried out with the RCM REMO. The investigated simulation was performed in the framework of the EU FP 6 project ENSEMBLES at a horizontal resolution of approximately 25 km x 25 km and a vertical resolution of 27 levels. The output of this simulation, which is driven by the GCM ECHAM5/MPI-OM, has also been studied in the ensemble in Chapter 2. The results are investigated for a reference period (1971–2000) and a future time period (2071–2100). Within the European domain, four sub-regions with different precipitation statistics and characteristics are selected: Southwestern Norway, the Alps, East Romania and Moldova, and Southern Italy (Figure 4.1).

4.2.2 Cluster analysis of the moisture flux divergence

In the first part of this chapter large-scale patterns of MFD at the time of heavy precipitation occurrence are identified in the RCM simulation. For this purpose a k-

means cluster analysis is carried out over Europe conditional on heavy precipitation events in the sub-domains. The investigation of pressure patterns within the clusters gives additional insight into the governing dynamic situations. Future changes in the cluster frequency are analyzed by projecting the cluster patterns to the future time period of the climate change scenario simulation.

Partitional clustering with the k-means method

The k-means algorithm is a partitional non-hierarchical cluster analysis which divides similar objects in a dataset into a fixed number k of groups which are well separated from each other. Initially k cluster centers are randomly selected. Each object is then assigned to the closest cluster center, measured by the minimum of the squared Euclidean distance (SED) between the field vector x and the respective cluster center vector y, given by

$$SED = \|x - y\|^2. \tag{4.1}$$

In the next step, an updated cluster center is calculated for each cluster. The objects in the dataset are again assigned to the clusters by calculating the SED and the cluster centers are updated. This process is repeated until the objects do not change clusters anymore and a minimum of the within-cluster sum of squares (WSS) is reached. The WSS is given by

$$WSS = \sum_{i=1}^{k} \sum_{x \in C_i} \|x - y_i\|^2, \tag{4.2}$$

where C_i is the cluster which x was assigned to and y_i is the corresponding cluster center.

For the k-means clustering method, the number of cluster needs to be chosen in advance. The quality of the classification result is to a large extent dependent on this predefined number k. However, its choice is not a trivial task and prior knowledge about the cluster structure of the dataset is necessary. Different statistical measures are applied to determine the optimal number of clusters. A description of the measures is given in Appendix C.

Application to the moisture flux divergence

The atmospheric water budget is described by the equation for the conservation of water vapor, which can be written in pressure coordinates as

$$\frac{\partial q}{\partial t} + \nabla q \vec{v} + \frac{\partial}{\partial p}(\omega q) = \frac{1}{g}\frac{\partial}{\partial p}(E - P). \tag{4.3}$$

Vertical integration of 4.3 over the whole atmosphere gives

$$\frac{\partial q_{vi}}{\partial t} + \int_{p}^{p_0} \nabla q\vec{v} = E - P, \tag{4.4}$$

where $\frac{\partial q_{vi}}{\partial t}$ describes the local rate of change of the vertically integrated water vapor. The term $\int_{p}^{p_0} \nabla q\vec{v}$ is the vertical integral of the MFD with q and $\vec{v}$ being the vertical profiles of the specific humidity and the wind, respectively. The sources and sinks of water vapor are represented by the evaporation E and the precipitation P.

The moisture flux divergence can thus be calculated using

$$MFD = E - P - \frac{\partial q_{vi}}{\partial t}. \tag{4.5}$$

More accurately, the moisture flux divergence would be calculated using $\int_{p}^{p_0} \nabla q\vec{v}$. Unfortunately, the wind components from the RCM output used in this study are only available at 6-hourly temporal resolution. Applying the divergence operator would not give meaningful results since the winds may have changed substantially within 6 hours. Ideally, the MFD would be determined directly during the RCM simulation at model time steps. Nevertheless, tests have shown that the offline calculation of MFD from hourly model output via the water balance 4.5 gives sufficiently similar results. The formulation is therefore used in the following. Since the focus of this study is on heavy daily precipitation totals, the analyses are carried out with daily averages of hourly calculated MFD.

The k-means cluster analysis is applied to the MFD for the entire European domain conditional on days when a heavy precipitation event is simulated by REMO for at least four grid points in the respective region. The restriction to four grid points sorts out days at which heavy precipitation has been simulated only for single grid points in the region and leads to a higher robustness of the results. Inspection of the data has shown that heavy precipitation occurs rarely at less than four grid boxes when it occurs. At this point a heavy precipitation event is defined as an exceedance over the empirical 95% quantile, which has been determined separately for each grid point in the sub-region over all data points in time. The maximum of all exceedances over the region at a time is considered. The winter (DJF) and the summer (JJA) seasons are examined separately, since the predominant synoptic situations are seasonally dependent. In the next step, the cluster centroid vector C composed of the k clusters with index $i = 1, ..., k$ is projected to each time step in the future time period 2071–2100 by application of a multivariate linear regression with coefficients a_i in the following way:

$$y = \sum_{i=1}^{k} a_i \cdot C_i, \tag{4.6}$$

with y being the time series of the daily regional averages of the MFD for the sub-region. The cluster patterns of moisture flux divergence are assumed not to change in

the future, which allows for investigating changes in the cluster frequency. In a next step, the projected percentual changes in heavy precipitation are calculated for the ith cluster as follows:

$$\Delta Pr_i = \frac{\overline{Pr_{ipres}} - \overline{Pr_{ifut}}}{\overline{Pr_{ipres}}} * 100, \tag{4.7}$$

where $\overline{Pr_{ipres}}$ and $\overline{Pr_{ifut}}$ are the averages over all heavy precipitation events belonging to the respective cluster, denoted by the indices $ipres$ and $ifut$ for present and future time period.

This calculation serves primarily to sort the clusters by the strength of the heavy precipitation change in decreasing order, which gives a first idea in which large-scale regimes of the moisture flux divergence the character of heavy precipitation in REMO may change most pronouncedly. Finally, a set of variables related to precipitation formation is analyzed conditional on the clustered regimes in the present and the future time period.

4.2.3 Set of covariates

The clusters of MFD can be considered as dynamic situations favoring heavy precipitation occurrence. Changes of variables related to precipitation formation are investigated for the time steps belonging to each of these synoptic situations, to sharpen the understanding for the influence of the large-scale dynamics on climatic changes concerning heavy precipitation at regional scales. For this purpose, the regional average of the variable for the sub-region in which heavy precipitation occurred is averaged over all time steps belonging to the respective cluster in the present and the future time period. The considered variables are q, which is the added amount of the vertically integrated water vapor q_v and liquid water content q_l, the vertical velocity ω, averaged over all pressure levels, the evaporation E, and the moisture flux divergence MFD itself.

In the second part of the study, the regional averages of the considered variables are used in all possible combinations as covariates in extreme value models for heavy precipitation. The combinations of covariates and their annotation are given in Table 4.2.

4.2.4 The extreme value model

The extreme value analysis of heavy precipitation and possible factors of influence is carried out with a non-homogeneous Poisson point process (PPP) model. This approach essentially unifies the peaks-over-threshold (POT) method with features of the generalized extreme value (GEV) distribution for block maxima. The estimated parameters of the PPP are commensurate to the GEV parameterization, which makes the

scale parameter σ independent on the threshold choice and allows for a direct extension of the model to covariates. In comparison to the block-maxima approach, the POT method takes a larger fraction of the dataset into account for analysis. An advantage of the PPP over the two parameter generalized Pareto distribution (GPD), is the fact that besides the exceedance itself the frequency of exceedances in a certain fraction of the data is considered. Here, the threshold is the 95% quantile of the regional maxima of daily precipitation in the respective sub-region.

Estimation of the PPP parameters is performed by minimizing the negative log-likelihood of the Poisson process. In this study the parameters shall depend on a set of covariates. The likelihood is here defined as:

$$L = \exp\left\{-\int_0^{T_e}\left[1+\xi\left(\frac{u-\mu_C}{\sigma_C}\right)\right]_+^{\frac{-1}{\xi}} dT\right\}\prod_{j=1}^{n_u}\frac{1}{\sigma_{Tj}}\cdot\left[1+\xi\left(\frac{\tilde{X}_j-\mu_{T_j}}{\sigma_{T_j}}\right)\right]_+^{\frac{-1}{\xi}-1} \tag{4.8}$$

with T_j being the time of the j-th exceedance and $\tilde{X}_j > u$ the value of the jth exceedance of the threshold u and $j = 1, \ldots, n_u$ with n_u being the number of exceedances. The interval $[0, T_e]$ describes the whole time period. It is furthermore $a_+ = a$ if $a > 0$ and zero otherwise. The model is extended by modeling the dependency of parameters μ and σ on the set of n covariates $C = (c_1, ..., c_n)$ in the following way:

$$\mu_C = \mu_0 + \sum_{i=1}^{n}\beta_i \cdot c_i, \qquad \sigma_C = \sigma_0 \cdot \exp\left\{\sum_{i=1}^{n}\gamma_i \cdot c_i\right\}, \tag{4.9}$$

The shape parameter ξ is held invariant with respect to the covariates.

At first, the model is fitted without covariates to determine initial values for the parameter estimation of the covariate-dependent models. In the next step, the parameters of the so determined statistical model are used as initial values for the models including all possible combinations of the covariates described in section 4.2.3. The minimization of the negative log-likelihood is achieved using the simulated annealing optimization technique, which belongs to the class of stochastic global optimization methods (Goffe et al. 1994). This technique finds a solution, which is very close to the global optimum. The estimated parameters slightly differ from each function evaluation to the other. To account for these random deviances, the optimization is repeated 20 times and the average of each parameter is considered.

The optimal model from a set of plausible models can be determined by the Aikaike Information Criterion (AIC, Aikaike (1973)), which is given by

$$AIC = -2\log L + 2k, \tag{4.10}$$

where k is the number of parameters.

The AIC does not only consider the likelihood of a model, but also the number of estimated parameters. In this way, the effect of overfitting due to a large number of free parameters is penalized. The model with the minimum AIC value is considered as the best to fit the data. In contrast to the likelihood ratio test, the AIC can be used to compare models which are not nested. The relative likelihood that the ith model rather than the one with the minimum AIC is the best to fit the data (Aikaike 1981), is determined by evaluating

$$L_i = exp((AIC_{min} - AIC_i)/2). \tag{4.11}$$

From this measure one can calculate the Aikaike weights w_i (Burnham and Anderson 2004), which can be interpreted as the probability of a certain model to be the best one out of a set of M models.

$$w_i = \frac{exp((AIC_{min} - AIC_i)/2)}{\sum_{k=1}^{M} exp((AIC_{min} - AIC_k)/2)}. \tag{4.12}$$

The AIC is a criterion to chose the best model out of a set of candidate model, but not able to assess the predictive skill of a model. If all candidate models fit the data unsatisfactorily, the AIC selects the best out of a range of bad models.

Model verification is therefore carried out using a cross-validation technique. The parameters of the covariate-dependent models are estimated for a training period, which is the whole time period except for one season, and a target period, which is the season that has been left out. The probabilities of daily precipitation totals to exceed a certain threshold are predicted with the daily values of the covariates for each day of the target period. The procedure is repeated by removing and predicting all 30 seasons of the time period successively. In this way, a 30-season time series of predicted daily probabilities for threshold exceedance is carried out.

A model's ability to predict the exceedance of a threshold is assessed with the Brier score (BS, Brier (1950)). It is defined as the mean squared error over a sample of length n between the predicted probability $0 \leq \lambda \leq 1$ to exceed the threshold and an indicator function $I(x_i > u)$, which is 1 when the threshold u is exceeded by the observation, and 0 otherwise.

$$BS = \frac{1}{n} \sum_{i=1}^{n} (I(y_i > u) - \lambda_i)^2 \tag{4.13}$$

where the y_i denote the values of daily precipitation. The values of λ_i are the daily probabilities predicted from the covariate-dependent parameters of the Poisson point process for each day, defined as $\lambda_i = (1 + \xi \frac{u-\mu_i}{\sigma_i})^{-1/\xi}$.

The relative improvement of a model compared to a reference model is determined by the Brier skill score (BSS), which can be interpreted as a goodness-of-fit test for the statistical model:

Table 4.1: Summary of the optimal cluster numbers for the sub-regions.

Region	DJF	JJA
Southwest Norway	6	7
Alps	7	6
East Romania / Moldova	6	6
South Italy	6	5

$$BSS = 1 - \frac{BS}{BS_{ref}}. \tag{4.14}$$

The reference model is represented by the climatological probability for exceedance of the threshold. The values of the BSS range between $-\infty$ and 1, and describes the gain of predictive skill against the reference model.

4.3 Results of the cluster analysis

Conditional on heavy precipitation in each sub-region, the k–means algorithm is applied over the entire European domain for k values from 3 to 12 to determine the optimal cluster solution. The graphics for the determination of the optimal cluster number are given in Appendix C. Cluster solutions with fewer clusters are favored since the patterns appear to be better separated from each other compared to solutions with more clusters. Table 4.1 summarizes the determined optimal cluster numbers for the different sub-regions in both seasons.

4.3.1 Winter

The clusters of the moisture flux divergence are displayed in conjunction with the mean sea level pressure (MSLP) anomalies in each cluster, obtained by subtracting the projected MSLP climatology over the years 1971–2000, shown in Figure 4.2. The clusters conditional on heavy precipitation over Southwest Norway (Figure 4.3(a)) mostly go along with flow from western to southern directions, indicated by large spatial gradients of the MSLP anomaly. Icelandic low pressure conditions dominate the synoptic patterns. Convergent regimes of moisture flux are present in all clusters, which is indicated by negative MFD values and blue contour colors. In Cluster 1, 2, and 3 a low pressure anomaly is located a little west of Southwestern Norway, the main flow is from southwest to south, and the moisture flux converges within the region itself. In Cluster 4, 5, and 6, the dominating flow is from the northwest, caused by a low pressure anomaly north of the region and a strong north-south pressure gradient.

The clusters are sorted according to the magnitude of the heavy precipitation change (Future–Present) in decreasing order at time steps belonging to the same cluster pattern of MFD. The changes in heavy precipitation are shown in Figure 4.3(b) for each cluster, with the error bars denoting the 90% confidence intervals estimated with a Wilcoxon rank sum test. Large uncertainties are indicated, which is due to large variability in the intensity of events in the sub-regions for each cluster. However, this analysis serves primarily to sort the clusters by the strength of the heavy precipitation change in decreasing order, which gives an idea in which large-scale regimes of the moisture flux divergence the character of heavy precipitation may change most pronouncedly.

The changes are with about 25% largest in Cluster 1, 2, and 3, i. e. in the situations with southwestern to southern flow directions, whereas the changes are negligible for Cluster 4, 5, and 6. Inspection of the cluster frequency in present and future time period (Figure 4.3(c)) indicates that Cluster 2, 3, and 4 occur less frequently in the future time period. Only minor increases are found for Cluster 1, which obtain the largest changes in heavy precipitation, as well as for cluster 5 and 6. In total, the frequency of all cluster, i.e. the frequency of heavy precipitation events, decreases by about 5% (not shown).

The clusters of MFD associated with heavy precipitation over the Alps in winter (Figure 4.4(a)), can roughly be divided into two classes in terms of the circulation. In Cluster 1, 2, 3, and 7, westerly to northerly flow conditions over the Alps are predominant, depending on the location of the low pressure anomaly. In Cluster 4, 5, and 6, a low pressure system is located directly over the Alps or west of it, causing flow from southwestern to southern directions. In the clusters of the first type, the moisture flux converges over the Atlantic ocean in the region of the British Isles and on the northern flank of the Alps, whereas in clusters of the second type, moisture flux convergence (MFC) is present over the entire Alpine region and along the windward Mediterranean coasts.

The changes in heavy precipitation (Figure 4.4(b)) are positive in all clusters and range from 15% for Cluster 7 to about 30% for Cluster 1. Both Cluster 1 and 7, in which the flow direction is from the north and the moisture flux converges in particular on the northern flank of the Alps, increase in frequency in the future (Figure 4.4(c)). On the contrary, Cluster 4, 5, and 6, which are associated with flow from the southwest and moisture flux convergence also on the Alpine south side, show decreasing changes.

Most clusters associated with heavy precipitation over East Romania and Moldova (Figure 4.5(a)) exhibit a regionally bounded low pressure anomaly located over the sub-region, which causes flow conditions from the southeast. A similar flow direction is also found for Cluster 2, in which a strong low pressure system is located over Italy. All clusters exhibit some MFC in East Romania and Moldova, but the largest magnitudes, spreading over the entire surrounding region, are found in Cluster 2.

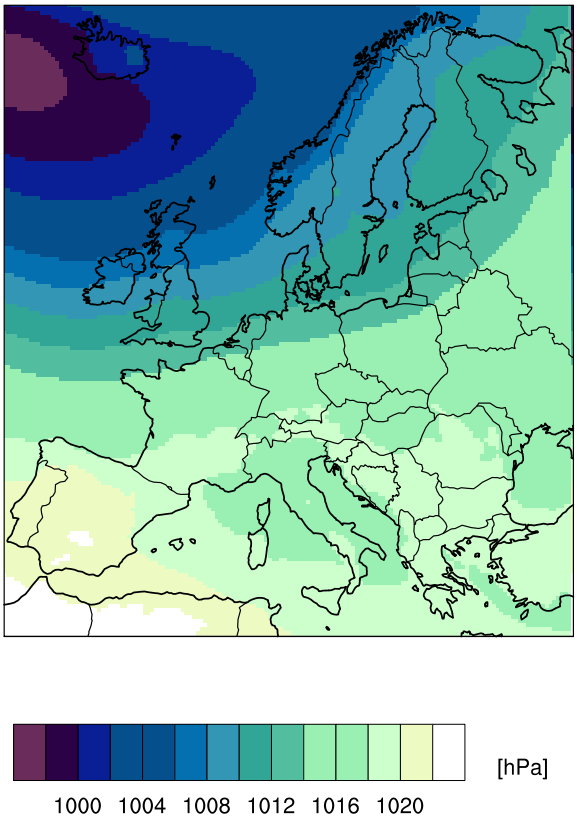

Figure 4.2: Simulated climatology of the MSLP in hPa over the time period 1971–2000 in winter.

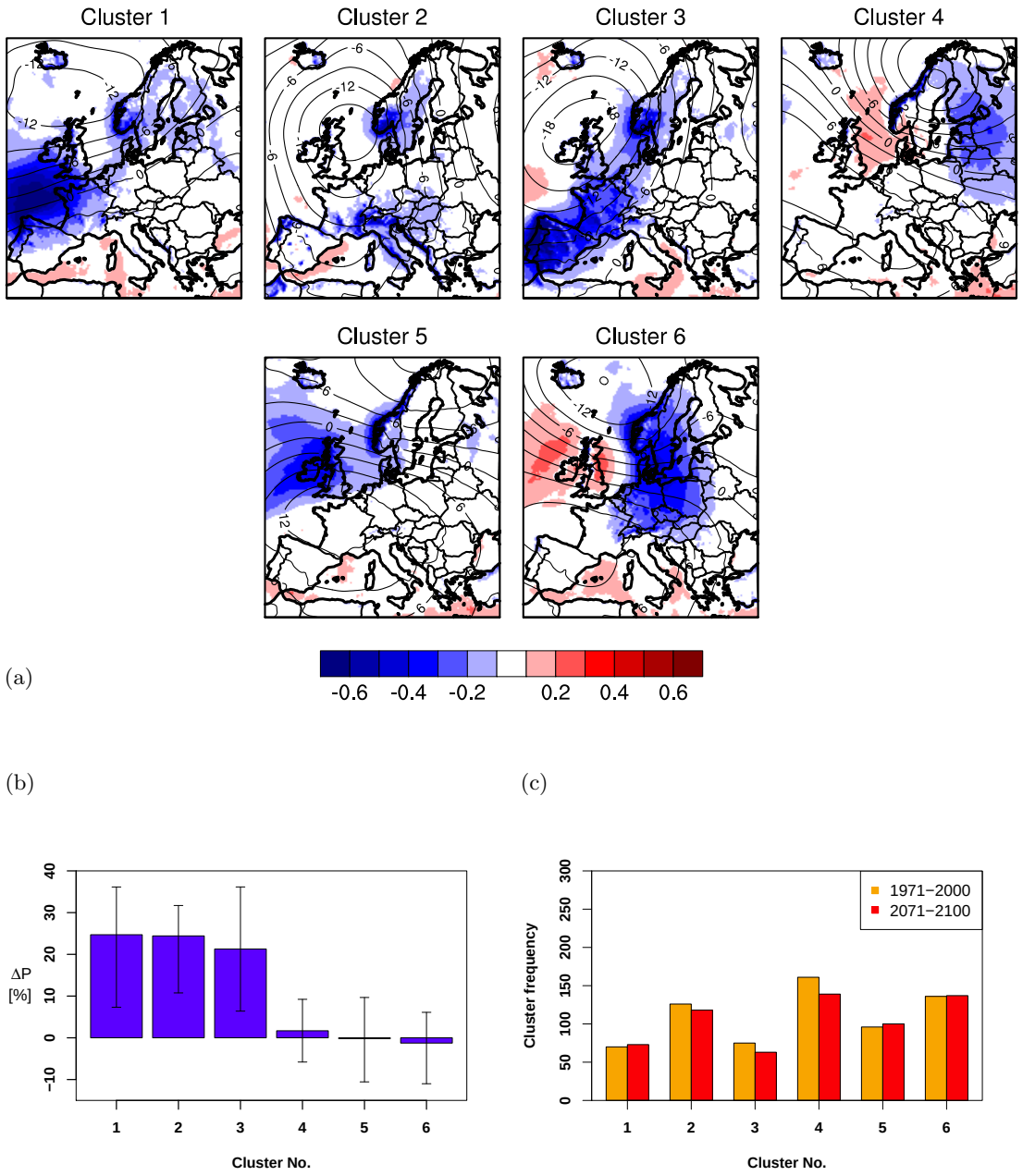

Figure 4.3: (a) Clusters of MFD conditional on heavy precipitation over Southwest Norway in winter. Filled contours mark the pattern of MFD (positive values, red) or MFC (negative values, blue). Cluster are sorted in decreasing order by the strength of the heavy precipitation change signal. Black lines show the MSLP isobars. (b) Relative changes (2071–2100 minus 1971–2000) of the mean exceedances over the 95% quantile of precipitation for each cluster in %. The error bars denote the 90 % confidence intervals estimated with a Wilcoxon rank sum test. (c) Frequency of the clusters in present (yellow) and future (red).

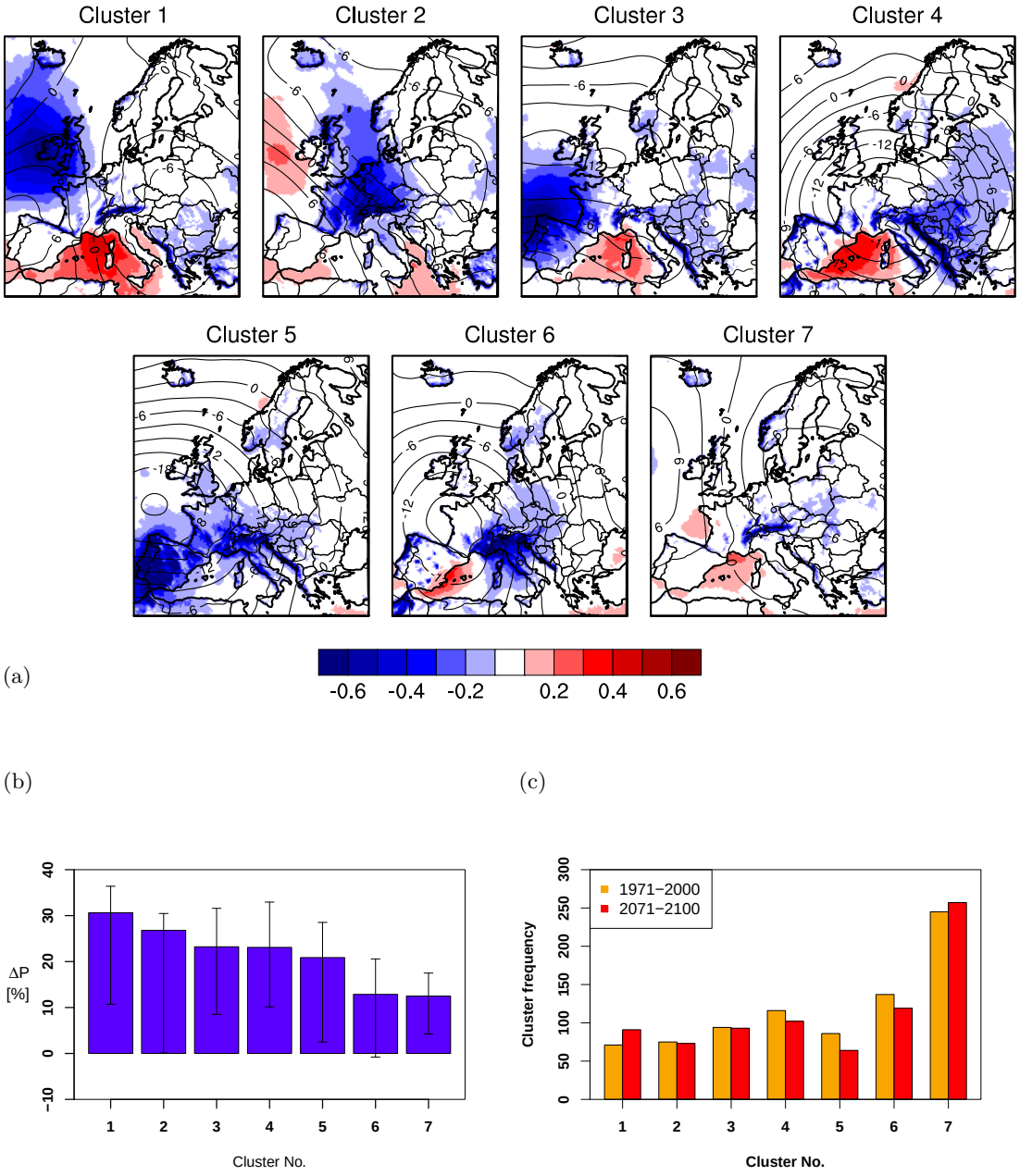

Figure 4.4: As 4.3, but for the Alps in winter.

The changes in heavy precipitation (Figure 4.5(b)) range from 21% in Cluster 1 to -7% in Cluster 6. The cluster which obtains the strongest changes in heavy precipitation is at the same time the most frequent one. The frequency of Cluster 1 as well as Cluster 3 and 4 increases towards the future (Figure 4.5(c)), whereas the other ones exhibit decreasing trends. The patterns becoming more frequent resemble the ones which become more frequent for the Alps (Figure 4.4(a)). In particular Cluster 4 for East Romania/Moldova is essentially equivalent to Cluster 1 for the Alps. This may indicate a change in the circulation in favor of more northerly flow conditions in the Alps and more southeasterly conditions in East Romania and Moldova.

The clusters for heavy precipitation over South Italy can broadly be classified into two types. The first type is characterized by flow conditions from the northwest to west, caused by low pressure anomalies centered over or close to the region (Cluster 1, 3, and 4). The other type exhibits pressure conditions causing more easterly directed flow (Cluster 2 and 5). Whereas for the first type, the moisture flux converges most strongly along the windward west coasts of Italy, the second type exhibits convergence mainly along the eastern coasts and on Sicily. Striking is Cluster 7, which is characterized by a strong low pressure anomaly west of Italy causing southwesterly flow and strong MFC over entire Italy and its surroundings.

The precipitation changes are positive between 2 and 23 % in Cluster 1, 2, and 3 (Figure 4.6(b)). Cluster 4, 5, and 6 exhibit negative changes down to -10 %. It is striking that Cluster 7, for which the strongest decrease in heavy precipitation is detected, shows the pattern with the strongest MFC over the South Italian region. Cluster 1 and 4, which are associated with a low pressure anomaly over Italy, increase in frequency towards the future (Figure 4.6(c)). The patterns with easterly flow conditions (Cluster 2 and 5) are projected to become less frequent.

For each cluster, the anomalies from the regional averages over the present and future time series of the vertically integrated water vapor q, the moisture flux divergence MFD, the evapotranspiration E, and the vertically integrated vertical velocity ω are determined. Figure 4.7 displays the standardized results for the present in lighter colors and the future time period in darker colors. The standardization is done by dividing the anomalies by the standard deviation of the variable over the whole time period.

Since the clusters have been calculated for the time steps with heavy precipitation occurrence only, the results can be considered also as the anomalies compared to time steps with no heavy precipitation occurrence. For all sub-regions, the precipitable water q exhibits mostly positive anomalies. As expected based on the Clausius-Clapeyron relation, it increases in the future time period for all clusters. Negative MFD anomalies which indicate a convergent behavior of the moisture flux, are present in all clusters except for Cluster 5 in South Italy (Figure 4.7(d)). It is striking that the most pronounced anomalies along with pronounced future changes occur simultaneously for q and MFD. In Southwest Norway, the Alps, and East Romania and Moldova (Figure 4.7(a)-(c)),

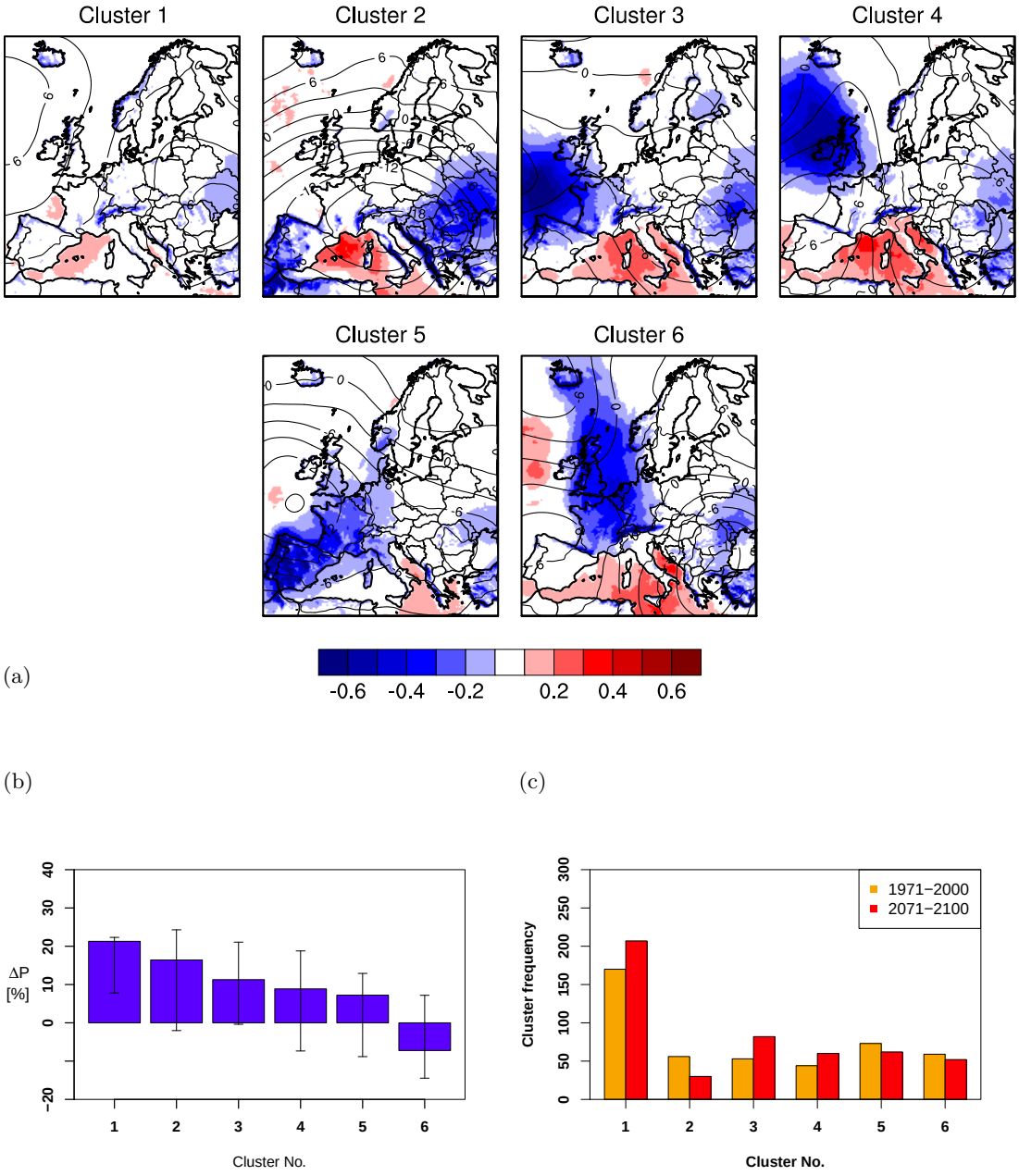

Figure 4.5: As 4.3, but for East Romania and Moldova in winter.

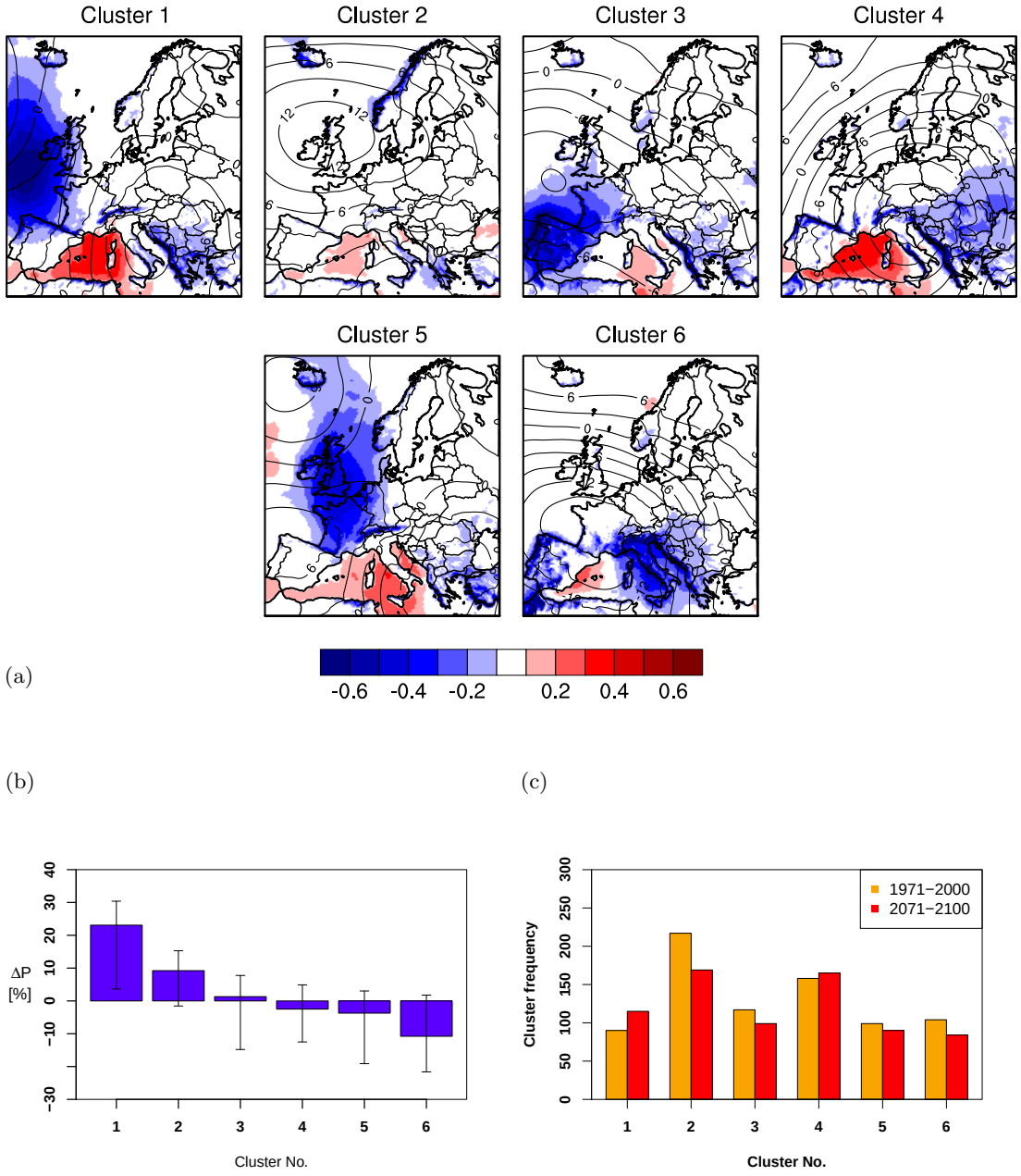

Figure 4.6: As 4.3, but for South Italy in winter

positive changes in the MFC are found in the clusters showing the strongest changes in heavy precipitation. In South Italy, MFC increases only for cluster 6, whereas the other patterns tend towards less convergent conditions.

For the vertical velocity ω negative values imply an upward and positive a downward direction of the wind. Positive values can indicate large-scale subsidence and more stable conditions, whereas negative values would stand for general rising of air masses within the sub-region. As expected because of the highly dynamic situations leading to heavy precipitation occurrence, the anomalies are all negative in Southwest Norway. But also for the other sub-domains, negative anomalies of ω are found for most clusters. For the future, the analyses indicate more upward winds over the Alps and more subsident conditions over East Romania and Moldova in some clusters. Evaporation anomalies are mainly positive for South Italy and Southwest Norway. For the future, increasing tendencies are projected in particular for East Romania/Moldova and South Italy.

4.3.2 Summer

For summer, the climatology of the MSLP, from which the anomalies displayed in conjunction with the clusters are calculated, is shown in Figure 4.8. In summer, heavy precipitation occurrence over Southwest Norway is accompanied by clearly less dynamic situations than in winter (Figure 4.9(a)). Nevertheless, low pressure anomalies are present and in most clusters located slightly west or north of the sub-region, causing westerly to southerly flow. The MFC magnitudes are in particular large along the windward coast of Southwest Norway. In Cluster 6 and 7, southwesterly flow conditions go together with convergent conditions over the entire region and its surroundings.

The magnitude of change in heavy precipitation (Figure 4.9(b)) reaches up to 20% in Cluster 1. It is striking that the largest changes occur in rather less dynamic situations, whereas the changes are negligible for Cluster 6 and 7, which disclose a clear pressure anomaly. The number of most clusters conditional on heavy precipitation occurrence is projected to change only little towards the future (Figure 4.9(c)). Only Cluster 3, which occurs most frequently, exhibits a larger decrease in frequency.

The cluster patterns for heavy precipitation over the Alps in summer, displayed in Figure 4.10(a), show also much less dynamic conditions than in winter. Only Cluster 1 shows a low pressure anomaly over the Alps, associated with flow from the northwest. The moisture flux converges in particular on the Alpine north side, but in most clusters the whole Alpine region is affected.

Positive, but weak and insignificant changes in heavy precipitation are found in Cluster 1, 2, and 3 (Figure 4.10(b)), while the other ones are associated with negative changes down to -15% in Cluster 6. Inspection of the cluster frequencies indicates that the number of heavy precipitation events decreases towards the future (Figure 4.10(c)).

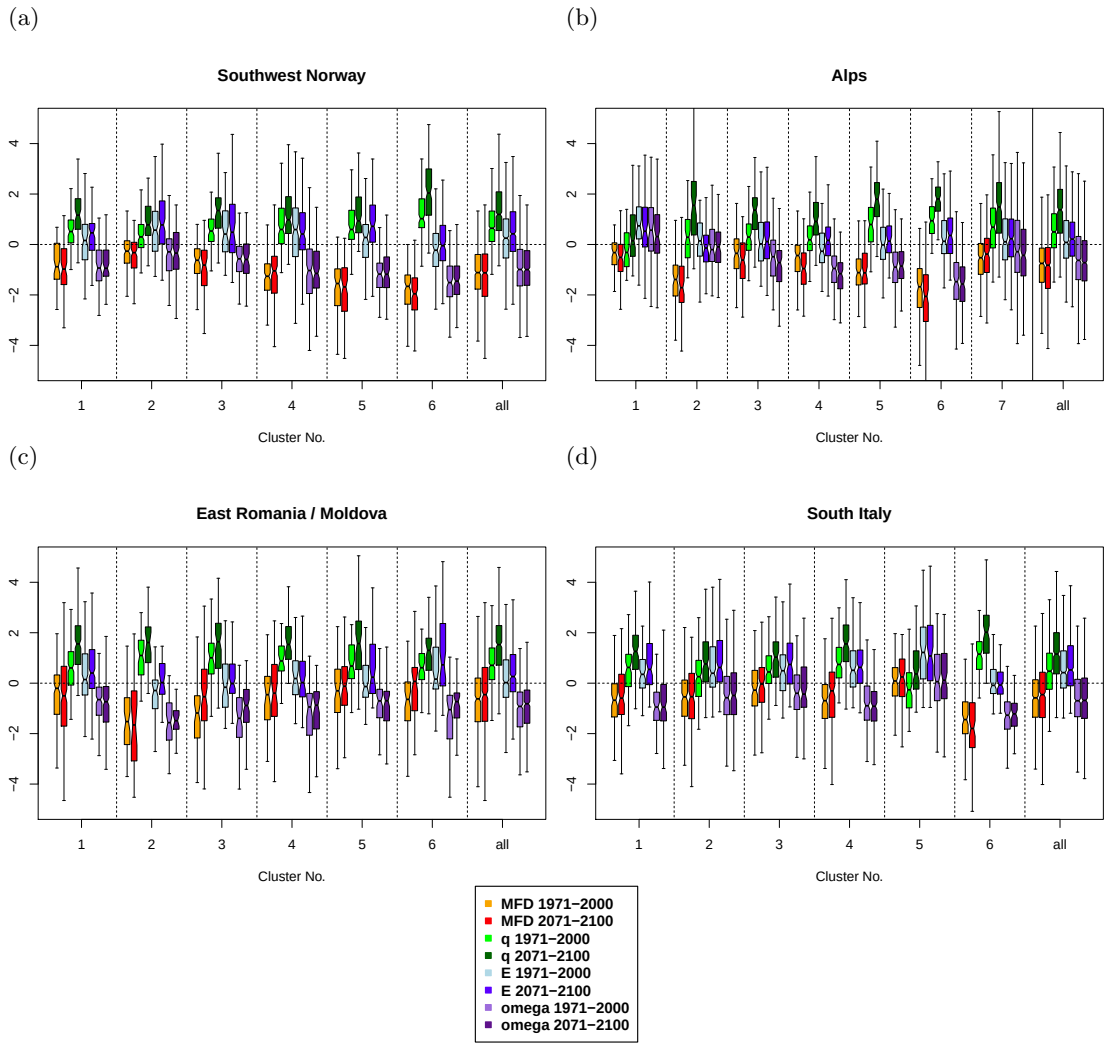

Figure 4.7: Regional average anomalies for present and future in winter of MFD (yellow and red), q_v (light green and green), E (light blue and blue), and ω (light purple and purple) conditioned on each cluster and for all time steps with heavy precipitation occurrence. The boxes denote the interquartile range, the whiskers extend to the most extreme data points. For (a) Southwest Norway, (b) the Alps, (c) East Romania and Moldova, (d) South Italy.

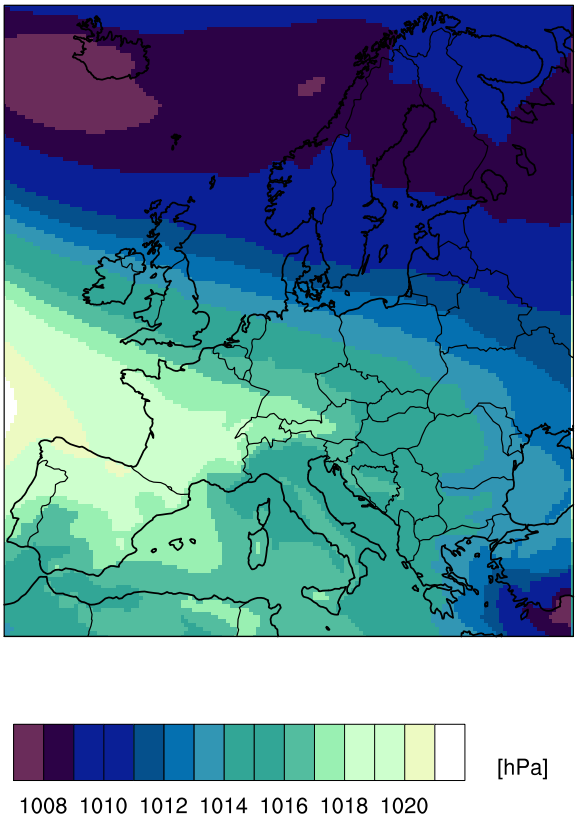

Figure 4.8: Simulated climatology of the MSLP in hPa over the time period 1971–2000 in summer.

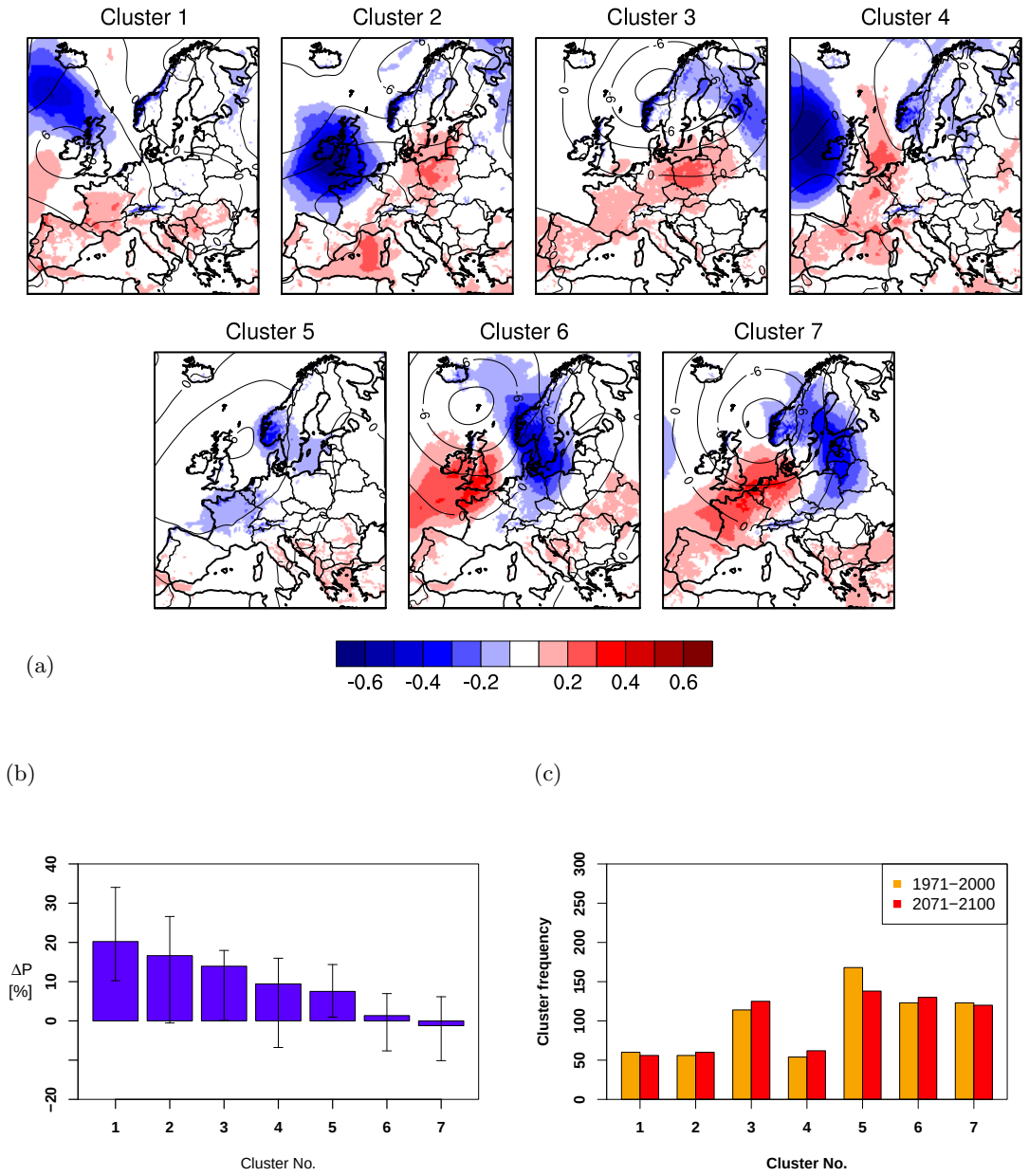

Figure 4.9: (a) Clusters of MFD conditional on heavy precipitation over Southwest Norway in summer. Filled contours mark the pattern of MFD (positive values, red) or MFC (negative values, blue). Cluster are sorted in decreasing order by the strength of the heavy precipitation change signal. Black lines show the MSLP isobars. (b) Relative changes (2071–2100 minus 1971–2000) of the mean exceedances over the 95% quantile of precipitation for each cluster in %. The error bars denote the 90 % confidence intervals estimated with a Wilcoxon rank sum test. (c) Frequency of the clusters in present (yellow) and future (red).

In particular, the patterns associated with negative changes in heavy precipitation become less frequent.

The clusters conditioned on heavy precipitation over East Romania and Moldova in summer go along with very weak pressure anomalies and there is no clear indication for favorable flow conditions. MFC is present over the sub-region in Cluster 5 and in Cluster 6, whereas even a divergent pattern is found for Cluster 4.

Heavy precipitation increases by up to 23 % in Cluster 1–5, while weak decreasing changes are found for Cluster 6 (Figure 4.11(b)). As for the Alps in summer, decreasing trends in the number of clusters dominate, which indicates a decrease in the total number of heavy precipitation events. However, the magnitudes of the changes in heavy precipitation cannot be attributed to the changes in the cluster number.

For heavy precipitation over South Italy (Figure 4.12(a)), similar to East Romania and Moldova, the clusters exhibit no relevant pressure anomalies determining the flow situation. At the same time, the MFD is weak or shows even positive, divergent values (Cluster 5) in the sub-region. These findings indicate a mainly convective nature of heavy precipitation in this sub-region. Inspection of the convective versus large-scale fraction of the heavy precipitation events (not shown) confirms this suggestion.

Heavy precipitation decreases for all six regimes (Figure 4.12(b)). The strongest changes in Cluster 5 constitute -40%. In the other patterns, the projected changes range between 23 and 25 %. Also for South Italy, the number of corresponding days with heavy precipitation decreases for most clusters (Figure 4.12(c)).

Figure 4.13 shows the anomalies and changes of regional averages in precipitation-related variables for each cluster in each of the four sub-regions in summer. It is striking that the anomalies are in general weaker for summer than for the winter. The anomalies of the vertically integrated water vapor are positive in particular in the warmer regions East Romania/Moldova (Figure 4.13(c)) and South Italy (Figure 4.13(d)). As in winter, the projected future changes of the vertically integrated water vapor are strong for all regions. Meaningful anomalies of the MFD are only found for Southwest Norway (Figure 4.13(a)). They show the largest changes in Cluster 1–4 which are associated with the largest heavy precipitation changes. Over the Alps (Figure 4.13(b)), the conditions become more divergent in all clusters. In South Italy, the strongest negative changes in heavy precipitation for South Italy occur together with a divergent pattern of the moisture flux. The absence of convergent anomalies in this region is reflected by the fact that the convective fraction of precipitation amounts for the majority of the decreasing trend (not shown). Changes in evaporation are not relevant in Southwest Norway and in the Alps, but decreasing trends are detected for all clusters in East Romania/Moldova and South Italy, which reflects the drying tendencies in these regions. The anomalies of the vertical velocity are mainly negative, indicating upwards directed air movements. Whereas the upward vertical velocities increase for Southwest Norway in the clusters with the strongest increases in heavy precipitation, the vertical velocities

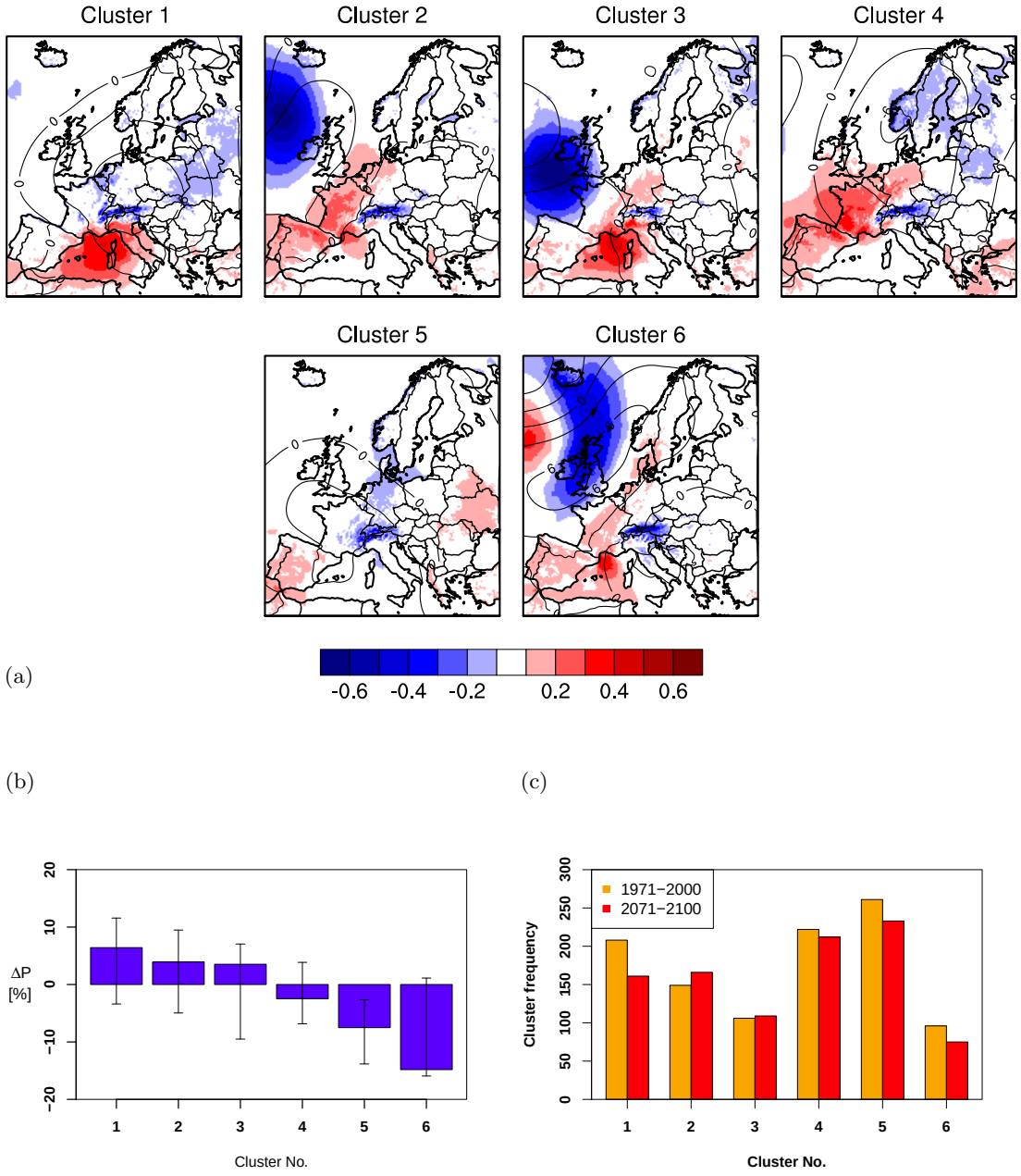

Figure 4.10: As 4.9, but for the Alps in summer.

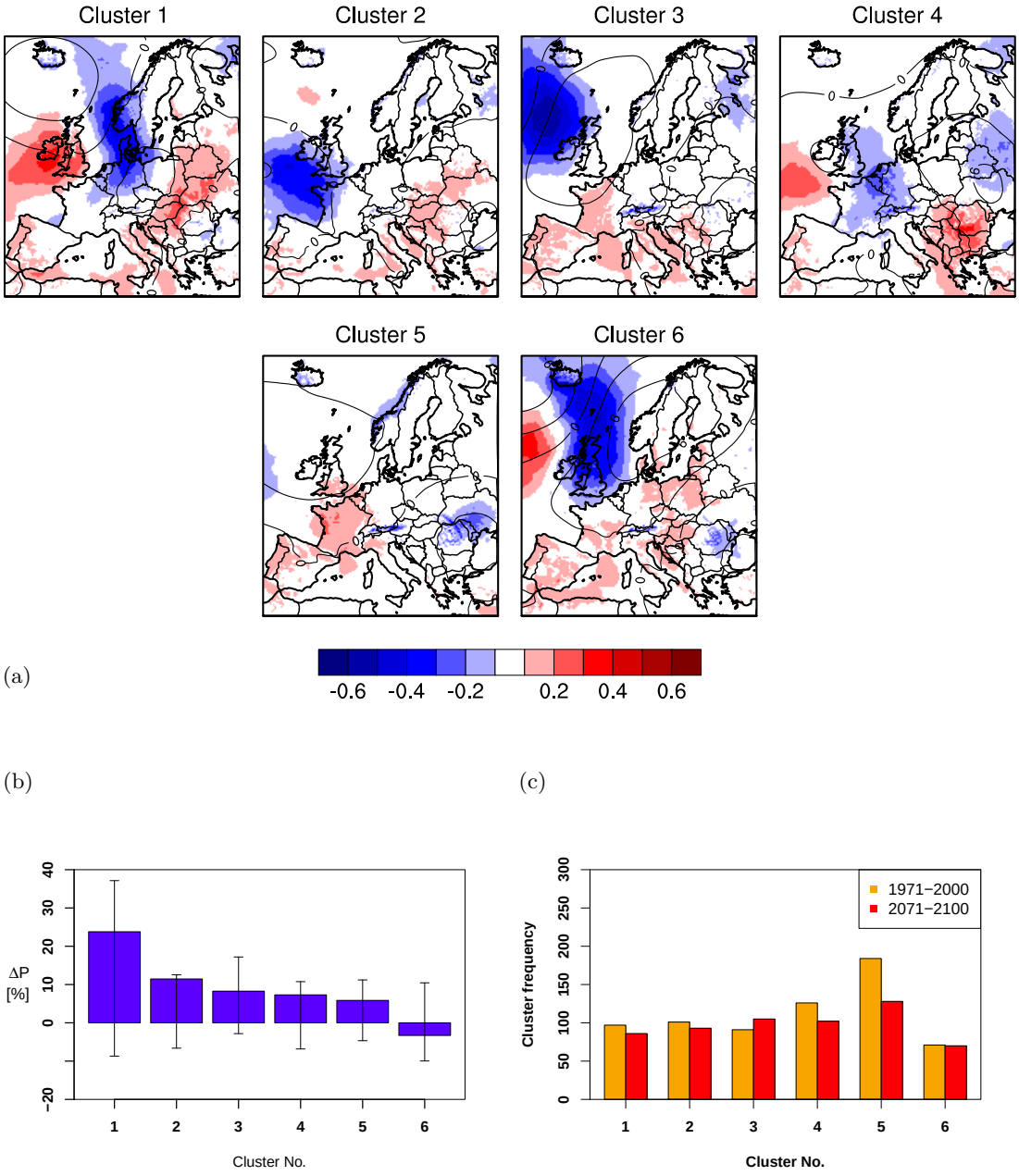

Figure 4.11: As 4.9, but for the East Romania and Moldova in summer.

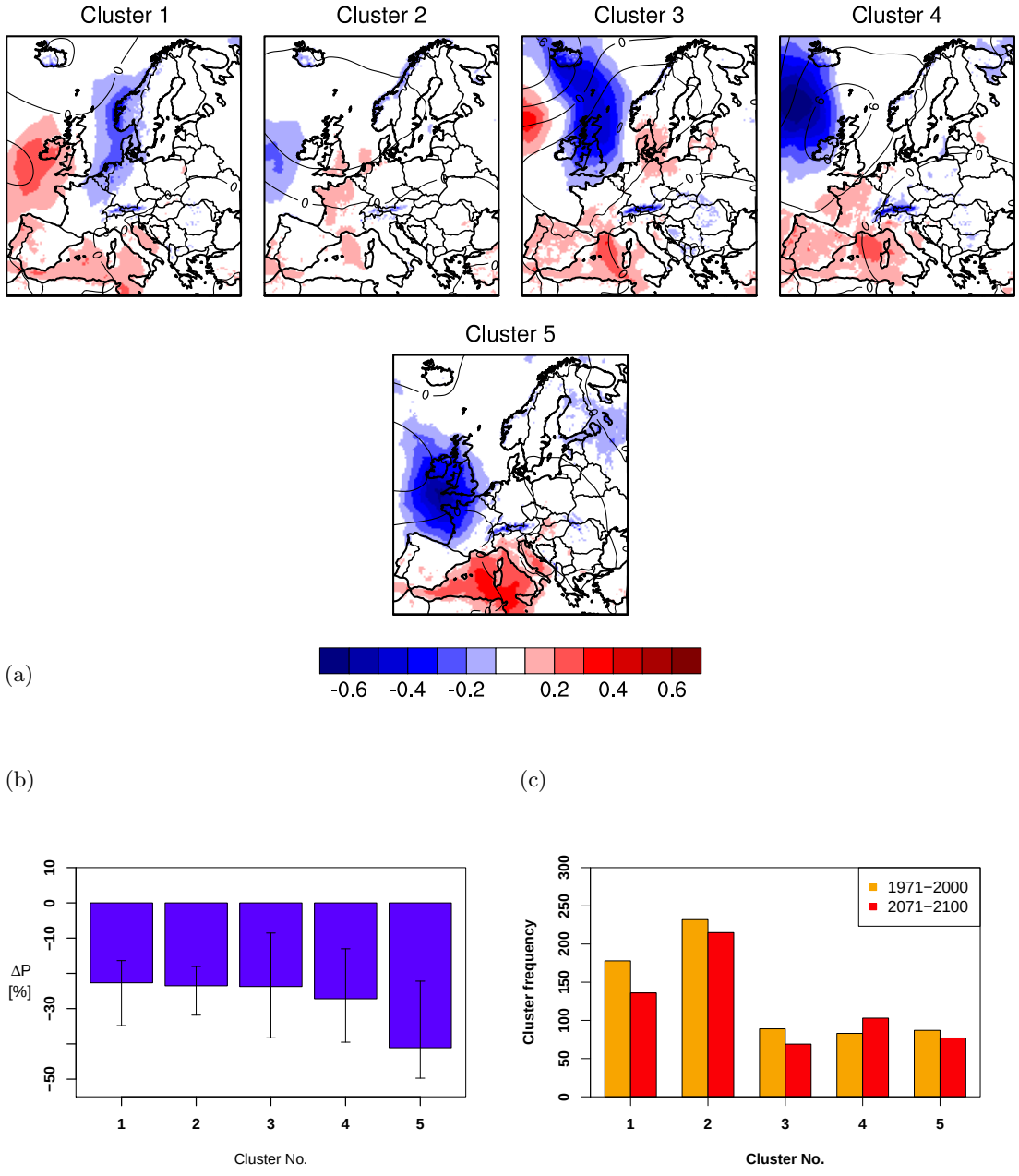

Figure 4.12: As 4.9, but for South Italy in summer.

in South Italy and Romania change towards slightly more downward and thus stable conditions, in particular in the clusters with the strongest negative heavy precipitation changes.

4.4 Covariates for heavy precipitation on regional scales

In this section, extreme value statistics are used to examine the best predictors from a set of variables related to heavy precipitation formation on climatic time scales over Europe. The role of dynamic versus thermodynamic covariates is analyzed in present and future. On the dynamic side, vertical velocity ω is investigated as covariate. The moisture variables q_v and q_l and the evaporation E serve as thermodynamic covariates. A combination of both effects is represented by the moisture flux divergence MFD, which can be modified both by changes in the flow and by changes in the water vapor. The combinations of covariates are numbered from 1 to 31 (Table 4.2).

4.4.1 Model selection with the Aikaike information criterion

Figures 4.14–4.17 show bar plots of the AIC values for the set of statistical models for heavy precipitation including the regional covariates q_v, q_l, E,MFD, and ω in each sub-region and season, in present and future time period. As described above, the minimum AIC denotes the best model out of a set of candidate models. Yet, it is possible that the difference between the best model and the subsequent models are insignificant. In the Figures 4.14–4.17, the best four models are highlighted in black. The relative probability that a certain model is the best one of the set can be analyzed by calculating the Aikaike weights, which are shown in the Tables 4.3–4.6.

Figure 4.14 illustrates the AIC for Southwestern Norway. In winter (Figure 4.14a and 4.14b) the best models include the moisture flux divergence MFD, either alone or in combination with other covariates. Additionally, models with a smaller number of covariates are favored before models with more covariates. In the summer (Figure 4.14c and 4.14d), the vertical velocity ω is an important covariate besides and in combination with the MFD. This appears to be even more relevant in the future (Figure 4.14d). Table 4.3 shows the corresponding Aikaike weights, indicating that the MFD alone has the highest probability to be the best predictor in winter. In the present time period, the combination of MFD and q_l has some probability, too. The Aikaike weights further indicate that in summer, ω gains relevance in the future time period.in the future time period.

As in Southwest Norway, the best models for heavy winter precipitation in the Alps (Figure 4.15) include the MFD as predictor. The Aikaike weights (Table 4.4) clearly indicate MFD alone to represent the best model in the present time period. In the future, q_l becomes important in addition to MFD in winter, and this model is the best

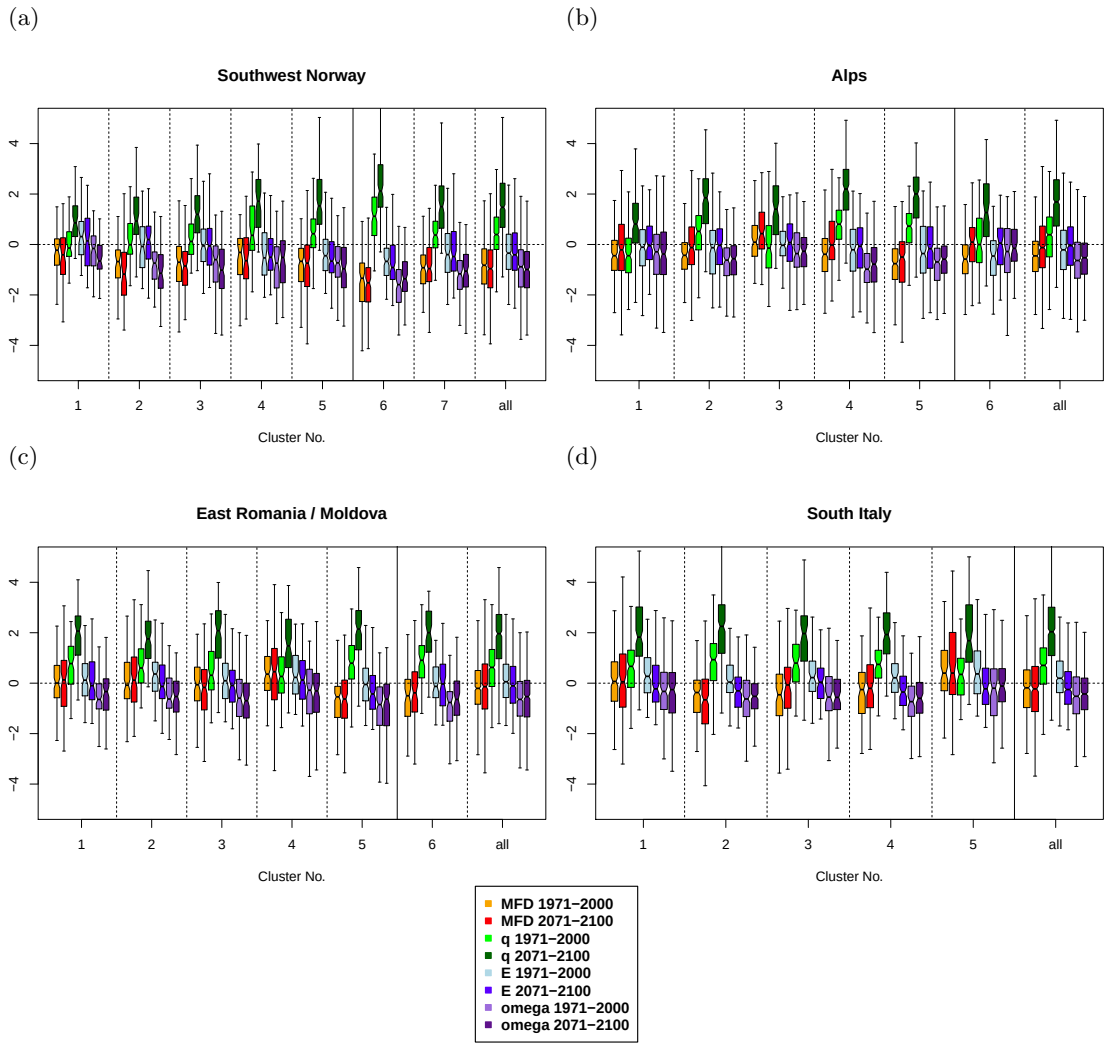

Figure 4.13: Regional average anomalies for present and future in summer of MFD (yellow and red), q_v (light green and green), E (light blue and blue), and ω (light purple and purple) conditioned on each cluster and for all time steps with heavy precipitation occurrence. The boxes denote the interquartile range, the whiskers extend to the most extreme data points. For (a) Southwest Norway, (b) the Alps, (c) East Romania and Moldova, (d) South Italy.

Table 4.2: Numbering of models including all possible combinations of covariates.

Model No.	Covariates
1	q_v
2	q_l
3	E
4	MFD
5	ω
6	q_v, q_l
7	q_v, E
8	q_v, MFD
9	q_v, ω
10	q_l, E
11	q_l, MFD
12	q_l, ω
13	E, MFD
14	E, ω
15	MFD, ω
16	q_v, q_l, E
17	q_v, q_l, MFD
18	q_v, q_l, ω
19	q_v, E, MFD
20	q_v, E, ω
21	q_v, MFD, ω
22	q_l, E, MFD
23	q_l, E, ω
24	q_l, MFD, ω
25	E, MFD, ω
26	q_v, q_l, E, MFD
27	q_v, q_l, E, ω
28	q_v, q_l, MFD, ω
29	q_v, E, MFD, ω
30	q_l, E, MFD, ω
31	q_v, q_l, E, MFD, ω

Table 4.3: Selection of the best models for heavy precipitation in Southwest Norway according to their Aikaike weights.

	DJF_{pres}		DJF_{fut}		JJA_{pres}		JJA_{fut}	
Rank	Model	w_i	Model	w_i	Model	w_i	Model	w_i
1	MFD	0.814	MFD	1.000	MFD, ω	0.732	ω	0.916
2	MFD, q_l	0.186	MFD, ω	0.000	ω	0.268	MFD, ω	0.062
3	MFD, ω	0.001	MFD, q_v	0.000	MFD, ω, E	0.000	ω, E	0.001
4	MFD, E	0.000	MFD, q_l	0.000	ω, E	0.000	MFD, ω, q_v	0.000

with a probability of 89.4%. In summer, MFD and ω are the best predictors and ω becomes more relevant in the future, similar to Southwest Norway. Whereas the best model in the present period consists of MFD alone, the Aikaike weights in Table 4.4 show clear evidence for the combination of MFD and ω to fit the data best in the future.

In East Romania and Moldova, the models with the lowest AICs for winter (Figure 4.16a and 4.16b) include ω and the vertically integrated cloud water q_l as covariates. The Aikaike weights (Table 4.5) indicate that ω alone represents the best model in the present time period and the combination of ω and q_l has a probability of 25.3% to be first. Yet, the latter is the best model in the future with very high probability. Models including E, while excluding ω or q_l perform worst over the Alps in winter. However, E improves as predictor in the future time period. In contrast to the winter months, q_l is not relevant in summer (Figure 4.16c and 4.16d). Instead ω is important as only covariate, indicated by high Aikaike weights (Table 4.5) or in combination with the vertically integrated water vapor or MFD. As in winter, the models of which E is part perform better in the future.

In contrast to the other sub-regions, it strikes for South Italy (Figure 4.17) that models with only one predictor do not exhibit the lowest AICs. The best models comprise both q_v and E. In the present time period in winter, the corresponding Aikaike weights (Table 4.6 indicate that the best model includes the MFD in addition to q_v and E. Though, in the future time period MFD is omitted. Also in the summer, the model including MFD loses probability to perform best. Figure 4.17 further indicates that E becomes more likely single predictor, both for winter and for summer.

4.4.2 Cross validation

The Aikaike information criteria give information on which model out of a set of candidate models performs best, but it is possible that the selected model is only the best in a set of bad models. A goodness-of-fit test of the identified statistical model is therefore assessed using a cross validation technique and the Brier skill score (BSS).

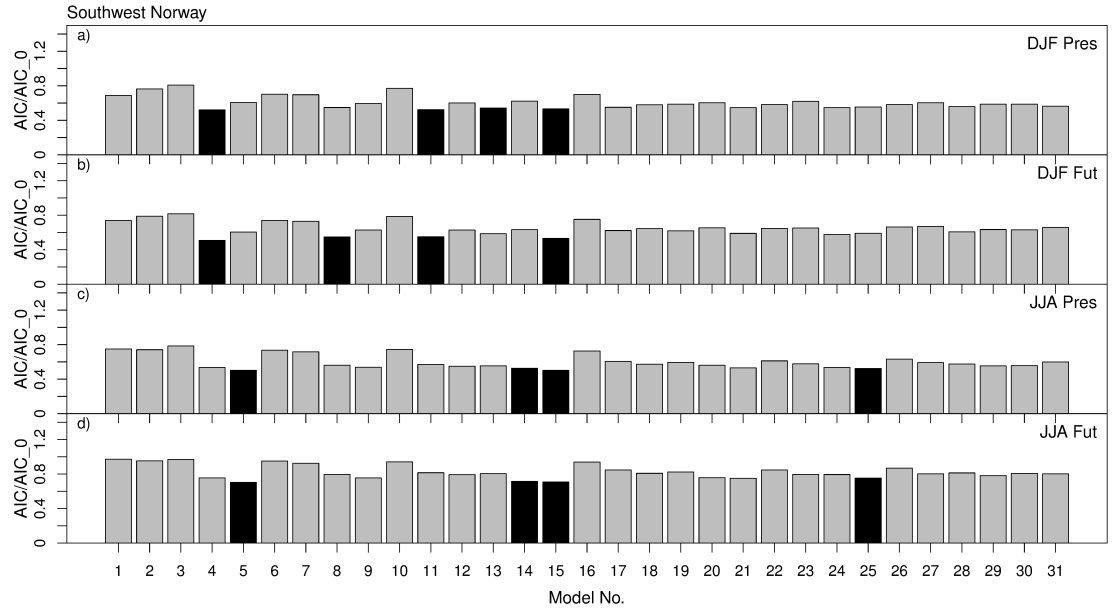

Figure 4.14: AICs of each model out of the set (see Table 4.2) relative to the statistical model without covariates (AIC_0) for Southwest Norway. a) DJF present, b) DJF future, c) JJA present, d) JJA future. The best four models are marked in black.

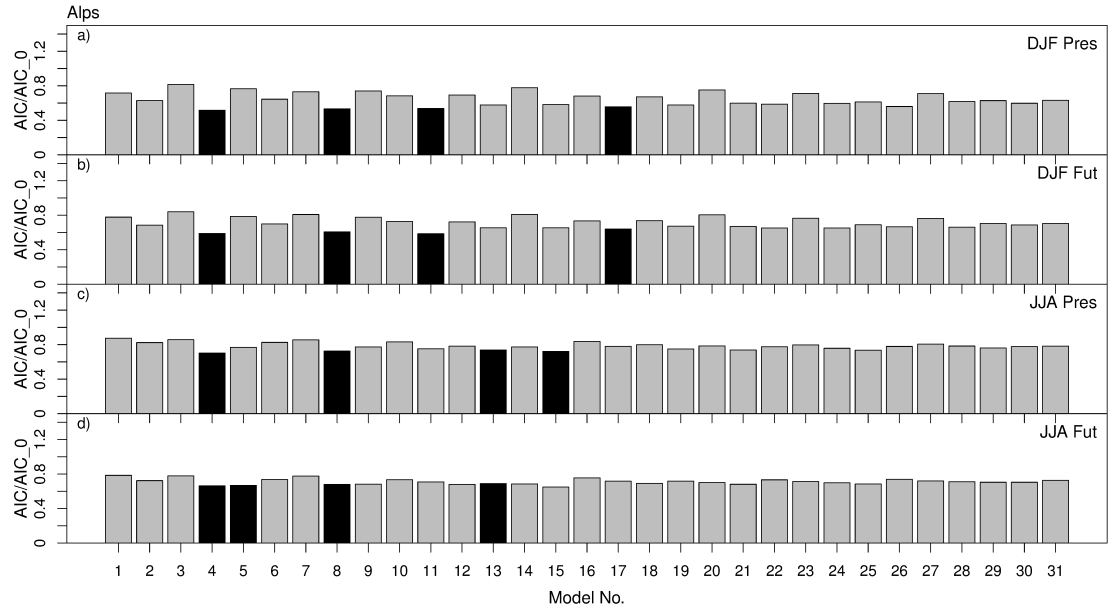

Figure 4.15: As Figure 4.14, but for the Alps.

Table 4.4: As Table 4.3, but for heavy precipitation in the Alps.

	DJF_{pres}		DJF_{fut}		JJA_{pres}		JJA_{fut}	
Rank	Model	w_i	Model	w_i	Model	w_i	Model	w_i
1	MFD	1.000	MFD, q_l	0.894	MFD	1.000	MFD, ω	1.000
2	MFD, q_v	0.000	MFD	0.106	MFD, ω	0.000	MFD	0.000
3	MFD, q_l	0.000	MFD, q_v	0.000	MFD, q_v	0.000	ω	0.000
4	MFD, q_v, q_l	0.000	MFD, q_v, q_l	0.000	MFD, ω, E	0.000	MFD, q_v	0.000

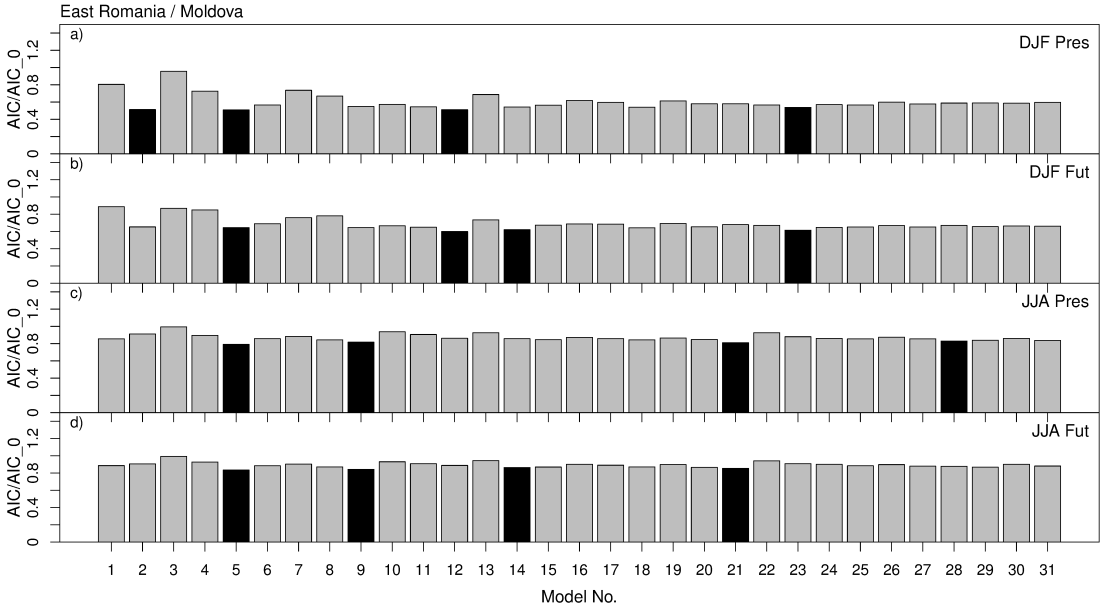

Figure 4.16: As Figure 4.14, but for East Romania and Moldova.

Table 4.5: As Table 4.3, but for heavy precipitation in East Romania and Moldova.

	DJF_{pres}		DJF_{fut}		JJA_{pres}		JJA_{fut}	
Rank	Model	w_i	Model	w_i	Model	w_i	Model	w_i
1	ω	0.615	ω, q_l	0.997	ω	1.000	ω	0.987
2	ω, q_l	0.253	ω, q_l, E	0.003	MFD, ω, q_v	0.000	ω, q_v	0.013
3	q_l	0.132	ω, E	0.000	ω, q_v	0.000	MFD, ω, q_v	0.000
4	ω, q_l, E	0.000	ω, q_v, q_l	0.000	MFD, ω, q_v, q_l	0.000	ω, E	0.000

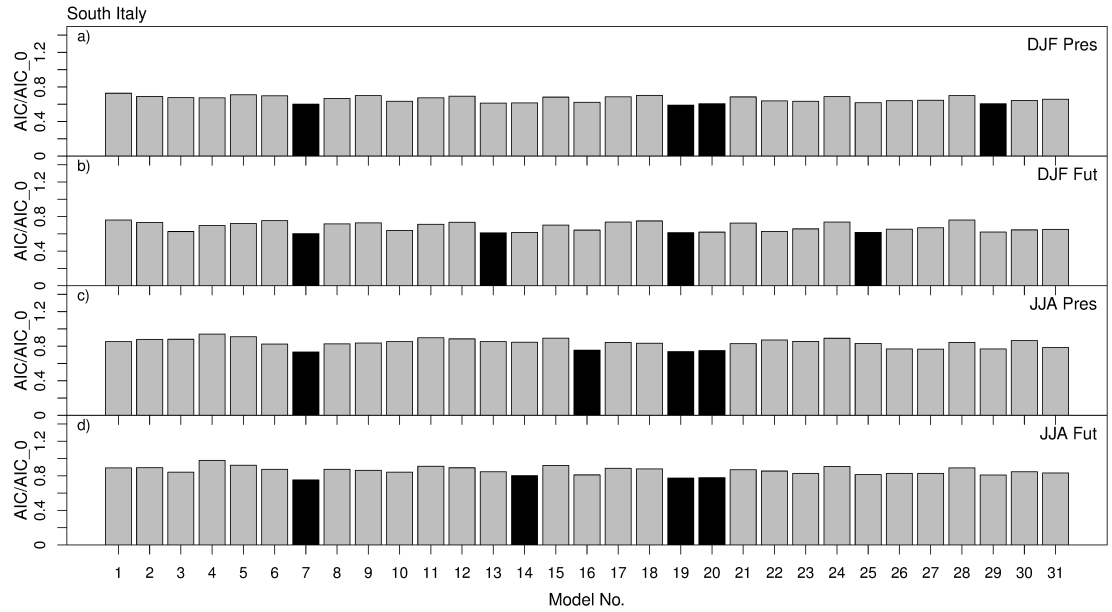

Figure 4.17: As Figure 4.14, but for South Italy.

Table 4.6: As Table 4.3, but for heavy precipitation in South Italy.

	DJF_{pres}		DJF_{fut}		JJA_{pres}		JJA_{fut}	
Rank	Model	w_i	Model	w_i	Model	w_i	Model	w_i
1	MFD, q_v, E	0.999	q_v, E	0.997	q_v, E	0.879	q_v, E	1.000
2	q_v, E	0.001	q_v, E	0.002	MFD, q_v, E	0.120	MFD, q_v, E	0.000
3	MFD, ω, q_v, E	0.000	MFD, q_v, E	0.001	ω, q_v, E	0.001	ω, q_v, E	0.000
4	ω, q_v, E	0.000	ω, q_v, E	0.000	q_v, q_l, E	0.000	ω, E	0.000

In the cross-validation procedure, explained in Chapter 4.2.4, the predictive skill of a model is assessed by successively removing one year of the time period for estimating the parameters of the covariate-dependent models and predicting the probabilities of daily precipitation totals to exceed a certain threshold in the removed year. The BSS is determined for each separate year as well as for the entire time period. In this way, information on the prediction uncertainty is obtained. The AIC analysis has revealed a preference for selection of models with one or two covariates. Therefore, the cross validation is carried out for model 1–15 (Table 4.2) only. The BSS is calculated for different thresholds, which are the climatological quantiles ranging from 95% to 99%.

In Figure 4.18–4.21 box-whisker plots of the BSS are presented for each sub-region, separately for winter and summer in present and future. The boxes mark the interquartile range of BSS values across the years in the 30-year time period and the whiskers extent to the most extreme data points.

For Southwest Norway the importance of the MFD as covariate is confirmed by the analysis of the BSS in both seasons, indicated by the highest BSS values for this covariate (Figure 4.18). Besides the MFD as only covariate, some predictive skill is awarded to models including MFD combined with a second variable, e.g. q_v or q_l. In addition, the relevance of ω is stressed, which in summer is at least of same relevance as MFD, and even more relevant in the future. These results reflect the findings from the AIC analysis in the section before. The values of the BSS for the best models are in the range between 0.2 and 0.3 on average over the 30-year period, which implies a 20–30 % gain of predictive skill compared to the reference model, i.e. the climatological probability for threshold exceedance. It can also be seen that the predictive skill decreases as the threshold increases. This is however less the case for summer than for winter.

The analysis of the BSS for the Alps 4.19 confirms the MFD as best performing covariate for heavy precipitation in both seasons. As for Southwest Norway, ω is more relevant in summer than in winter, in particular in the future time period. The values of the BSS for the best model range between 10% and 30%, depending on the threshold.

In agreement with the AIC analysis in the section before, ω is identified also by the cross validation as best covariate for heavy precipitation in East Romania and Moldova (Figure 4.20). The variability of the BSS values across the 30 years, illustrated by the whiskers, is large in winter, which implies uncertainty in the estimation of the BSS for the whole time period. The models including ω show an average gain in predictive skill of 30% compared to the reference model in winter. The BSS values remain relatively constant across the thresholds. Also in summer, the best predictive skill is awarded to ω, but is much smaller than in winter.

For South Italy, only very small BSS values are found for winter (Figure 4.21). In summer though, the combination of q_v and E (Model No. 7) as best predictors is confirmed. The gain of predictive skill for this model is about 20% against the reference

model.

The results of this chapter so far have shown that different regional covariates are the best predictors for heavy daily precipitation events in different sub-regions and seasons. Whereas the MFD is the best predictor in the colder regions, Southwest Norway and the Alps, the vertical velocity ω is dominant in the East European sub-region. Again a contrasting picture is found for South Italy, where the evaporation in combination with the vertically integrated water vapor exhibits the best model. These findings indicate that different processes are responsible for heavy precipitation formation. The processes are to some extent dependent on the temperature. It is striking that in Southwest Norway and in the Alps ω is more important in the summer, in particular in the future time period. Seeing that ω is a good predictor in the warmer East European region leads to the conclusion that ω becomes more important in warmer climatic conditions. But there are limits: In the warmest region, South Italy, it is the local availability of water, represented by q_v, evaporating from the ground (E), which determine the probability of heavy precipitation occurrence. In this dry region the limited availability of water causes a limit to the relative humidity, in contrast to the more northern regions, where the air is on average closer to saturation.

4.4.3 Parameter combinations of the identified models

The parameter combinations of the Poisson point process models with the most suitable covariate identified by the analyses in section 4.4.1 and 4.4.2 for the future time period are given in Table 4.7 for each region. The parameters have been estimated based on centered and scaled covariate vectors, which makes them independent of the range of the variable and comparable. The influence of the MFD as regional predictor for the Alps and for Norway is large in winter, in particular in the location parameter for which the covariate dependency represented by β_1 is up to 24% of μ_0. As expected, the relation is negative, i.e. heavy precipitation will increase when the moisture flux is strongly convergent. Large dependencies are also found for the dynamic covariate ω, in particular for Southwest Norway in summer. Negative values here denote that increased upward directed velocities cause stronger precipitation events. In the Alps and East Romania/Moldova in winter also the column-integrated liquid water q_l significantly contributes to a positive shift of the location parameter. The strongest influence in South Italy comes from the evaporation E in both seasons, indicating that the probability for heavy precipitation strongly depends on the local availability of water. In summer, the dependency of the scale parameter on q_v is strongly negative in relative terms. Less column water vapor thus means a higher day-to-day variability in the probability for heavy precipitation occurrence. This might indicate that heavy precipitation occurs less frequently, but with higher intensity, such as in strong convective events.

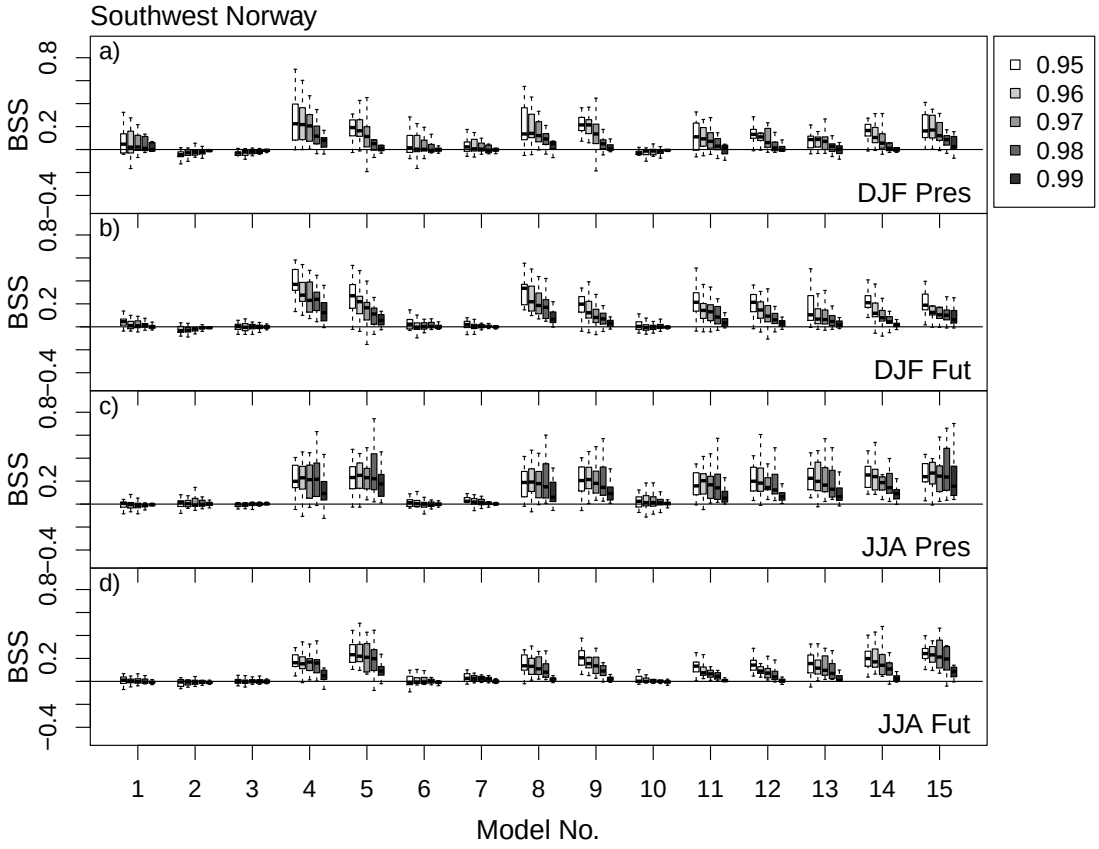

Figure 4.18: Brier skill scores for the first 15 combinations of covariates from Table 4.2 for Southwest Norway. The skill scores are calculated to assess the skill of predicting of the probabilities for exceeding different thresholds, which are climatological quantiles ranging from 95% to 99%. The boxes show the interquartile range and the whiskers extent to the maximum and minimum yearly BSS over the cross-validated time period of 30 years. The rows of the panel show the results for a) winter present, b) winter future, c) summer present, d) summer future.

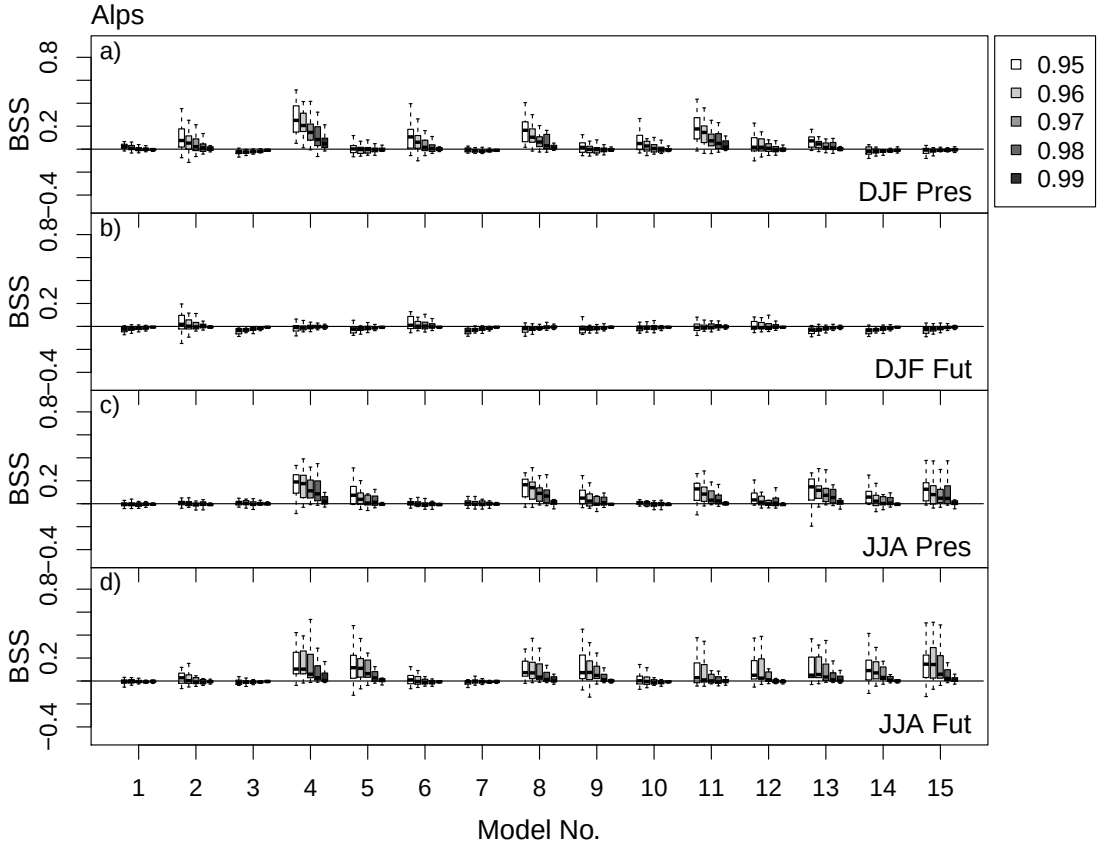

Figure 4.19: As figure 4.18, but for the Alps.

Table 4.7: Parameter combinations for the PPP models. β_1 and γ_1 describe the dependency of the location and scale parameter on the first covariate, β_2 and γ_2 the dependency on the second covariate. They are marked in bold font.

Region	Covariates	μ_0	β_1	β_2	σ_0	γ_1	γ_2	ξ
Southw. Norway DJF	MFD	79.86	**-19.65**	-	2.11	**-0.16**	-	-0.09
Southw. Norway JJA	ω	82.52	**-14.11**	-	2.84	**0.11**	-	-0.16
Alps DJF	MFD, q_l	78.99	**-10.83**	**9.74**	3.04	**-0.19**	**-0.06**	-0.05
Alps JJA	MFD, ω	89.35	**-11.89**	**2.98**	2.71	**-0.08**	**-0.04**	0.08
East Rom./Mol. DJF	ω, q_l	35.63	**-6.45**	**4.47**	2.23	**-0.04**	**-0.04**	-0.15
East Rom./Mol. JJA	ω	66.77	**-7.22**	-	3.15	**0.02**	-	0.17
South Italy DJF	q_v, E	73.29	**6.24**	**14.66**	2.54	**0.04**	**0.16**	-0.02
South Italy JJA	q_v, E	45.93	**4.11**	**6.58**	3.09	**-0.27**	**-0.19**	-0.16

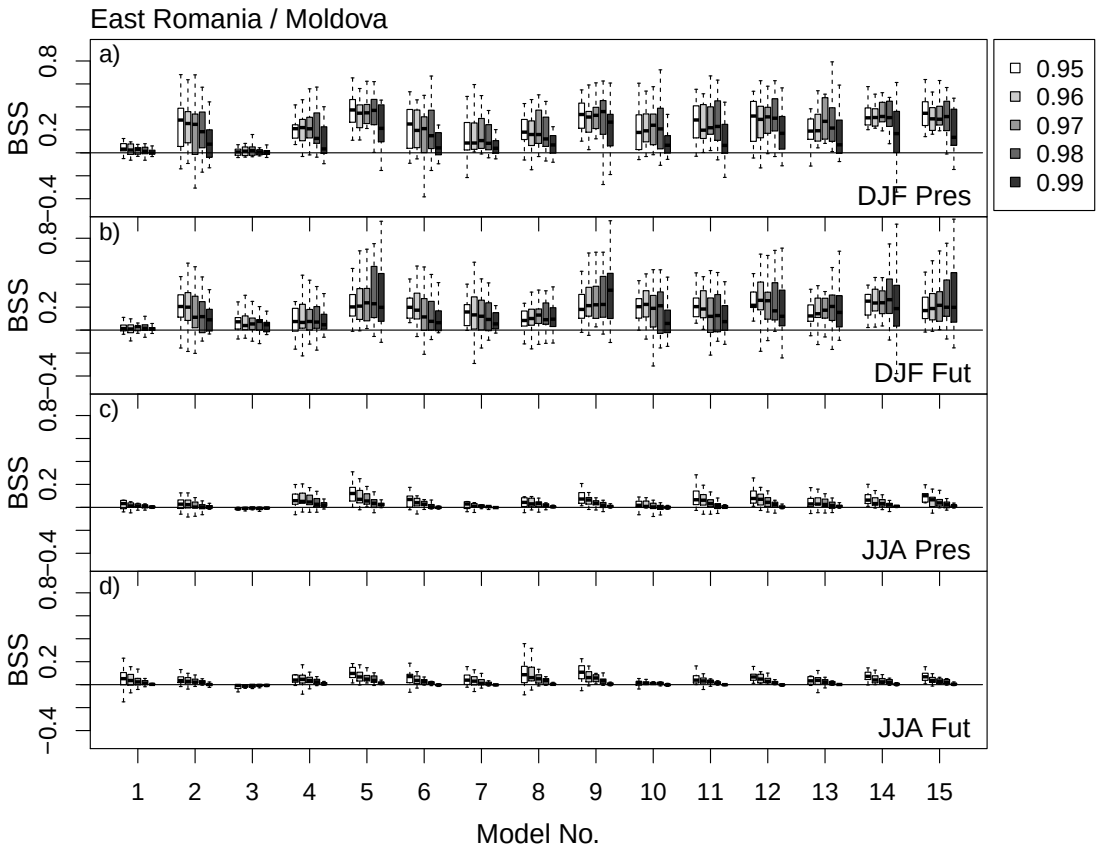

Figure 4.20: As figure 4.18, but for East Romania and Moldova.

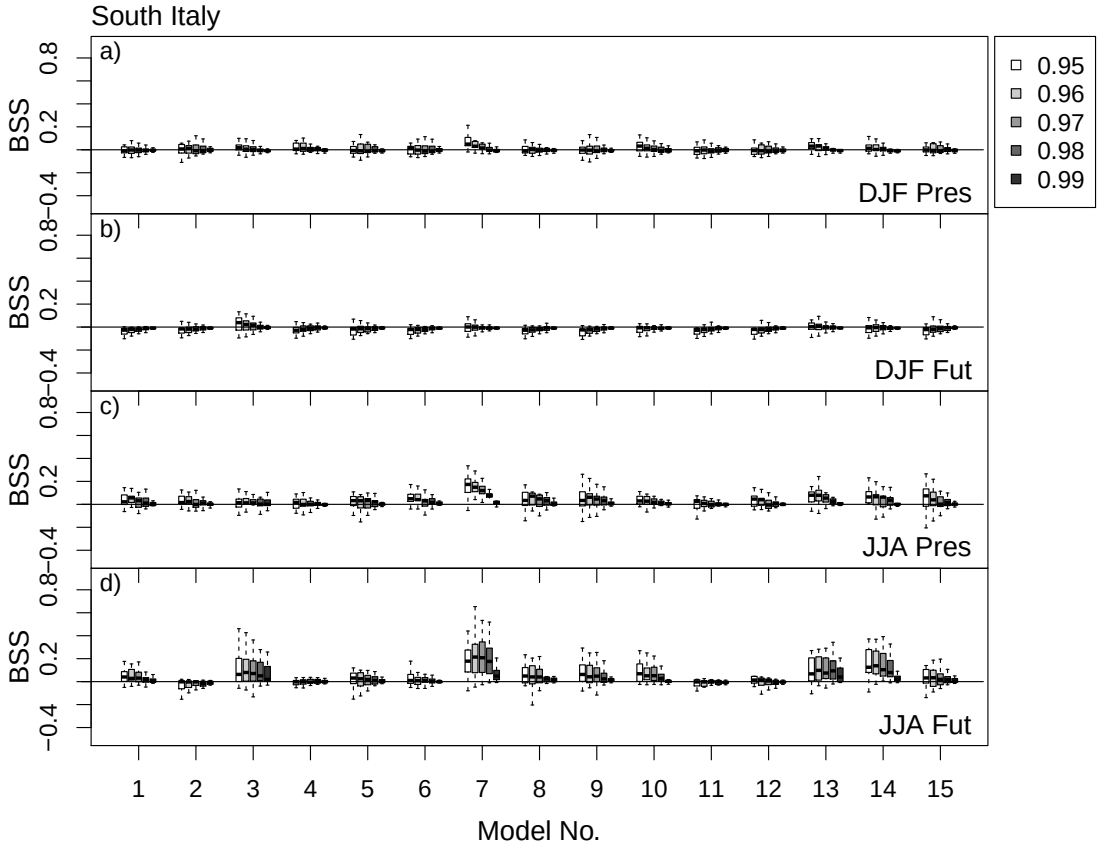

Figure 4.21: As figure 4.18, but for South Italy.

4.5 Discussion and Conclusions

In this chapter a cluster analysis of the moisture flux divergence has been applied to the European domain conditioned on heavy precipitation occurrence in four European sub-regions with different climatic characteristics. Suitable covariates for heavy precipitation based on the moisture balance equation have been identified in the second part.

In the colder and more dynamically influenced regions Southwest Norway and the Alps, the MFD clearly plays a large role for changes of heavy precipitation. In particular strong changes are found for synoptic situations with high MFC anomalies over the respective sub-region. Furthermore, characteristic synoptic patterns favorable for heavy precipitation formation are identified, such as flow from the southwest to south for Southwest Norway and from the northwest to north for the Alps in winter. There is a tendency that such situations become slightly more frequent in the future. Inspection of the simulated winds in 850 hPa (not shown) confirms a future shift by 10 degrees southwards on average in Southwest Norway. Yet, in general, shifts in the wind directions are small.

The anomalies and changes of the MFD and the vertically integrated water vapor are connected, but MFD clearly rules out the latter as predictor for heavy precipitation in Southwest Norway and the Alps. Also, the regional averages of q_v are not anomalously high in general at the times of heavy precipitation occurrence. The lesson learned from this is that its is not the actual amount of vertically integrated water vapor by itself which controls heavy precipitation, but rather the vertically integrated moisture flux which converges in the region. Since $MFC = -\nabla q\vec{v}$, this leads to the conclusion that heavy precipitation changes are steered by both the dynamics and the moisture amount and do not necessarily scale immediately with the Clausius-Clapeyron like change in water vapor over the same region. It is therefore rather the large-scale than the regional changes in q_v in conjunction with the dynamics that play the decisive role for heavy precipitation changes.

For warmer climate conditions, as for the future in Southwest Norway and the Alps, in particular in summer, and in East Romania/Moldova in both seasons in present and future, the importance of the vertical velocity as predictor for heavy precipitation increases, whereas the MFD loses importance. The advection of moisture thus plays a less important role and the local dynamics gain relevance compared to the large-scale dynamics. The vertical velocities are connected to the formation of clouds, which is reflected by the column cloud liquid water being a relevant covariate besides ω in East Romania and Moldova in winter.

With warmer temperatures in summer, the water vapor gains importance as second best predictor in the same region. Together with the evaporation, q_v also plays a decisive role in South Italy in both seasons. The lower troposphere in these regions is

in particular in summer far below saturation on average. Therefore, the amount of q_v is anomalously high at the time of heavy precipitation occurrence (see Figure 4.13(d)). It is thus the availability of water vapor, which controls whether heavy precipitation can form. The local availability is reflected in the amount of water which can evaporate from the surface and is fed into the clouds. The importance of the evaporation is stressed by the large dependence of the parameters in the respective extreme value models on this covariate. Due to the future drying of the soil, less water can evaporate, which leads to negative trends in heavy precipitation. The decreasing influence of the dynamic predictors MFD and ω stresses the mainly thermodynamic nature of heavy precipitation in this region. The recycling ratio, which is the ratio of precipitation coming from water through evaporation in the region itself versus the precipitation of water advected to the region (Trenberth 1998), is large. The analyses of the changes in ω over the European domain (Figure 5.1, Chapter 5) further indicate more downwards directed and thus more divergent motions on average for the Mediterranean region, in particular in summer. This effect probably enhances the decrease of heavy precipitation in Southern Europe.

Summary of Chapter 5

In Chapter 4, dynamic and thermodynamic causes for heavy precipitation formation and projected future changes are analyzed from an RCM simulation using a cluster analysis and extreme value statistics. In particular for the dynamically influenced regions in winter, the cluster analysis reveals characteristic patterns of moisture flux divergence and synoptic scale flow favorable for heavy precipitation formation. The extreme value analysis indicates that the best suitable physical covariates for heavy precipitation – and thus the most important factors controlling the changes – are to a large extent dependent on the climatic conditions of the respective geographic region. The results highlight in particular a large importance of the dynamic covariates.

5 Final discussion and conclusions

In this study, causes for regional changes in heavy precipitation are investigated for Europe. In the following, the analyses and results are summarized, the findings across the chapters are linked together, and the most important aspects are conclusively discussed. Finally, the answers to the research questions posed in Chapter 1.1 are given and some outlook to possible continuations of the study is presented.

5.1 Summary of the results

In the first part (Chapter 2), robust climatic trends in highest quantiles of daily precipitation totals are analyzed in an ensemble of regional climate model simulations using non-stationary extreme value statistics. Positive trends in heavy precipitation are found for the entire domain in winter, with strongest changes over the northern parts of Europe. In summer, the changes are mainly negative in southern Europe, despite strong positive trends in the near-surface temperatures. The changes are found to be robust in terms of inter-simulation agreement for the largest part of the domain. Exceptions are for example the mountainous regions in winter.

The second aspect of the first part is the investigation of thermodynamic factors of influence for heavy precipitation. In this context, the Clausius-Clapeyron scaling of heavy precipitation is assessed on regional scales. On a grid-point basis only a limited scaling of changes in heavy precipitation with the vertically integrated water vapor is found. Besides the fact that the changes in the column water vapor reach up to 15 $\%/K$ according to the season and the simulation, whereas heavy precipitation changes range between 2 and 6 $\%/K$, spatial correlations between the trends in both variables are not detected everywhere in Europe. In particular, a weak relationship is found over Scandinavia. Instead, changes in heavy precipitation rather follow the pattern of changes in the vertically integrated cloud liquid water and show high correlations with the latter in different parts of Europe.

In the second part of the study (Chapter 3) thermodynamic relations and their connections with heavy precipitation occurrence are analyzed in observational datasets and in present-day RCM simulations for different European sub-domains during the summer months. The connections of water vapor and cloud water with near-surface temperatures are examined with focus on the Clausius-Clapeyron relation. Whereas the vertically integrated water vapor follows the Clausius-Clapeyron relation for low

and moderate temperatures, a weaker connection is found at the highest end of the temperature range. An explanation for the latter is an undersaturated atmosphere due to a limited availability of water vapor caused by reduced advection of moisture in the less dynamic synoptic situations that prevail at high temperatures. The cloud water increases with temperature in the colder range, but decreases at higher temperatures, probably due to an increase in the amount of convectively formed clouds from which water is more effectively removed by precipitation on sub-daily timescales.

In addition, the connection of heavy summer precipitation with the thermodynamically important variables water vapor and cloud water is further investigated in satellite observations and in the REMO simulations using an extreme value statistical model. It is found that high quantiles of precipitation do not exhibit a distinct relationship with the vertically integrated water vapor in any of the sub-regions, neither in the observations, nor in the model simulation. Consistently with the findings from Chapter 2, the vertically integrated cloud water represents a more appropriate predictor for the intensity of heavy daily precipitation totals in the summer season on regional scales. Instead of being controlled by the availability of water vapor at the time of occurrence, heavy precipitation in summer appears to be thermodynamically determined by the efficiency of the cloud formation, which is related to the structure of the boundary layer.

Whereas the focus of Chapter 2 and 3 lies in particular on the thermodynamic aspects of heavy precipitation occurrence and future changes, the impact of the atmospheric dynamics is examined in Chapter 4. The moisture flux divergence combines the availability of water vapor with the advection of moisture and balances evaporation and precipitation as sources and sinks of water in the water balance equation. A cluster analysis of the MFD is applied to an RCM simulation for the European domain with focus on four European sub-regions to investigate the synoptic situations favorable for heavy precipitation formation. In the second part of Chapter 4, dynamic and thermodynamic factors are combined by being examined as covariates for heavy precipitation using an extreme value analysis. The choice of the covariates MFD, vertical velocity ω, column water vapor q_v, column cloud liquid water q_l, and evaporation E is based on the atmospheric water balance equation. From all possible combinations of these variables, the ones most suitable to explain heavy precipitation variability and changes are identified by analysis of the Aikaike information criterion and through application of a cross validation procedure. Characteristic synoptic situations associated with strong regional moisture flux convergence favor heavy precipitation events over Southwest Norway and over the Alps. There is a tendency that such situations become slightly more frequent in the future. The importance of the large-scale dynamics is corroborated by the finding that the moisture flux divergence is the best predictor for heavy precipitation in these regions. Going to East Romania and Moldova, where the climate is less strongly influenced by the large-scale advection of moisture, the vertical velocity ω, represent-

ing the local dynamics, is most suitable to fit the heavy precipitation distribution. As suggested in Chapter 2, the availability of water through local evaporation is decisive for heavy precipitation formation in South Italy, the region with the driest climate.

5.2 Discussion

The results of this study have shown that a purely thermodynamic scaling of heavy precipitation changes has limits on regional scales. Instead, the best regional covariates for heavy precipitation depend on the climatic characteristics of the respective region. Both thermodynamic and dynamic aspects have to be considered.

Concerning heavy precipitation changes over Europe, two aspects have been mentioned in particular and will be discussed in more detail by linking the findings from Chapter 2, 3, and 4. First (a), in the higher latitudes, the simulated changes in heavy precipitation are largest for Europe, but still weaker in magnitude than the changes in precipitable water, besides not being well correlated. At the same time, the increases in precipitable water are as strong or even stronger than suggested by the Clausius-Clapeyron relation. Second (b), in the south of Europe, in particular in summer, the changes in heavy precipitation are negative over large parts. Besides, it is indicated both in Chapter 2 and 3 that the increase in precipitable water in the warmest regions and for the highest temperature range is weaker than predicted by the Clausius-Clapeyron relation, associated with negative changes in the relative humidity.

(a)

In the first case the region is strongly influenced by the large-scale dynamics, in particular in winter. In Chapter 4 the moisture flux divergence, which incorporates both moisture content and atmospheric transports, is identified as the best covariate for heavy precipitation in Southwest Norway. The occurrence of heavy precipitation is thus controlled by the moisture which is advected by storms and converges in this region. In synopsis with the result from Chapter 2 that changes in heavy precipitation are weaker than changes in the vertically integrated water vapor, the dynamics may play the decisive role for changes in heavy precipitation here. Some tendencies for shifts in the dynamics are indicated by changes in the cluster frequencies, but the clusters of MFD may not be represent the changes adequately. Yet, indications for alterations in the dynamics are found by inspection of the changes in ω (Figure 5.1). Also related to the first aspect is the finding that the changes in heavy precipitation scale somewhat better with the column cloud liquid water than with the total column water vapor. The condensation rate and thus the formation of clouds is controlled by the vertical velocity as dynamic factor and the moist static stability of the boundary layer as thermodynamic aspect (Weaver and Ramanathan 1997). The vertical velocities over northern

Europe show mainly decreasing trends (Figure 5.1), i.e. changes towards a weakening of the upward motion of air masses. This is in particular the case over the Norwegian Sea and along the west coast of Norway, where the projected changes in heavy precipitation and cloud liquid water are weakest. It might thus be an explanation why the changes in cloud liquid water and heavy precipitation are damped compared to the changes in vertically integrated water vapor. The influence of ω and static stability effects on heavy precipitation is also discussed by O'Gorman and Schneider (2009a), who assess a scaling for heavy precipitation which is based on the condensation rate, being related to the moist-adiabatic derivative of the saturation water vapor as thermodynamic part and ω accounting for the dynamic influence. The moist-adiabatic derivative of the saturation water vapor is related to the moist static stability. The authors argue that the increase in the moist-adiabatic derivative of saturation water vapor is weaker than the increase in vertically integrated saturation water vapor due to a weakening of the moist-adiabatic temperature lapse rate caused by increased latent heat release. As a consequence, the increase in the condensation rate is damped. The scaling (for equations see Appendix B) has been calculated on grid-point basis with the data from the REMO simulation analyzed in Chapter 2 and 4. In Figure 5.2 the thermodynamic and the full scaling, including ω, are shown for winter. For northern Europe, the thermodynamic part indicates smaller changes than those in the vertically integrated water vapor analyzed in Chapter 2, but also does not explain the variance in heavy precipitation changes across the region. The full scaling appears to explain the changes in heavy precipitation better. In Southwest Norway, which was one of the subregions analyzed in Chapter 4, the explained variance R^2 of heavy precipitation changes by the full scaling is 51 % and the explained variance by the thermodynamic scaling is 19 %. Thus an interaction of dynamic and thermodynamic factors is suggested, which is in agreement with the finding from Chapter 4 that the MFD, which includes both aspects, is the best predictor for heavy precipitation in this region. One can conclude from this discussion that the changes in the dynamic factors play a decisive role for the changes in cloud liquid water, and thus for the changes in heavy precipitation.

(b)

It has been found in Chapter 2 and 3 that over southern Europe in summer the increase in the vertically integrated water vapor is weaker than suggested by the Clausius-Clapeyron relation. In the climate projections to the future this is reflected by decreasing trends in relative humidity (see Figure A.1, Appendix A). In particular the fact that the magnitudes are weaker over the land masses than over water indicates that the changes in precipitable water are limited by the local availability of water which is provided by evaporation from the ground. In accordance with this, the combination of evaporation and the vertically integrated water vapor is identified as best suitable

(a)

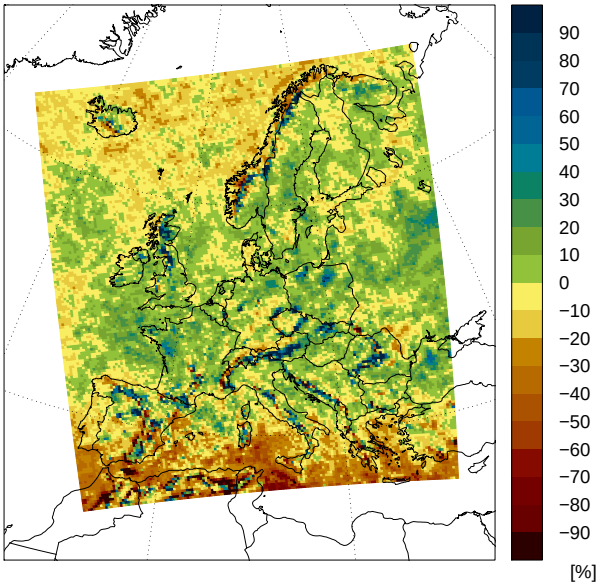

(b)

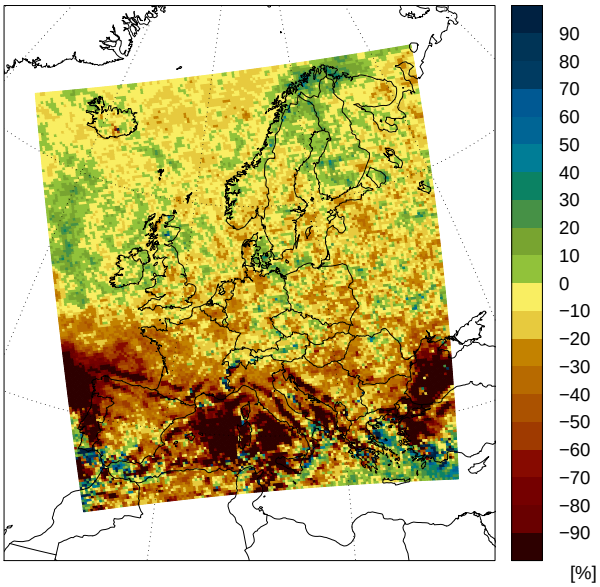

Figure 5.1: Change in the vertical velocity ω in $\%/K$ for (a) winter and (b) summer in the RCM REMO at 25 km spatial resolution.

(a)

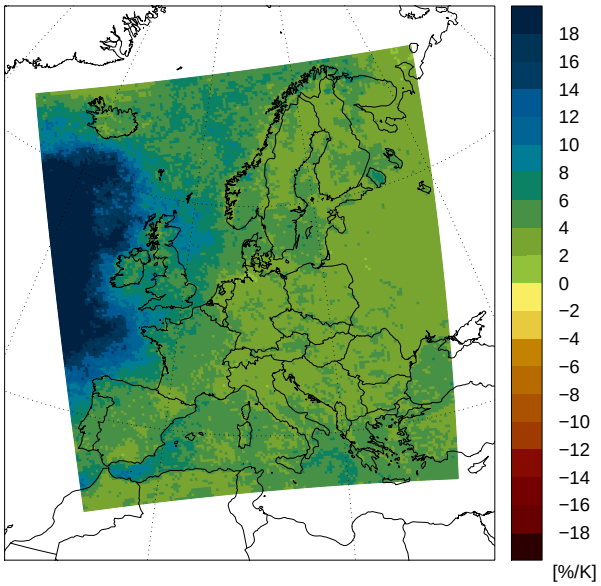

(b)

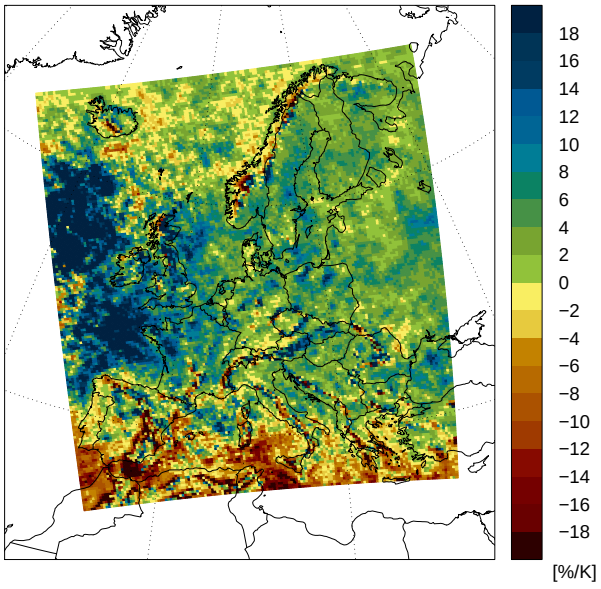

Figure 5.2: a) Thermodynamic part of the scaling conditional on heavy precipitation occurrence in $\%/K$ for winter in the RCM REMO at 25 km spatial resolution. b) Full scaling including ω.

(a)

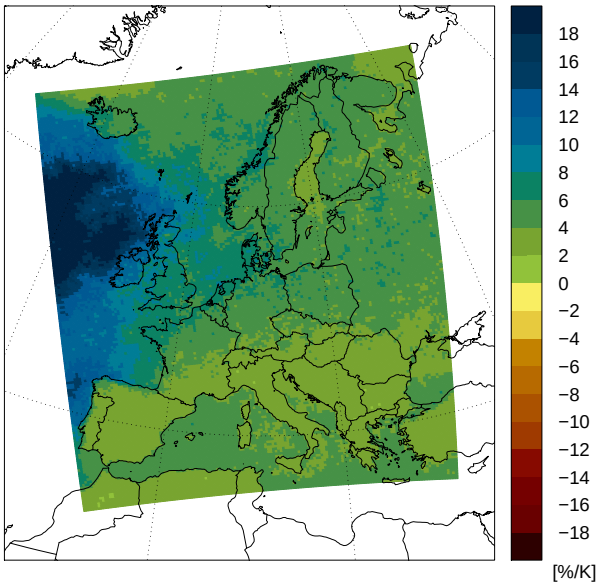

(b)

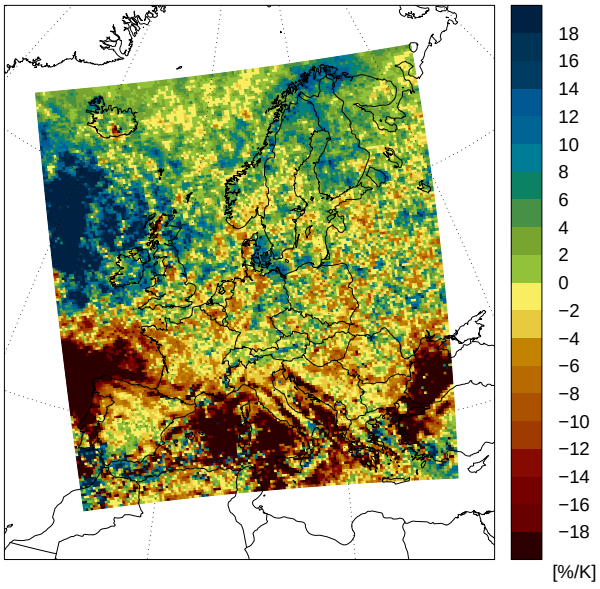

Figure 5.3: a) Thermodynamic part of the scaling conditional on heavy precipitation occurrence in $\%/K$ for summer in the RCM REMO at 25 km spatial resolution. b) Full scaling including ω.

covariate model for heavy daily precipitation totals in Chapter 4. The weaker increase in precipitable water leads to a decreasing probability for saturation and thus condensation, which controls parts of the changes in cloud liquid water and heavy precipitation. As for northern Europe the thermodynamic scaling by O'Gorman and Schneider (2009a) (Figure 5.3) exhibits weaker values than the changes in precipitable water analyzed in Chapter 2 and can explain a good part of the spatial variance of the changes in heavy precipitation ($R^2 = 44\%$). Nevertheless, the thermodynamic aspects do not necessarily explain why the changes in cloud liquid water and heavy precipitation are negative in many parts of southern Europe in summer. Inspection of Figure 5.1(b) shows that the projected changes in ω are negative in this regions, too, indicating stronger subsidence and weaker upward air motions. The strongest changes occur over Italy and the Mediterranean. As mentioned already in Chapter 2, in the southernmost regions the strong changes in ω might be due to a poleward shift of the subsiding branches of the Hadley cell (Lu et al. 2007). However, a possible shift of the Hadley cell is limited to the north due to the conservation of angular momentum (Held and Hou 1980). The changes in the dynamics further northwards might instead be related to the changes in the meridional temperature gradient. The negative changes in ω counteract the thermodynamic aspects of changes in the condensation rate and lead to negative signs of changes in heavy precipitation. The importance of the dynamics is also confirmed by the extreme value analysis in Chapter 4: Besides q_v and E, the dynamic covariates ω and MFD are included in the best covariate dependent models (Table 4.6).

The concluding discussion of the most important features of changes in heavy precipitation over Europe makes clear that for a complete understanding in the considered regions, the thermodynamic aspects always have to be viewed in conjunction with the dynamic ones, which often play a decisive role. This is supported by the findings for other sub-regions, such as the Alps and eastern Europe. Yet, the way how the dynamic and thermodynamic aspects interact regarding changes in heavy precipitation is dependent to a large extent on the climatic characteristics of the regarded region.

5.3 The answers to the research questions

The answers to the research question which were posed in the beginning can be summarized as follows:

- **How is heavy precipitation projected to change regionally over Europe for a future climate change scenario? Are the changes robust across an ensemble of regional climate model simulations?**
  The results show robust trends for heavy precipitation over many parts of Europe in a warming climate. The trends differ both regionally and seasonally. In winter the changes are positive over most of the European continent, with the largest

changes in high quantiles over northern Europe. A north-south gradient in the trends can be observed, and in the most southern parts of Europe the trends are close to zero or even negative. In summer, despite strong increases in near-surface temperatures, negative trends in heavy precipitation occur over a large area which extends from central to southern Europe. These negative trends can reach up to -30 % in regions like Spain, southern France, southern Italy, or Greece. In northern Europe, changes in heavy precipitation are positive also in summer.

- **Is there an immediate scaling of changes in heavy precipitation and precipitable water, predicted by the Clausius-Clapeyron relation?**
  For many regions of Europe the results of this study question the dominant role of precipitable water as a governing factor for changes in heavy precipitation. It is shown that the trends in heavy precipitation are smaller than predicted by the Clausius-Clapeyron relation. The spatial pattern of changes in heavy precipitation correlates better with changes in cloud liquid water compared to vertically integrated water vapor. Cloud liquid water is also found to be a better covariate for heavy precipitation in some regions, in particular in summer. It is suggested that dynamic aspects, such as changes in the moisture convergence and vertical velocity, and changes in the moist static stability play an important role. Therefore, changes in column water vapor do not relate to changes in cloud condensate and precipitation in a straightforward way.

- **Which dynamic and thermodynamic mainly govern the formation of heavy precipitation events? How do they interact and cause changes of heavy precipitation in different regions of Europe?**
  In the colder and more dynamically influenced regions, the moisture flux divergence is identified as best covariate for heavy precipitation. Since it clearly rules out the water vapor as predictor, this confirms the finding that heavy precipitation changes are steered by both the dynamics and the moisture amount and do not necessarily scale immediately with the Clausius-Clapeyron like change in water vapor over the same region. Also for other regions, the dynamic aspects play a decisive role. The vertical velocity is related to the formation of clouds and is identified as best predictor for eastern Europe. For warmer climate conditions the local factors gain relevance compared to the large-scale aspects. In the warmest region, South Italy, the evaporation and the column water vapor are found to be the best predictors. It is suggested that in this region it is the local availability of water vapor, which controls whether heavy precipitation can form. However, the sign of the changes in heavy precipitation might be controlled by the vertical velocity.

5.4 Outlook

The importance of dynamic aspects for changes in heavy precipitation has been stressed in this study. In particular for the regions where the moisture flux divergence is identified as best covariate, it would be worth studying, from which regions the moisture is advected to the region where it precipitates in a heavy rain event. This may be possible through a build-in moisture tracking in a regional climate model, which is applied online with the simulation. In this way it would be possible to examine whether the locations of moisture source regions and the tracks of moisture change in a warmer climate. Also one could investigate how the atmospheric water vapor changes with climate in the source region and thus affects cloud formation and heavy precipitation in the target regions. The tracking of moisture in an RCM simulation could furthermore help to investigate to which extent the moisture for heavy precipitation is provided by local sources versus advection through synoptic scale systems. This study has indicated that the local availability of moisture is an issue in particular in southern Europe in summer.

A related aspect which should be further investigated is the decrease in the relative humidity in summer over the southern European land masses. It may be interesting to reconsider this aspect in conjunction with the scaling of O'Gorman and Schneider (2009a). In general, the scaling has been found to function better than the Clausius-Clapeyron scaling, but it just considers the saturation value of water vapor, which is only a function of temperature. Instead, the changes in the condensation rate and thus cloud liquid water and precipitation may be modified by the relative humidity in some regions, as this study has pointed out. A modification that accounts for this aspect might give an improved scaling for regional changes.

A Projected changes in the relative humidity

In the following figure, the relative projected trend of the relative humidity over the time period 1961–2100 is illustrated. The results are mentioned in the course of the discussion in Chapter 2, as well as in other parts, but the figure is not part of the publication underlying Chapter 2.

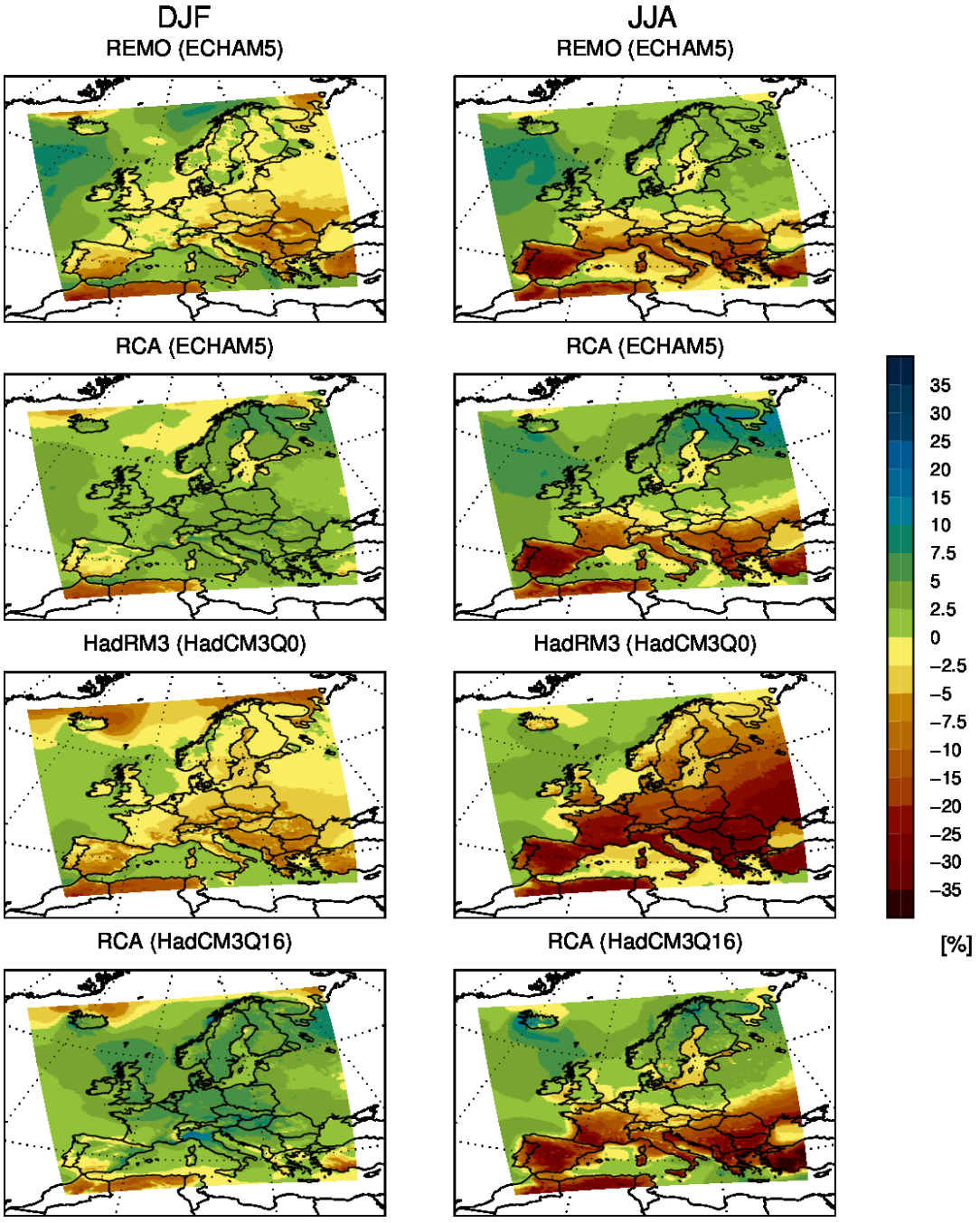

Figure A.1: Relative trends of the relative humidity over the time period 1961–2100 in % for winter (left) and summer (right).

B Application of the scaling by O'Gorman and Schneider (2009a) on regional scales

In their studies (O'Gorman and Schneider 2009a,b), the authors use a global scaling for heavy precipitation which is based on the scaling of the condensation rate c. Condensation is related to upward motion and adiabatic cooling and under the assumption of fixed relative humidity, the condensation rate needed to maintain the water vapor content close to saturation is given by

$$c = -\omega \left. \frac{dq_s}{dp} \right|_{\theta^*}, \tag{B.1}$$

where ω is the vertical velocity in pressure coordinates and $\left. \frac{dq_s}{dp} \right|_{\theta^*}$ is the vertical derivative of the saturation specific humidity, taken along a moist adiabat with constant equivalent potential temperature θ^* to account for the effect of latent heat release.

Heavy precipitation events often occur at temperatures higher than the climatological mean. Therefore, the precipitation scaling is evaluated at temperatures T_e conditional on heavy precipitation occurrence as follows

$$P_e \sim -\left\{ \omega_e \left. \frac{dq_s}{dp} \right|_{\theta^*, T_e} \right\}, \tag{B.2}$$

where P_e denotes a high quantile of precipitation, ω_e is the conditional vertical velocity, and $\{\cdot\}$ is a mass weighted integral over the troposphere. The full scaling thus consists of the thermodynamic part $\left. \frac{dq_s}{dp} \right|_{\theta^*}$ and the dynamic contribution incorporated by the vertical velocity ω_e.

For the regional application of the scaling here, B.2 is applied conditional on heavy precipitation, which is here events belonging to the range between the 92.5% and the 97.5% percentiles, at each grid point of a REMO simulation covering the European domain at a spatial resolution of 25 km (for further description of the simulation see Chapters 2 and 4). In Figure 5.2, the thermodynamic and the full scaling are shown for winter, in Figure 5.3 for summer.

C Determination of the optimal cluster number

C.1 Statistical measures

When applying partitional cluster algorithms like the k-means method, the optimal number of clusters has to be determined in advance. This is a key problem of such algorithms, since the optimal solution is in practice often difficult to find. Therefore, several statistical measures exist, which are helpful in this task. In order to find robust results for the cluster number, which are not restricted to a single statistical measure alone, different indices are applied here.

The $DVIndex$ introduced by Shen et al. (2005) is designed in a way that assumes the best cluster solutions to be compact and well separated from each other. The compactness of each cluster ($Intra$) is described by the average within-cluster sum of squares over all data points $\frac{1}{N}WSS(k)$ (Eq. C.1). A measure for the separation of the clusters is the ratio of the maximum to the minimum squared Euclidean distance (SED) (Eq. 4.1) between the cluster centroids, multiplied by the sum of the inverse $SEDs$ ($Inter$).

$$Intra(k) = \frac{1}{N}WSS(k) \tag{C.1}$$

$$Inter(k) = \frac{max_{i,j}(SED(i,j))}{min_{i \neq j}(SED(i,j))} \cdot \sum_{i=1}^{k} \left(\frac{1}{\sum_{j=1}^{k} SED(i,j)} \right) \tag{C.2}$$

Both measures are normalized by their maxima calculated for all cluster numbers $k > 2$:

$$IntraRatio = \frac{Intra(k)}{MaxIntra} \tag{C.3}$$

$$InterRatio = \frac{Inter(k)}{MaxInter}. \tag{C.4}$$

The $DVIndex$ is then defined as follows:

$$DVIndex(k) = IntraRatio(k) + \gamma * InterRatio(k), \tag{C.5}$$

where γ is a tuning parameter accounting for the noise in the data ($0 < \gamma < 1$) or to give the compactness more relevance compared to the separateness ($\gamma > 1$). Hoffmann (2012) found a value of 0.5 for γ to be appropriate for a weather pattern classification

and is thus be assumed to be appropriate here, too. The results of the $DVIndex$ for a range of γ values confirm the choice of γ to be reasonable.

Like the $DVIndex$, the $Validity$ index is also based on compactness and separation as measures for the goodness of the classification represented by a certain number of clusters. It was first introduced by Ray and Turi (2000) and is defined as

$$Validity(k) = \frac{Intra(k)}{min_{i \neq j}(SED(i,j))}. \tag{C.6}$$

For comparison and assessment of the robustness of the results, two more simple measures are applied in addition, which is the minimum SED ($MinSED$) and the maximum correlation between the cluster centroids ($MaxCorr$). The optimal cluster number is determined by finding a solution where $DVIndex$, $Validity$, and $MaxCorr$ should have a local minimum, and $MinSED$ should have a local maximum.

C.2 Results

Based on the measures described above, the optimal cluster numbers are determined for application in the four sub-regions for winter and summer. The numbers can mostly be detected by scanning the curves for a minimum of the $DVIndex$ or $Validity$ index, in conjunction with a local minimum SED. Also, a smaller number of clusters is generally favored before a larger number, because the clusters are preferred to be well separated from eachother. In this way, the following cluster numbers are found:

- Winter (Figure C.1)

  Southwest Norway, 6

  Alps, 7

  East Romania/Moldova, 6

  South Italy, 6

- Summer (Figure C.2)

  Soutwest Norway, 7

  Alps, 6

  East Romania/Moldova, 6

  South Italy, 5

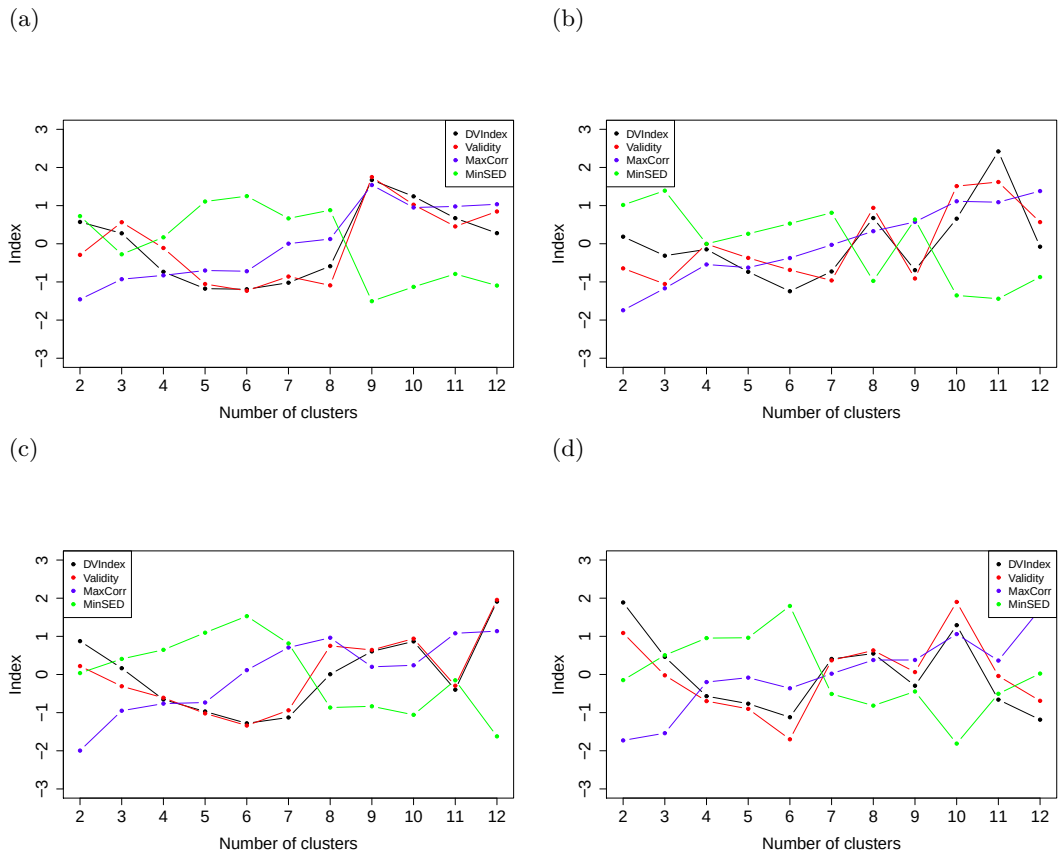

Figure C.1: Measures for determination of the optimal cluster number in the winter season for (a) Southwest Norway, (b) the Alps, (c) East Romania and Moldova, (d) South Italy.

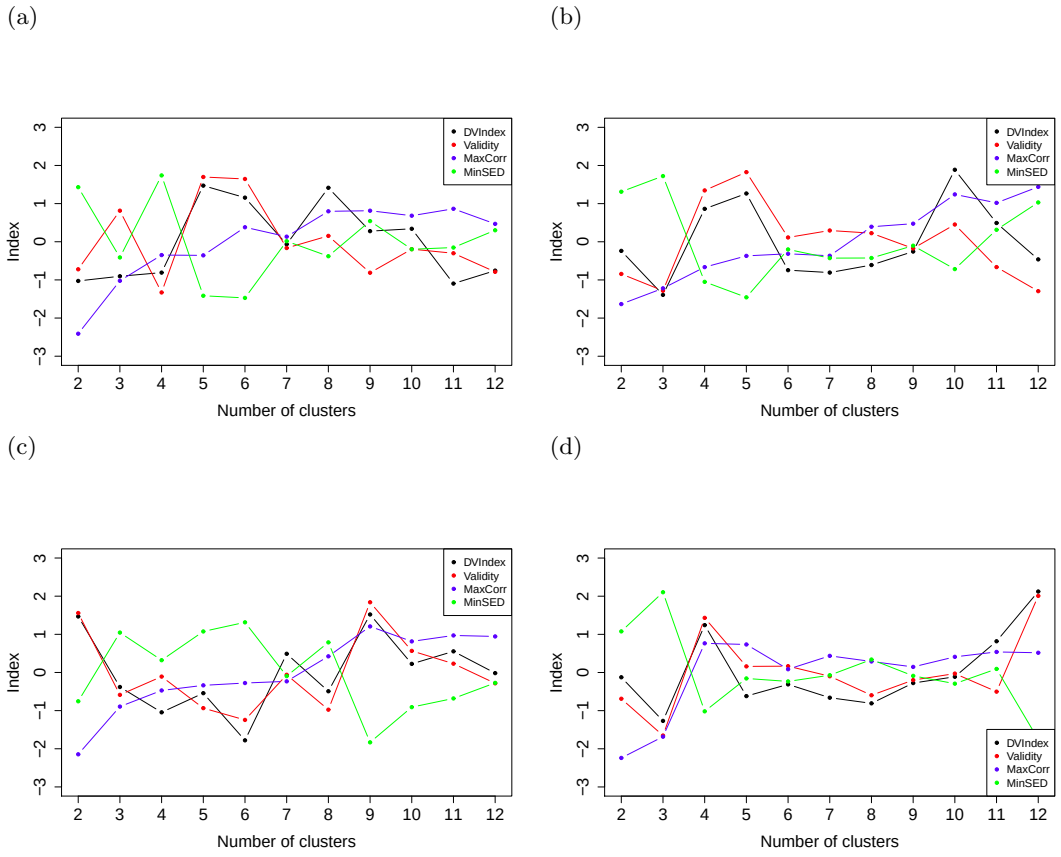

Figure C.2: Measures for determination of the optimal cluster number in the summer season for (a) Southwest Norway, (b) the Alps, (c) East Romania and Moldova, (d) South Italy.

Bibliography

Aikaike, H., 1973: Information theory and an extension of the maximum likelihood principle. *2nd International Symposium on Information Theory*, B. Petrov and F. Csaki, Eds., Budapest, Akademie Kiade, 267–281.

Aikaike, H., 1981: Likelihood of a model and information criteria. *Journal of Econometrics*, **16**, 3–14.

Allan, R. P. and B. J. Soden, 2008: Atmospheric warming and the amplification of precipitation extremes. *Science*, **321**, 1481–1484.

Allen, M. R. and W. J. Ingram, 2002: Constraints on future changes in climate and the hydrological cycle. *Nature*, **419**, 224–232.

Bengtsson, L., K. Hodges, and E. Roeckner, 2006: Storm Tracks and Climate Change. *J. Climate*, **19**, 3518â–3543.

Bengtsson, L., K. I. Hodges, and N. Keenlyside, 2009: Will extratropical storms intensify in a warmer climate? *J. Climate*, **22**, 2276–2301.

Berg, P., J. O. Haerter, P. Thejll, C. Piani, S. Hagemann, and J. H. Christensen, 2009: Seasonal characteristics of the relationship between daily precipitation intensity and surface temperature. *J. Geophys. Res.*, **114**, doi:10.1029/2009JD012008.

Boer, G., 1993: Climate change and the regulation of the surface moisture and energy budgets. *Clim. Dyn.*, **8**, 225–239.

Böhm, U., M. Kücken, W. Ahrens, A. Block, D. Hauffe, K. Keuler, B. Rockel, and A. Will, 2006: CLM-The climate version of LM: Brief description and long-term applications. *COSMO Newsletter*, **(6)**.

Boutle, I. A., S. E. Belcher, and R. S. Plant, 2010: Moisture transport in mid-latitude cyclones. *Q. J. R. Meteorol. Soc.*, **136**, 1–15.

Brier, G. W., 1950: Verification of forecasts expressed in terms of probability. *Mon. Wea. Rev.*, **78**, 1–3.

Buishand, T., 1989: Statistics of extremes in climatology. *Statistica Neerlandica*, **43 (1)**, 1–30, doi:10.1111/j.1467-9574.1989.tb01244.x.

Burnham, K. and D. Anderson, 2004: Multimodel Inference : Understanding AIC and BIC in Model Selection. *Sociological Methods & Research*, **33**, 261–304.

Chou, C., C.-A. Chen, P.-H. Tan, and K. Chen, 2012: Mechanisms for global warming impacts on precipitation frequency and intensity. *J. Climate*, **25 (9)**, 3291–3306, doi:10.1175/JCLI-D-11-00239.1.

Christensen, H., E. Kjellström, F. Giorgi, G. Lenderink, and M. Rummukainen, 2010: Weight assignment in regional climate models. *Clim. Res.*, **44**, 179–194.

Christensen, J. and O. Christensen, 2007: A summary of the PRUDENCE model projections of changes in european climate by the end of this century. *Clim. Change*, **81**, 7–30, 10.1007/s10584-006-9210-7.

Coles, S., 2001: *An Introduction to Statistical Modeling of Extreme Values*. Springer, New York, 208 pp.

Coles, S. and A. Stephenson, 2011: *ismev: An Introduction to Statistical Modeling of Extreme Values*. R package version 1.36.

Collins, M., B. B. B. Booth, G. R. Harris, J. M. Murphy, D. M. H. Sexton, and M. J. Webb, 2006: Towards quantifying uncertainty in transient climate change. *Clim. Dyn.*, **27**, 127–147, doi:10.1007/s00382-006-0121-0.

Davison, A. C. and R. L. Smith, 1990: Models for exceedances over high thresholds. *J. Roy. Stat. Soc. Series B*, **52**, 393–442.

Durman, C. F., J. M. Gregory, D. C. Hassell, R. G. Jones, and J. M. Murphy, 2001: A comparison of extreme european daily precipitation simulated by a global and a regional climate model for present and future climates. *Q. J. R. Meteorol. Soc.*, **127 (573)**, 1005–1015, doi:10.1002/qj.49712757316.

Embrechts, P., C. Klüppelberg, and T. Mikosch, 1997: *Modelling extremal events*. Springer, New York.

Emori, S. and S. Brown, 2005a: Dynamic and thermodynamic change in mean and extreme precipitation under climate change. *Geophys. Res. Lett.*, **32 (L17706)**.

Emori, S. and S. J. Brown, 2005b: Dynamic and thermodynamic changes in mean and extreme precipitation under changed climate. *Geophy. Res. Lett.*, **32**, doi: 10.1029/2005GL023272.

Frei, C., J. Christensen, M. Déqué, D. Jacob, R. G. Jones, and P. L. Vidale, 2003: Daily precipitation statistics in regional climate models: Evaluation and intercomparison for the European Alps. *J. Geophys. Res.*, **108**, doi:10.1029/2002JD002287.

Frei, C., C. Schär, D. Lüthi, and H. C. Davies, 1998: Heavy precipitation processes in a warmer climate. *Geophys. Res. Lett.*, **25**, 1431–1434.

Frei, C., R. Schöll, S. Fukutome, J. Schmidli, and P. Vidale, 2006: Future change of precipitation extremes in Europe: Intercomparison of scenarios from regional climate models. *J. Geophys. Res.*, **111**, doi:10.1029/2005JD005965.

Friederichs, P., 2010: Statistical downscaling of extreme precipitation using extreme value theory. *Extremes*, **13**, 109–132.

Friederichs, P., M. Goeber, S. Bentzien, A. Lenz, and R. Krampitz, 2009: A probabilistic analysis of wind gusts using extreme value statistics. *Met. Z.*, **18**, 615–629.

Frierson, D. M. W., 2008: Midlatitude static stability in simple and comprehensive general circulation model. *J. Atmos. Sci.*, **65**, 1049–1062.

Frierson, D. M. W., J. Lu, and G. Chen, 2007: Width of the Hadley cell in simple and comprehensive general circulation models. *Geophys. Res. Lett.*, **34**, doi:10.1029/2007GL031115.

Genio, A. D. D., M.-S. Yao, and J. Jonas, 2007: Will moist convection be stronger in a warmer climate? *Geophys. Res. Lett.*, **34**, L16 703.

Gerber, E. P. and G. K. Vallis, 2009: On the zonal structure of the North Atlantic Oscillation and Annular modes. *J. Atmos. Sci.*, **66**, 332–352.

Goffe, W. L., G. D. Ferrier, and J. Rogers, 1994: Global optimization of statistical functions with simulated annealing. *Journal of Econometrics*, **60 (1–2)**, 65–99, doi:10.1016/0304-4076(94)90038-8.

Hanel, M. and T. A. Buishand, 2010: On the value of hourly precipitation extremes in regional climate model simulations. *J. Hydrology*, **393**, 265–273.

Haylock, M., N. Hofstra, A. Klein Tank, E. Klok, P. Jones, and M. New, 2008: A European daily high-resolution gridded dataset of surface temperature and precipitation for 1950–2006. *J. Geophys. Res.*, **113**, D20 119, doi:doi:10.1029/2008JD010201.

Hegerl, G., et al., 2007: *IPCC, 2007: Climate Change 2007: The Physical Science Basis. Contribution of Working Group I to the Fourth Assessment Report of the Intergovernmental Panel on Climate Change*. Cambridge University Press, Cambridge, U.K.

Held, I. and A. Y. Hou, 1980: Nonlinear axially symmetric circulations in a nearly inviscid atmosphere. *Journal of the Atmospheric Sciences*, **37**, 515–533.

Held, I. M. and B. J. Soden, 2006: Robust responses of the hydrological cycle to global warming. *J. Climate*, **19**, 5686–5699.

Hoffmann, P., 2012: Quantifying the influence of climate change on the urban heat island of hamburg using different downscaling methods. Ph.D. thesis, University of Hamburg.

Hohenegger, C., P. Brockhaus, C. S. Bretherton, and C. Schär, 2009: The soil moisture-precipitation feedback in simulations with explicit and parameterized convection. *J. Climate*, **22**, 5003–5020.

Hohenegger, C., A. Walser, W. Langhans, and C. Schär, 2008: Cloud-resolving ensemble simulations of the August 2005 Alpine flood. *Q. J. R. Meteorol. Soc.*, **134**, 889–904.

Jacob, D., 2001: A note to the simulation of the annual and inter-annual variability of the water budget over the Baltic Sea drainage basin. *Meteorol. Atmos. Phys.*, **77**, 61–73.

Jacob, D. and R. Podzun, 1997: Sensitivity studies with the regional climate model REMO. *Meteorol. Atmos. Phys.*, **63**, 119–129.

Jacob, D., et al., 2001: A comprehensive model intercomparison study investigating the water budget during the BALTEX-PIDCAP period. *Meteorol. Atmos. Phys.*, **1-4**, 19–43.

Jacob, D., et al., 2007: An intercomparison of regional climate models for Europe: model performance in present-day climate. *Clim. Change*.

Katz, R. W., 1999: Extreme value theory for precipitation: sensitivity analysis for climate change. *Adv. Wat. Res.*, **23**, 133–139.

Katz, R. W., M. B. Parlange, and P. Naveau, 2002: Statistics of extremes in hydrology. *Adv. Wat. Res.*, **25**, 1287–1304.

Kjellström, E., F. Boberg, M. Castro, H. Christensen, G. Nikulin, and E. Sánchez, 2010: Daily and monthly temperature and precipitation statistics as performance indicators for regional climate models. *Clim. Res.*, **44**, 135–150.

Kjellström, E., et al., 2005: A 140-year simulation of European climate wit the new version of the Rossby Centre regional atmpospheric climate model (RCA3). Tech. Rep. 108, SMHI, SE-60176, Sweden, 54 pp.

Klein Tank, A. and Coauthors, 2002: Daily dataset of 20th–century surface air temperature and precipitation series for the European Climate Assessment. *Int. J. of Climatol.*, **22**, 1441–1453.

Klok, E. and A. Klein Tank, 2009: Updated and extended European dataset of daily climate observations. *Int. J. Climatol.*, **29**, 1182–1191.

Korty, R. L. and T. Schneider, 2007: A climatology of the tropospheric thermal stratification using saturation potential vorticity. *J. Climate*, **20**, 5977–5991.

Kunz, M. and C. Kottmeier, 2006: Orographic enhancement of precipitation over low mountain ranges, part II: Simulations of heavy precipitation events over Southwest Germany. *J. Appl. Meteorol. Climatol.*, **45 (8)**, 1041–1055.

Lenderink, G., 2010: Exploring metrics of extreme daily precipitation in a large ensemble of regional climate model simulations. *Clim. Res.*, **44**, 151–166.

Lenderink, G., B. van den Hurk, E. van Meijgaard, A. van Ulden, and J. Cuijpers, 2003: Simulation of present-day climate in RACMO2: first results and model developments. Tech. Rep. 252, 24 pp., KNMI.

Lenderink, G. and E. van Meijgaard, 2008: Increase in hourly precipitation extremes beyond expectations from temperature changes. *Nature Geoscience*, **1**, 511–514.

Lindstrot, R., R. Preusker, H. Diedrich, L. Doppler, R. Bennartz, , and J. Fischer, 2012: 1d-var retrieval of daytime total columnar water vapour from meris measurements. *Atmos. Meas. Tech.*, **5**, 631–646, doi:doi:10.5194/amt-5-631-2012.

Lionello, P., U. Boldrin, and F. Giorgi, 2008: Future changes in cyclone climatology over Europe as inferred from a regional climate model simulation. *Clim. Dyn.*, **30**, 657–671.

Lorenz, D. and E. DeWeaver, 2006: The Response of the Extratropical Hydrological Cycle to Global Warming. *J. Climate*, **20**, 3470–3484.

Lorenz, P. and D. Jacob, 2010: Validation of temperature trends in the ENSEMBLES regional climate model runs driven by ERA40. *Clim. Res.*, **44**, 167–177.

Lu, J., G. A. Vecchi, and T. Reichler, 2007: Expansion of the Hadley cell under global warming. *Geophys. Res. Lett.*, **34**, doi:10.1029/2006GL028443.

Mariotti, A., N. Zeng, Y.-H. Yoon, V. Artale, A. Navarra, P. Alpert, and L. Z. X. Li, 2008: Mediterranean water cycle changes: transition to drier 21st century conditions in observations and CMPI3 simulations. *Environ. Res. Lett.*, **3**, doi:10.1088/1748-9326/3/4/044001.

Meehl, G. A., J. M. Arblaster, and C. Tebaldi, 2005: Understanding future patterns of increased precipitation intensity in climate model simulations. *Geophys. Res. Lett.*, **32 (L18719)**, doi:10.1029/2005GL023 680.

Muller, C. J., P. O'Gorman, and L. E. Back, 2010: Intensification of precipitation extremes with warming in a cloud resolving model. *Preprint*, **1**, 1–17.

Nakicenovic, N. and R. Swart, 2001: Emissions scenarios. special report of the IPCC. Tech. rep., Cambridge University Press, Cambridge, MA, USA.

Naveau, P., M. Nogaj, C. Ammann, P. Yiou, D. Cooley, and V. Jomelli, 2005: Statistical methods for the analysis of climate extremes. *Comptes Rendus Geoscience*, **337 (10–11)**, 1013–1022, doi:10.1016/j.crte.2005.04.015.

O'Gorman, P. and T. Schneider, 2009a: Scaling of precipitation extremes over a wide range of climates simulated with an idealized GCM. *J. Climate*, **22**, 5676–5685.

O'Gorman, P. A. and C. J. Muller, 2010: How closely do changes in surface and column water vapor follow clausius-clapeyron sclaing in climate change simulations? *Environ. Res. Lett.*, **5**, doi:10.1088/1748-93226/5/2/025207.

O'Gorman, P. A. and T. Schneider, 2009b: The physical basis for increases in precipitation extremes in simulations of 21st-century climate change. *Proc. Nat. Acad. Sci.*, **106**, 14 773–14 777.

Pall, P., M. R. Allen, and D. A. Stone, 2007: Testing the Clausius-Clapeyron constraint on changes in extreme precipitation under CO_2 warming. *Clim. Dyn.*, **28**, 351–363.

Parker, D. J., 2002: The response of CAPE and CIN to tropospheric thermal variations. *Quarterly Journal of the Royal Meteorological Society*, **128**, 119–130.

R Development Core Team, 2010: *R: A Language and Environment for Statistical Computing*. Vienna, Austria, R Foundation for Statistical Computing, ISBN 3-900051-07-0.

Radermacher, C. and L. Tomassini, 2012: Thermodynamic causes for future trends in heavy precipitation over Europe based on an ensemble of regional climate model simulations. *J. Climate*, **25 (21)**, 7669–7689, doi:http://dx.doi.org/10.1175/JCLI-D-11-00304.1.

Ray, S. and R. H. Turi, 2000: Determination of the number of clusters in k-means clustering and application in colour image segmentation. *Proceedings of the 4th International Confernece on Advances in Pattern Recognition and Digital Techniques, New Delhi, Narosa*, 137–143.

Ribatet, M., 2011: *POT: Generalized Pareto Distribution and Peaks Over Threshold*. R package version 1.1-1.

Riemann-Campe, K., K. Fraedrich, and F. Lunkeit, 2009: Global climatology of Convective Available Potential Energy (CAPE) and Convective Inhibition (CIN) in ERA-40 reanalysis. *Atm. Res.*, **93**, 534–545.

Sanchez-Gomez, E., S. Somot, and M. Déqué, 2009: Ability of an ensemble of regional climate models to reproduce weather regimes over Europe-Atlantic during the period 1961-2000. *Clim. Dyn.*, **33**, 723–736.

Schär, C., D. Lüthi, U. Beyerle, and E. Heise, 1999: The soil-precipitation feedback: A process study with a regional climate model. *J. Climate*, **12**, 722–741.

Schulz, J., et al., 2009: Operational climate monitoring from space: the EUMETSAT Satellite Application Facility on Climate Monitoring (CM–SAF). *Atmospheric Chemistry and Physics*, **9**, 1687–1709.

Semenov, V. A. and L. Bengtsson, 2002: Secular trend in daily precipitation characteristics: Greenhouse gas simulation with a coupled AOGCM. *Clim. Dyn.*, **19**, 123–140.

Semmler, T. and D. Jacob, 2004: Modeling extreme precipitation events - a climate change simulation for Europe. *Global and Planetary Change*, **44**, 119–127.

Seneviratne, S. I., T. Corti, E. L. Davin, M. Hirschi, E. B. Jaeger, I. Lehner, B. Orlowsky, and A. J. Teuling, 2010: Investigating soil moisture - climate interactions in a changing climate: A review. *Earth–Science Reviews*, **99 (3–4)**, 125–161, doi: 10.1016/j.earscirev.2010.02.004.

Shen, J., S. Chang, E. Lee, Y. Deng, and S. Brown, 2005: Determination of cluster number in clustering microarray data. *Appl. Math. Comput.*, **169**, 1172–1185.

Sherwood, S. C., W. Ingram, Y. Tsushima, M. Satoh, M. Roberts, P. L. Vidale, and P. A. O'Gorman, 2010: Relative humidity changes in a warmer climate. *J. Geophys. Res.*, **115**, doi:10.1029/2009JD012585.

Smith, R. L., 1999: Trends in rainfall extremes, unpublished manuscript.

Smith, R. L., 2003: Statistics of extremes, with applications in environment, insurance and finance. *Extreme Values in Finance, Telecommunications and the Environment*, B. Finkenstadt and H. Rootzen, Eds., Chapman and Hall/CRC Press, London, 1–78.

Soden, B. J., D. L. Jackson, V. Ramaswamy, M. D. Schwarzkopf, and X. Huang, 2005: The radiative signature of upper tropospheric moistening. *Science*, **310**, 841–844.

Tomassini, L. and D. Jacob, 2009: Spatial analysis of trends in extreme precipitation events in high-resolution climate model results and observations for Germany. *J. Geophys. Res.*, **114**, 1–20.

Trenberth, K., 2011: Changes in precipitation with climate change. *Climate Research*, **47**, 123–138.

Trenberth, K. E., 1998: Atmospheric moisture recycling: Role of advection and local evaporation. *J. Climate*, **12**, 1368–1381.

Trenberth, K. E., A. Dai, R. M. Rasmussen, and D. B. Parsons, 2003: The changing character of precipitation. *Bull. Am. Meteorol. Soc.*, 1205–1217.

Ulbrich, U., J. G. Pinto, H. Kupfer, C. Leckebusch, T. Spangehl, and M. Reyers, 2008: Changing Northern Hemosphere storm tracks in an ensemble of IPCC climate change simulations. *J. Climate*, **21**, 1669–1679.

Van Aalst, M. K., 2006: The impacts of climate change on the risk of natural disasters. *Disasters*, **30 (1)**, 5–18, doi:10.1111/j.1467-9523.2006.00303.x.

Weaver, C. P. and V. Ramanathan, 1997: Relationships between large-scale vertical velocity, static stability, and cloud radiative forcing over northern hemisphere extra-tropical oceans. *Journal of Climate*, **10**, 2871–2887.

Zängl, G., 2007: To what extent does increased model resolution improve simulated precipitation fields? A case study of two North-alpine heavy-rainfall events. *Met. Z.*, **16 (5)**, 571–580.

Acknowledgements

At this point I would like to acknowledge to everybody who made a contribution to the success of my PhD thesis. First of all I would like to thank my advisors: Lorenzo Tomassini, who was willing to supervise this thesis and guided me into the world of extreme value statistics. Daniela Jacob, who gave me the chance to work in the REMO group and provided an excellent framework to perform regional climate modeling. I wish to thank both for the helpful discussions and comments regarding my work. Also I would like to thank Andreas Hense, for chairing my advisory panel and giving helpful advice, in particular on meteorological and statistical matters.

I was given the opportunity to be part of the *International Max Planck Research School on Earth System Modeling*. In this context I wish to express sincere thanks to Antje Weitz, Cornelia Kampmann, and Wiebke Böhm for their engagement and the immense support.

I would like to express my gratitude to the coordinators of the NCAR Advanced Study Program, for giving me the opportunity to join their Summer Colloquium on *Statistical Assessment of Extreme Weather Phenomena under Climate Change* in June 2011 and for the great organization of this workshop. Besides all other contributors, I wish to thank in particular Rick Katz and Eric Gilleland, who made a great effort to give the participants competent insights and understanding of extreme value theory.

The greatest part of this PhD work was financed by the EU FP7 project *SafeLand*, whose coordinators and participants I would like to thank for the pleasant project meetings and open discussions across fields. Furthermore, I am thankful for being given the chance to carry out some of the RCM simulations analyzed in this thesis in the framework of this project. A large part of the RCM data used in this work were provided by the EU FP6 Integrated Project ENSEMBLES whose support I gratefully acknowledge. The satellite data used in this work were provided by the *The ESA Due GlobVapour Project* and by *EUMETSAT Satellite Application Facility on Climate Monitoring (CM SAF)*. In this context I would like to thank in particular Nadine Schneider, Marc Schröder, Martin Stengel, and Frank Kaspar, for providing the data and giving support on data usage.

I would kindly like to thank Cathy Hohenegger and Bjorn Stevens, for valuable scientific discussions and advice on cloud and precipitation processes. Petra Friederichs, for her advice and support regarding statistical methods. Kathrin Riemann-Campe, for providing the CAPE-algorithm developed in her thesis. Paul O'Gorman for sharing

information and programming code on his scaling methods. Bettina Diallo for her great assistance on graphical editing.

I wish to thank my colleagues from the REMO-Group. I has been a very nice and welcoming working atmosphere and I could often benefit from a great willingness of everybody to discuss scientific problems and share knowledge. In particular I would like to thank my office mates: Katharina Bülow for responding to any question I could possibly have when I was starting my PhD studies and always cheering me up with some sweets in the right moment. Thomas Raub for supporting me in particular in the final stage – with comments on my work, dark chocolate, and a sympathetic ear. Special thanks go to my lunch companions and the 15.31 aggro table soccer crew, who provided diversion in the right moments and structured my days with cheerful and mind-clearing breaks.

Many thanks go to my parents, who gave me the chance to study and always supported me in every respect. And finally Daniel, for keeping me grounded under any circumstances and enriching my life with lots of happy moments.



ISSN 1614-1199